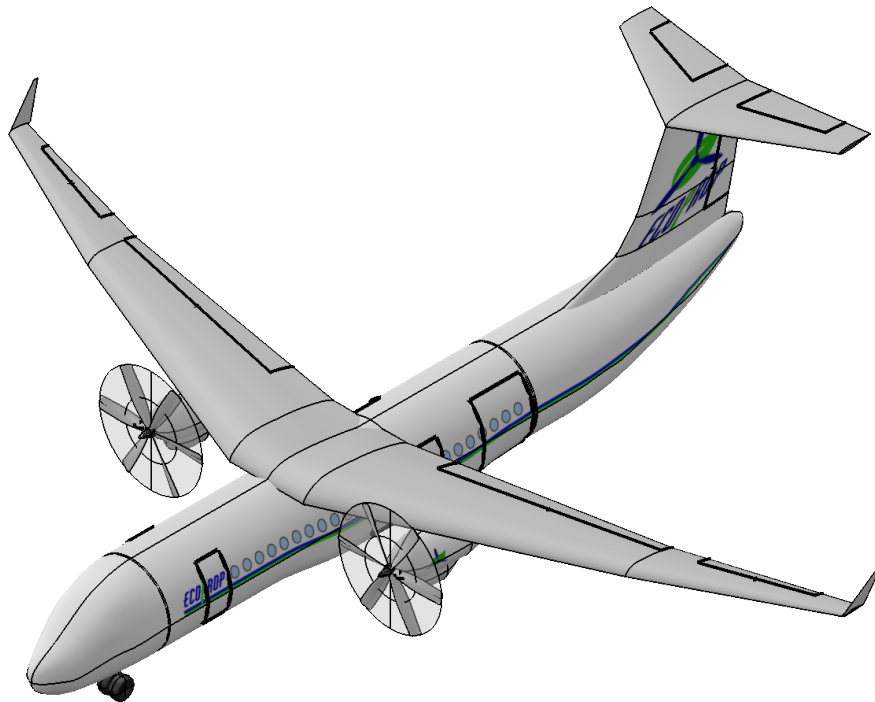# AIAA 2022-2023 Undergraduate Team RFP

Hybrid-electric Regional Turboprop

Final Design Report

ECOPROP

Department of Mechanical and Aerospace Engineering
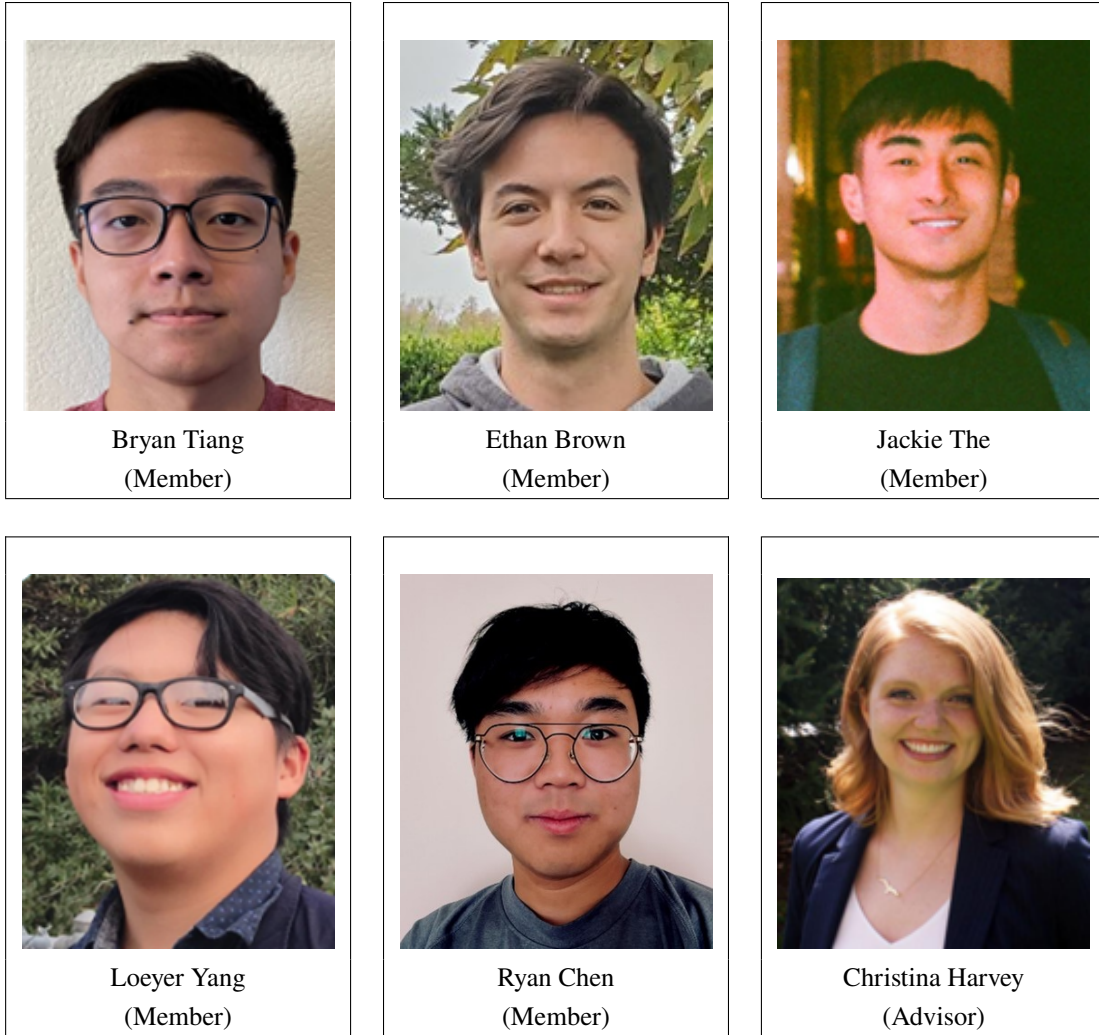University of California, Davis

Bryan Tiang
(Member)

Ethan Brown
(Member)

Jackie The
(Member)

Loeyer Yang
(Member)

Ryan Chen
(Member)

Christina Harvey
(Advisor)
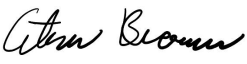
Table 1   Member Affiliations

Name	AIAA#	Signature
Bryan Tiang	1423101	
Ethan Brown	1423009	
Jackie The	1422885	
Loeyer Yang	1422964	
Ryan Chen	1422956	
Christina Harvey	948231	

Contents

List of Figures

List of Tables

I. Summary

A. Executive Summary

As a result of the COVID-19 pandemic, the demand for flights dropped significantly. Now as the pandemic comes to an end demand for regional flights between cities has been growing particularly quick. Considering the stricter emission requirements for airliners, there is also a growing market for regional aircraft with better fuel economy and reduced carbon and nitrogen oxide emissions. This is an opportunity to develop a hybrid-electric regional turboprop aircraft for regional flights to target this market. After considering a series of conceptual aircraft designs, we decided on a twin-engine hybrid-electric turboprop that has a T-tail empennage and a large wingspan with the potential use of a strut-braced wing. The aircraft must be competitive with similar regional turboprops, fulfill the requirements from the Request for Proposal (RFP), be compliant with FAR 23 and FAR 25 regulations, and have a technical readiness by 2035.

With this concept, we conducted a preliminary aircraft sizing to determine an initial estimate of the takeoff weight. We continue to refine this weight estimation by incorporating different performance constraints defined by the RFP and FAR regulations. The wing loading and power loading plots are developed to choose a feasible design space for the aircraft. In addition, we estimated the wing weight and selected a parallel powertrain architecture, which helped determine the power and weight for each major component. A process of iterations resulted in a maximum takeoff weight of 50,000 pounds.

Following FAR regulations, RFP requirements, and the comparable aircraft as a guide, we determined the fuselage diameter and structural thickness, as well as the layout of the required cargo, cockpit, seats, exits, and cabin amenities. We also incorporated estimates for landing gear and battery volumes. This process resulted in an 83.0 foot long fuselage with a 9.10 foot diameter.

Considerations for aerodynamics were taken into account when determining the wing and the empennage. The airfoil selected for our current wing is the ATR-72 airfoil due to the high $C_{L_{max}}$ required to fulfill the take-off climb requirement. However, as the airfoil is highly cambered, it is more suitable for low speed cruising. The tail of our current design adopts a T-tail configuration where the horizontal tail and vertical tail have the symmetric NACA 0012 and NACA 0009 airfoil respectively. The elevated position of the horizontal tail keeps it clear of the wake and prop-wash by the main wing and propellers, increasing its effectiveness.

After determining the previous configurations, we improved the weight of the aircraft once more by determining the weights of the components as weight groups. The new estimated weight of the aircraft is 64,482 pounds. Furthermore, the component weights and their relative center of gravity (CG) positions were found which determined the overall CG of the aircraft. In addition, the neutral point was calculated to determine the static margin of our aircraft, which equals 9.1%, indicating static longitudinal stability. Lastly, we estimated the cost of the aircraft to be $35 million per unit.

B. Dimensioned three-view drawings (all units in ft unless stated otherwise)
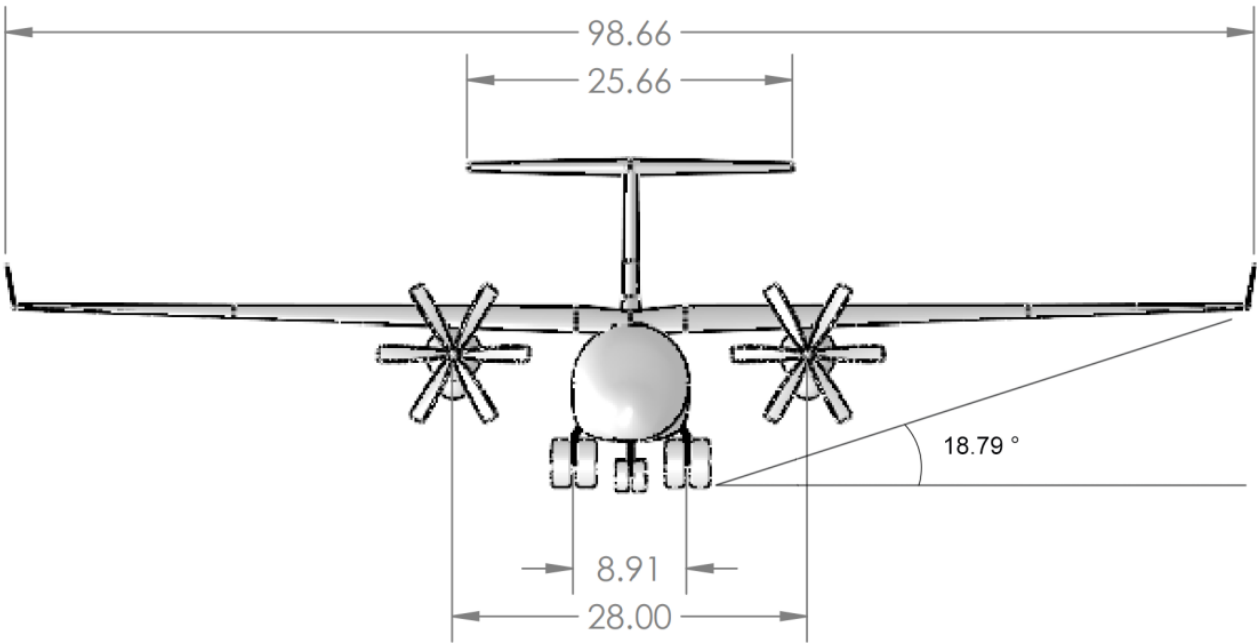
Fig. 1   Front view dimension
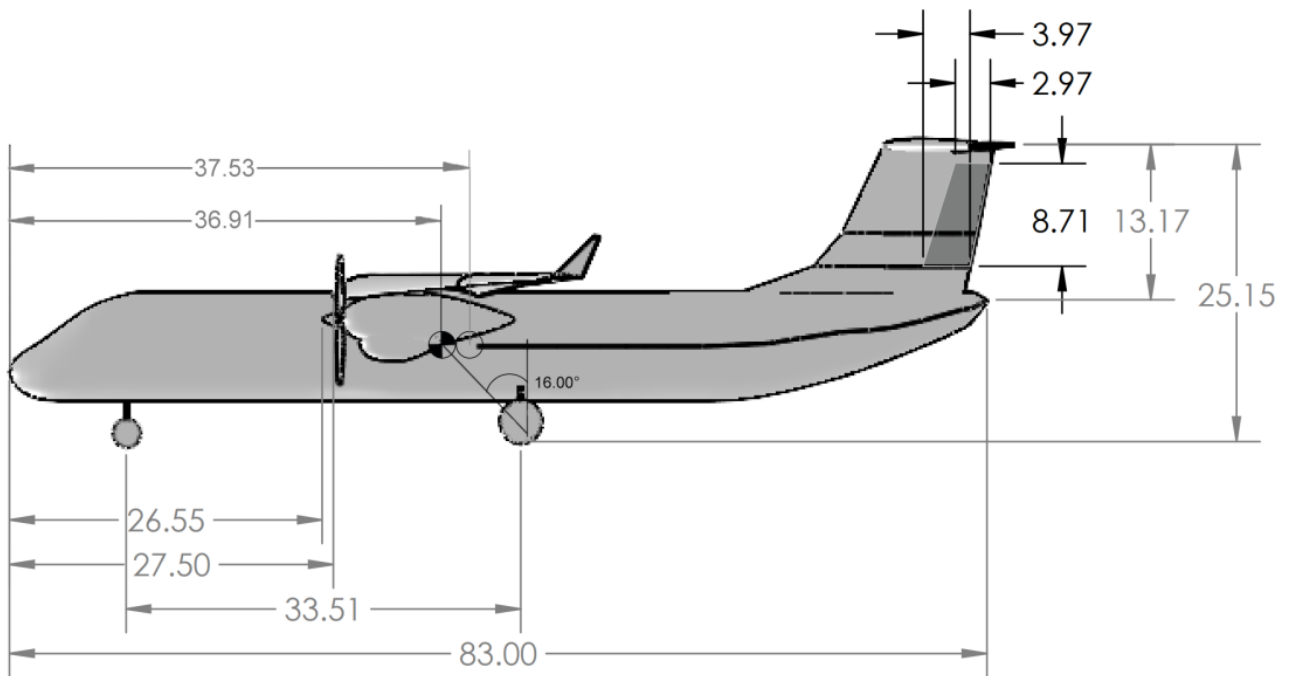
Fig. 2   Left view dimension
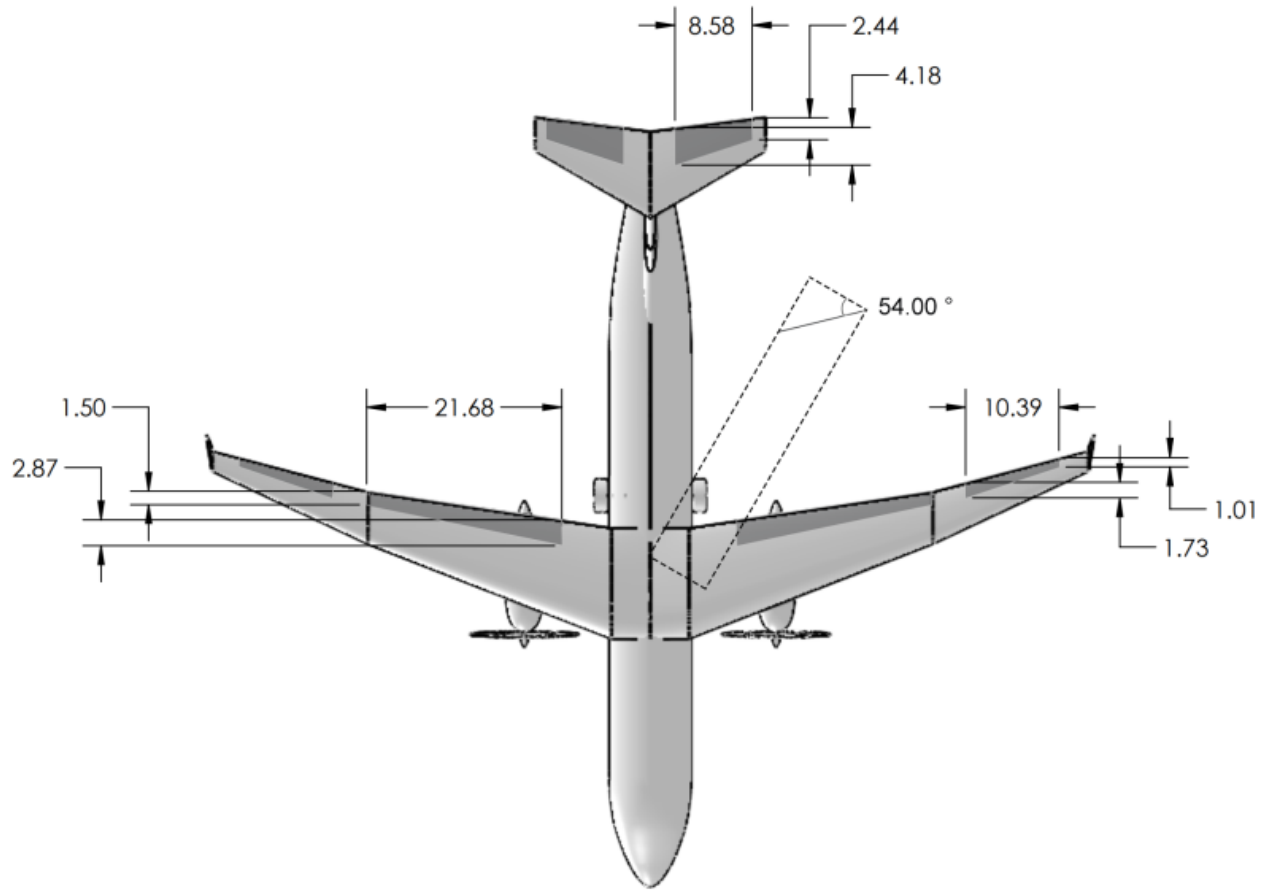
Fig. 3   Top view dimension

C. Major Geometric and Performance Parameters

Table 2 Comparable Aircraft Specifications vs. EcoProp

Parameters	Dash 8 Q300/Q400	ATR 72	SAAB 2000	EcoProp
Aircraft Weights				
Max Take-off Weight [lb]	43,000 [9]	41,005 [10]	50,700 [11]	64,000
Empty Weight [lb]	39,500 [9]	24,802 [10]	29,940 [11]	47,740
Max Payload Weight [lb]	13,500 [9]	10,141 [10]	14,600 [11]	12,660
Aerodynamic Parameters				
Cruise C_L	-	-	-	1.55
Landing C_L	-	-	-	2.6
Takeoff C_L	-	-	-	2
Cruise L/D	-	-	-	17
Aircraft Sizing Parameters				
Power Loading [lb/hp]	12.17	10.41	12.21	8
Wing Loading [lb/ft^2]	90.73	77.18	84.5	84
Wingspan [ft]	90 [9]	80.7 [12]	81.23 [11]	97
Wing Area [ft^2]	689 [9]	557.4 [12]	600 [13]	730
Aspect Ratio (AR)	12.6	11.99	11	13
Average Wing $\frac{t}{c}$	-	-	-	0.135
Length [ft]	73 [9]	74.5 [12]	89.5 [11]	83.0
Height [ft]	24.57 [9]	24.9 [12]	25.36 [11]	11.9
Fuselage Max Diameter [ft]	8.83 [9]	8.42 [12]	7.58 [14]	9.10
Engine				
Engine	PW 123	PW 120	RR Allison AE 2100	PW 150A
Engine Architecture [hp]	Conventional	Conventional	Conventional	Parallel
Engine Power [hp]	4,706 [9]	5,000 [15]	4,152 [11]	9,625
Engine Cruise SFC [lb/(hp hr)]	-	-	0.460[16]	0.433[16]
Key Safety and Operational Performance Parameters				
Cruise Mach no.	0.62 [17]	0.5 [18]	0.41 [19]	0.46
Range (Max Passengers) [nmi]	841 [9]	1,000 [10]	1,170 [20]	1,000
Fuel Capacity [lb]	5,000 [9]	4,409 [10]	6,160 [11]	6,000
Fuel Burn Per 500 nmi Trip [lb]	3,070 [21]	2,998 [22]		2,700
Fuel Burn Per Seat [lb/Seat]	61	42	-	39.8
Take off Field Length [ft]	3,280 [23]	3,822 [10]	4,005 [11]	4,500
Landing Field Length [ft]	2,560 [23]	3,169 [10]	3,937 [14]	4,500
Static Margin [%]	-	-	-	7.5
Business Parameters and Economic Estimates				
Passengers [persons]	50 [23]	50 [10]	50-58 [20]	50
Cabin Crew [persons]	2 [23]	2 [24]	2 [20]	1
Cockpit Crew [persons]	2 [25]	2 [24]	-	2
Cost per Aircraft (New) [$/aircraft]	17,000,000 [26]	26,000,000 [27]	15,000,000 [14]	35,000,000

II. Introduction

A. Estimated Market Size

Our preliminary research indicates that the market size for regional jets in 2021 was $10.47 billion dollars, [28] and the size of this market is projected to increase to $16.58 billion by the year 2028 [28]. Additionally, the demand for regional flight are forested to increase by 70% to 6 trillion asks by 2035[29]. The regional jet market covers both short and medium length flights [30] varying between a range of 830 nmi to 3450 nmi. We are aiming for a target range of 1000-1500 nmi with our turboprop aircraft.

With a 70% drop in year-on-year passenger demand for aircraft travel due to COVID-19, there subsequently was a large increase in interest for smaller short-haul flights in 2021. But this rebound in interest was not similarly felt by long-haul aviation, which is still experiencing low demand relative to pre-pandemic projections [31] leading to uncertainty in the investment in future larger wide-body, long-haul aircraft. The simultaneous boost in sales to aircraft like the A321neo [31] and the continued development of electric and hybrid electric aviation engines could indicate a permanent shift in the market towards airline fleets consisting of less long-haul aircraft towards these smaller, more regional, short-haul aircraft.

Short-haul and regional air routes are a currently under-served market, with 500-1000 nmi trips largely dominated by ground vehicles. Regional aircraft can utilize smaller regional airfields to also fly these trips [32]. Interstate trips of these distances, such as from San Francisco to Los Angeles, can be better served by smaller aircraft with some electric propulsion [33].

Additionally, the use of these hybrid electric and fully electric aircraft can counter the inefficiencies and emissions of traditional fuel powered aircraft when traveling shorter trips and carrying smaller payloads. With less time in cruise and more time during high-drag conditions like takeoff and landing, traditional engines can be fuel inefficient [34]. The onset of hybrid architectures can allow regional flights to reemerge in the face of fuel costs and environmental concerns. It also has the possibility of making prices for these trips more affordable and attractive for consumers.

B. Potential Challenges

Fuel cost is 20 - 40% of an airline's operating cost [35], so airlines will want their planes to have maximum fuel efficiency. Reducing emissions has also emerged as a goal for the commercial airline industry as a whole. As a result, airlines have become more keen on replacing jet fuel with alternative fuels and energy sources such as bio-fuels, hydrogen, and electricity [36].

The hybrid jet engine is a relatively new addition to the aviation industry, and requires new technology to further progress. This poses many challenges such as:

1) Weight management: Unlike conventional jet engines, hybrid jet engines require batteries that greatly add to the weight of the aircraft. A hybrid electric aircraft will have a constant battery weight throughout the flight as

opposed to a decreasing fuel weight in conventional aircraft[37]. With the additional weight, lighter materials may be needed to compensate. The placement of the batteries also affects the stability and maneuverability of the aircraft. In addition to the batteries, there is the weight of the electrical or hybrid powertrain and any additional components to support it [37].

2) Complexity: Hybrid jet engines consist of more components than a traditional combustion jet engine. This makes designing, building, and maintenance of the engine more difficult.

3) Cost: Hybrid jet engines require the development of new technology to make it economically and physically feasible to transport passengers over short range flights. Since a hybrid electric aircraft will require more components, the production cost will increase as well.

4) High Voltage Machines: For aircraft applications, high voltage machines (generator, motor) are necessary to provide the necessary thrust and electrical power. The power density of electrical machines needed for a hybrid jet engine is 10 to 15 kW/kg [38], however, there are physical limitations to the specific power conventional motors can provide. Currently, there is interest in superconducting machines (cryogenic) utilizing high temperature superconducting coils (HTS) because it can achieve high torque while maintaining high efficiency. A superconducting machine (including the weight of the cryogenic cooling system) can achieve a specific power of 9 kW/kg [39]. However, superconducting machines require a cryogenic cooling system, which can add significant weight to the aircraft.

5) Energy Storage: The range of the hybrid electric aircraft will depend on the type of energy storage used. High specific energy, life cycle, and stability are important considerations for energy storage. Lithium Ion batteries are commonly used in ground applications because of their long life cycles. However, the specific energy of a Li-ion battery is 250 Wh/kg whereas it is 12,000 Wh/kg for jet fuel [39]. Li-ion batteries are prone to thermal runaway, an uncontrolled chemical reaction that occurs within the cell which can lead to fire. Some battery energy storage alternatives that are being considered are Li-air batteries and Li-S batteries. Li-air batteries can provide a higher specific energy of 1000-2000 Wh/kg, however the electrolyte can decompose quickly and decrease the life cycle [39]. Li-S batteries can provide 500 Wh/kg and also have a life cycle of 500 cycles similar to Li-ion batteries [39]. The main challenges with Li-S batteries is the degradation of the cathode and overheating. Alternatives to batteries are flywheels and super-capacitors. Flywheels can store electrical energy as mechanical energy and have a specific energy of 100 Wh/kg [39]. Super-capacitors have a low energy density of 10-15 Wh/kg, but will have a much longer life cycle, temperature performance, and efficiency [39].

6) Power Distribution and Control: The ability to control the voltage, current, and frequency of electrical energy allows for the control of the electrical machines and for the generation, distribution, and storage of electrical energy. One of the challenges for power distribution is the choice between DC or AC distribution. DC distribution allows electrical decoupling between electrical machines which will allow the generator and the propulsor motor

to run at their optimal speeds without the need for a mechanical gearbox [38]. The cons of a DC system is the dependency on solid switching components with two conversion stages which will lead to power loss [38]. The advantages of an AC system is the removal of the solid state switching loss [38]. However, an AC distribution system will have coupling between the motor and the generator, which reduces the controllability of the system [38].

7) High Voltage Insulation: The use of high voltage in hybrid electric engines will require more insulation due to the partial discharge effect. The partial discharge effect degrades the wiring insulation due to internal discharges. The higher voltage and higher altitudes will magnify these effects [37]. High voltage electrical components need proper electrical insulation along with good thermal conductivity so that the electrical components are sufficiently cooled. This insulation needs to be light, strong, and compact to decrease the weight and volume of the conductors. One promising material is boron-nitride nanotubes (BNNT), but the high cost of this material will need to be considered. A Micro-multilayer Multifunctional Electrical Insulation (MMEI) system of polymer insulation films, e.g. Kapton PI and PFA as a bond layer is a commercially viable insulation option. MMEI has multifunctionality by providing high partial discharge resistance, improved durability, EMI shielding, and high thermal dissipation [40].

8) Safety: A hybrid-electric aircraft will have a greater reliance on electrical components, therefore increasing the criticality of the fault management system's effectiveness. Due to the nature of high voltages, electrical arcs which can cause short circuits in the system are a risk. Failures such as a short circuit in the electrical components can occur quickly and can lead to greater damage if not detected in a timely manner. It is necessary that the fault management system can quickly detect and isolate the electrical faults in order to protect the electrical components and preserve the reliability of the aircraft [37].

C. Aircraft Requirements

The following aircraft requirements in Table 3 were obtained from the Hybrid-electric Turboprop Request for Proposal (RFP) document by the American Institute of Aeronautics and Astronautics (AIAA). Note that the M represents a mandatory requirement while T stands for a tradable requirement.

Table 3   RFP Requirements

Category	Requirements	M or T
Figure of Merit	20%+ Reduction in block fuel on 500 nmi mission vs current turboprops	M
	Reduction in emissions vs current turbo-props	M
Entry into Service (EIS)	2035 for airplane	M

	Engine(s) technology can be certified by 2034	M
Passenger Capacity	50 +0/-4 passengers in a single class seating arrangement at a 30 inch seat pitch	M
Range with Full Passengers	1000 nmi	M
Cruise Speeds	Minimum cruise of 275 KTAS	M
	Target cruise of 350 KTAS	T
Seat Width	Minimum seat width of 17.2 inch	M
	Target seat width of 18 inch	T
	At least a 2 inch armrest width	M
Cross-section	Stand up height in the aisle similar to competitive aircraft	M
	Baggage compartment is tall enough to be serviced ergonomically	M
	18 inch minimum aisle width	M
Wing Span	Maximum of ICAO Code B (< 24 m)	T
	Maximum of ICAO Code C (< 36 m)	M
Performance	Approach speed category C (< 141 knots)	M
	Maximum landing field length of 4,500 ft over a 50 ft obstacle to a runway with dry pavement (sea level ISA + 18°F day) at maximum landing weight	M
	Takeoff, and landing performance should also be shown at 5,000 ft above mean sea level (ISA + 18°F)	M
	Distance to climb up to initial cruising altitude less than 200 nmi	M
	Initial cruising altitude of at least FL280	M
	Show fuel burn performance per trip and per seat and compare with the appropriate competitive aircraft at 500 nmi	M
Climb Gradient	Meet 14 CFR 25.121 Climb Gradient Requirements	M
Certifications	Capable of VFR and IFR flight with an autopilot	M
	Capable of flight in known icing conditions	M
	Meets applicable certification rules in FAA 14 CFR Part 25	M
	Provide systems and avionics architecture that will enable autonomous operations	T
Crew	2 pilots and 1 cabin crew member for every 50 passengers	M
Pilot and Baggage Weights	Pilot/Crew weight of 190 lb	M
	Baggage weight per pilot of 30 lb and volume of at least 4 cubic feet per person	M
Passenger and Baggage Weights	200 lb per passenger	M
	40 lb and 5 ft^3 of baggage per passenger	M

D. Mission Profile

Figure 4 represents a predicted mission profile for our aircraft based on the RFP. Table 4 is a more detailed breakdown of the time and power requirements for each mission segment.
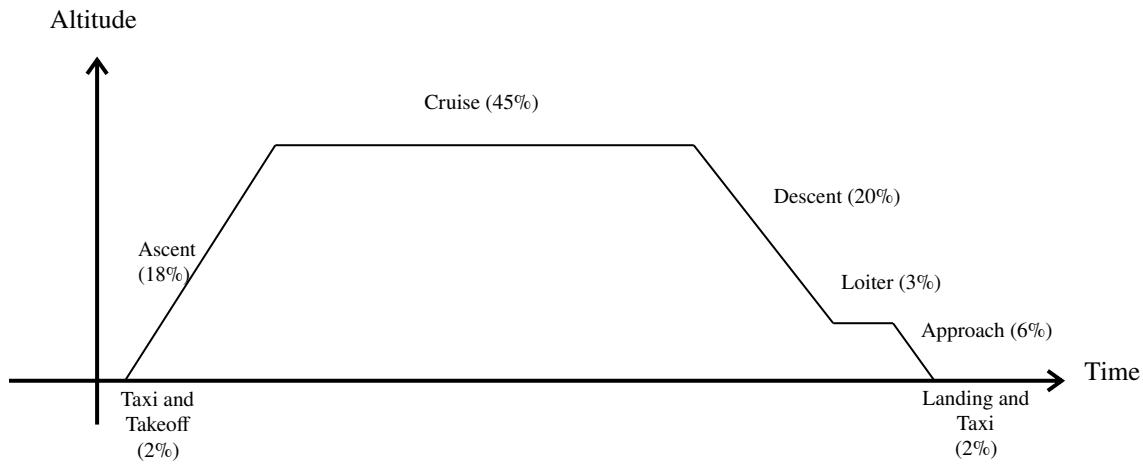
Fig. 4   Estimated mission profile for hybrid electric regional aircraft [1]

Table 4   Mission Profile

Segment	Portion of Total Time [%]	Estimated Power Requirement [hp] [41]
Taxi and Takeoff	2	5200
Ascent	18	4700
Cruise	45	2000
Descent	20	100
Loiter	3	1200
Approach	6	100
Landing and Taxi	6	1200

III. Configuration

A. Concept Designs

Figures 5, 6 and 7 show 3 initial concepts that our team considered.

1) Design 1
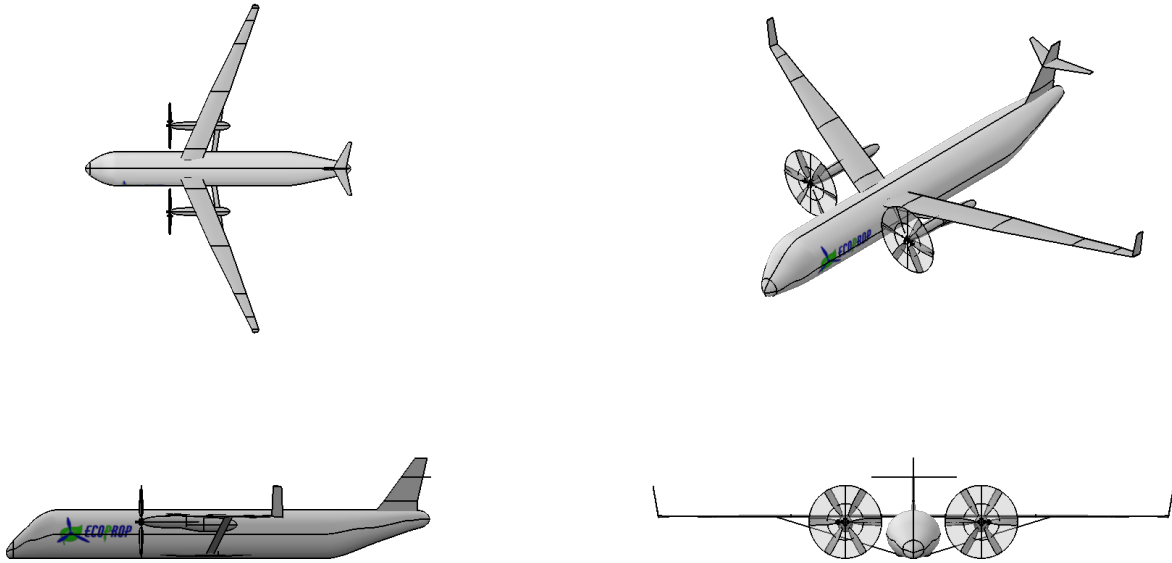
Fig. 5   Concept 1: A two-propeller, strut-braced wing aircraft, around 70 feet in length

2) Design 2
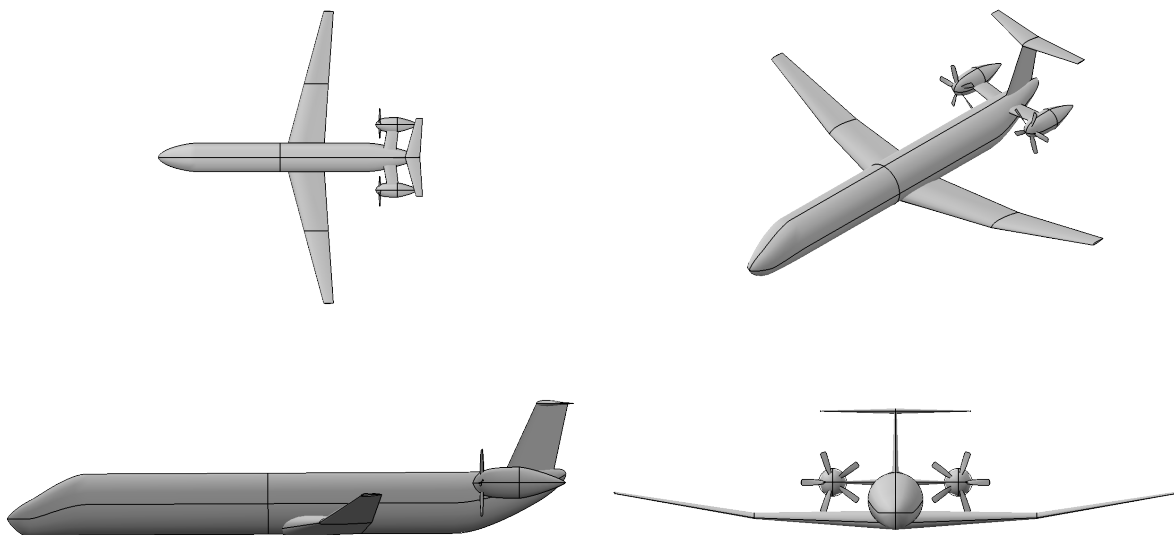
Fig. 6   Concept 2: A two rear propeller aircraft, around 80 feet in length

3) Design 3
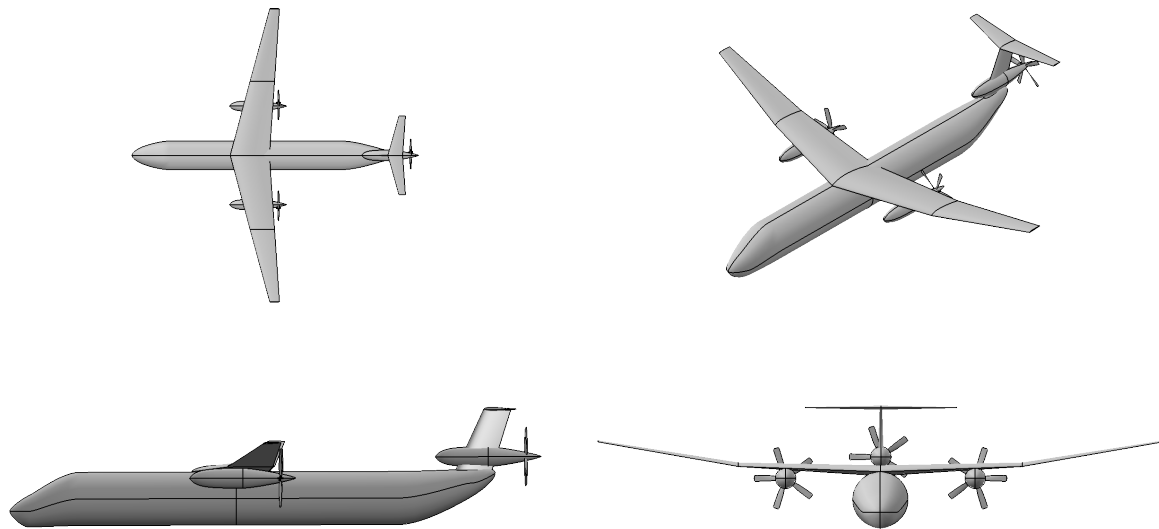
Fig. 7   Concept 3: A three propeller aircraft, around 80 feet in length

B. Design Advantages and Disadvantages

1) Design 1

Advantages

The use of a strut to support the wings allows for a much higher aspect ratio wing to be supported on the aircraft. This brings the design closer an ideally infinite wing, reducing induced drag and increasing the slope of the lift curve. Additionally, this aircraft can carry over the RFP specifications of 50 passengers, having enough size for around 70. This can be reduced for size or weight savings.

Disadvantages

The problem with this design is the size. The increased aspect ratio means the overall width of the plane is very large, and it may cause issues when parked at airports with limited or compact spaces. There is a specific requirement in the RFP to have a wingspan of less than the ICAO Code C limit and it might exceed that. This might be an issue that can be solved with folding wings, however this adds complexity and cost to the design.

2) Design 2

Advantages

Since the engine is attached to the rear of the aircraft, it is easier to reconfigure the wing and landing gears, while reducing its complexity. Additionally, in the scenario when the aircraft experiences engine failure in one of the engines, the yaw generated will be less significant.

Disadvantages

As the engine is placed behind the wing, it is very likely that the engine will be taking in disturbed air which reduces its efficiency. Without the engine attached to the wing, there is no longer a counter weight against the lift experienced by the wing. There is also a stricter requirement for ensuring that one engine failure doesn't cause the failure of the other engine.

3) Design 3

Advantages

The concept design consists of three propellers which will give the aircraft a high thrust to lift ratio, and the nature of the long wings will generate a high lift to drag ratio. Additionally, the propeller positioned at the rear end of the engine would reduce the noise heard by the passengers in the cabin.

Disadvantages

The three propellers would result in a more complex propulsion system, increasing its manufacturing and maintenance cost. The weight of the aircraft would be greater, requiring stronger landing gear to withstand its weight.

C. Considered Criteria

This section explains our thought process behind how each criteria was weighted for the Pugh Matrix.

1) Fuel and Emission Reductions:

Having a 20% reduction in block fuel and the reduction in emissions compared to existing turboprops are both figures of merit requirements for our customer. Since this is one of the main reasons for the hybrid electric aircraft proposal, we believe this is an important requirement that should be weighted as 5.

2) Range Requirements:

1000 nmi range for our aircraft is comparable to existing turboprop designs and is ideal for the regional and short haul flight goals. Being able to achieve this range requirement is important for the design to remain competitive. We believe this is an important requirement that should also be weighted as a 5.

3) Number of Passengers:

The number of passengers is mostly non-negotiable as to meet fuel per passenger per flight goals, but we feel that if the efficiency goals are substantial enough, then meeting lower end of this requirement (46 passengers), as stated in Table 3, is a worthy trade off. This is the reason we give it a weight of 4.

4) Target Cruise Speed:

While our target cruise speed is 350 KTAS, there is wide variability between this target speed and the minimum speed of 275 KTAS. In order to be competitive with newer turboprops, we want to aim on the higher end of this range or exceed it. However, there may be some potential benefits to reducing the cruise speed that may

outweigh general speed benefits. The larger range of accepted speeds does mean that we can give it a weight slightly lower than the previous criteria at 3.

5) Seating and Aisle Spacing:

There is room for variation to make the seats larger and more spacious, however our main goal is to increase efficiency. Therefore, if the sacrifice to aspects such as fuselage diameter or weight the plane are too great in order to increase the seat area, then that trade off will not always be worthwhile. We believe that a weight of 2 is most appropriate number for this criteria.

6) Landing and Takeoff Distances:

The landing and takeoff distances will likely be met by most designs, and we don't want to sacrifice the main objectives to reduce these distances more than required. Therefore we have assigned a weight of 2 for this criteria.

7) Distance of Climb to Cruise:

Similar to the previous requirement, we believe this can be met by most designs but optimization should not come at the cost of more important requirements. As a result, we have also assigned a weight of 2 to this criteria.

8) Time to Certify and Field Aircraft:

This is fairly important, as our customer would likely want to field these aircraft in a reasonable time frame. While we could introduce new technologies that would make meeting the main requirements easier, if certification of this new technology isn't done within the desired time frame, then the aircraft cannot be approved for use. We have decided that a weight of 3 is best for this criteria.

9) Aircraft Payload Weight:

We feel that primary values for the weight to support the engines and the airframe are of most importance. Once these are determined, a design window for modifications can be used to determine changes needed to accommodate the weights and sizes of baggage for crew, and passengers. While there are requirements for the weight of the payload, we feel that they dictate our aircraft design the least, therefore, we score it a 1.

D. Pugh Matrix

Based on the RFP we created the Pugh matrix shown in Table 5 to aid us in the selection of a concept.

Table 5   Pugh Matrix for Concept Selection

Requirements / Concepts	Category Weight	Concept 1	Concept 2	Concept 3
Reduction in emissions vs current turboprops	5	+1	0	0
1000 nmi Range with full passengers	5	0	0	0
50 +0/-4 passengers	4	+1	+1	+1
350 KTAS target cruise speed	3	0	0	+1
18" Aisle Width, 18 inch Seat Width and 30 inch Pitch	2	+1	0	0
4,500 ft over 50 ft obstacle takeoff and landing	2	0	+1	+1
Less than 200 nmi distance of climb to cruise	2	0	+1	+1
2035 for aircraft / engine technology certified by 2034	3	0	+1	0
Pilot, Crew, Passenger Baggage Size and Weight	1	+1	+1	0
Unweighted Totals:	–	4	4	4
Weighted Totals	–	12	12	11

E. Selection of Concept

Based on the weighted totals in Table 5, concept 1 and 2 are in a tie. However in our preliminary sizing study we ultimately found concept 1 to be both slightly lighter and cheaper therefore we decided to move forward with it.

IV. Preliminary Sizing

A. Preliminary Weight Estimations

In this section, we conducted a preliminary estimate for the weights in lb for each of the concepts.

Starting with the weight of the crew and their baggage, W_{crew}, which is calculated with the following equation:

$$W_{Crew} = (190 + 30) \cdot (N_{Pilots} + N_{Attendants}) \tag{1}$$

where N_{Pilots} is the number of pilots and $N_{Attendants}$ is the number of attendants. The values for 190 and 30 were the weights suggested by the RFP from Table 3.

The weight of the passengers and their baggage, $W_{Passengers}$ is calculated with the following equation:

$$W_{Passengers} = (200 + 40) * (N_{Passengers}) \tag{2}$$

where $N_{Passengers}$ is the number of passengers. The values for 200 and 40 were the weights suggested by the RFP from Table 3.

To calculate the fuel fraction, we first need to establish the fuel fractions of all the flight segments. The fuel fractions for takeoff, climb, descent, and landing are shown in Table 6.

Table 6   Fuel Fractions ([3], Table 3.2)

Mission Segment	Fuel Fraction	Value
Takeoff	W_1/W_0	0.970
Climb	W_2/W_1	0.985
Descent	W_4/W_3	0.990
Landing	W_6/W_5	0.995

The fuel fractions for the cruise and loiter segments will need to be calculated separately. The equation for the cruise segment, W_3/W_2, is ([3], Eqn 3.6):

$$\frac{W_3}{W_2} = \exp\left\{\frac{-R \cdot C}{V_{\text{cruise}}\frac{L}{D}_{\max}}\right\} \tag{3}$$

where R is the range of the aircraft, C is the specific fuel consumption in [lbf/(lbf hr)], V_{cruise} is the cruise velocity and $\frac{L}{D}_{\max}$ is the max lift-to-drag ratio

The equation for the loiter segment, W_5/W_4, is ([3], Eqn 3.8):

$$\frac{W_5}{W_4} = \exp\left\{\frac{-E \cdot C}{0.866\frac{L}{D}_{\max}}\right\} \tag{4}$$

where E is the endurance of the aircraft. Additionally, there is a factor of 0.866 for the L/D value since props are most efficient at that value ([3], p. 41)

Because Eqn 3 and 4 are for jets they will be corrected for propellers through the use of this equation ([3], Table 3.4)

$$C = C_{\text{bhp}} \cdot \frac{V_{\text{cruise}}}{550\eta_{\text{p}}3600} \tag{5}$$

where C_{bhp} is the amount of fuel needed to produce one horsepower at the propeller shaft [lb/hr/hp]. For cruise this value is 0.5 and loiter it is 0.6 ([3], Table 3.4). The additional 3600 and 550 are conversion factors. The fuel fraction can then be determined with Eqn 6 ([3], Eqn 3.13):

$$\frac{W_{\text{f}}}{W_0} = \left(1 - \frac{W_6}{W_5}\frac{W_5}{W_4}\frac{W_4}{W_3}\frac{W_3}{W_2}\frac{W_2}{W_1}\frac{W_1}{W_0}\right)1.06^* \tag{6}$$

*We multiply the fuel fraction by 1.06 to account for trapped fuel weight.

The empty weight fraction, W_{e}/W_0, is found with the Eqn 7 ([4], Eqn 2.3):

$$\frac{W_{\text{e}}}{W_0} = AW_0^C \tag{7}$$

For our purposes, values of the regression constants are A = 0.96 and C = -0.05 ([3], Table 3.1).

With all the weight fractions found, we can then estimate the takeoff weight of the aircraft with Eqn 8 ([3], Eqn 3.4):

$$W_0 = \frac{W_{\text{Crew}} + W_{\text{Passengers}}}{1 - \frac{W_{\text{f}}}{W_0} - \frac{W_{\text{e}}}{W_0}} \tag{8}$$

The takeoff weight found with Eqn 8 assumes that our airplane uses only fuel. In order to hybridize it, we will also need to estimate the mass of the battery by including a battery mass fraction term. For our aircraft we will assume that

20% of the cruise segment will be powered by electricity and that 45% of the fuel in the plane will be utilized for the cruise segment. To find the energy required for this, we will need the energy density of the fuel, which is assumed to be 5,443 Wh/lb [39], and the efficiency of the fuel, which is 0.28 [42]. We also assume our batteries are lithium-air batteries which will have an energy density of about 453 Wh/lb [39].

Therefore, the equation for our battery mass, W_{Bat}, is:

$$W_{\text{Bat}} = \frac{W_{\text{f}} \cdot 5,443 \cdot 0.45 \cdot 0.28 \cdot 0.2}{453} \tag{9}$$

We then obtain a battery mass fraction by dividing W_{Bat} with W_0 which was found previously. The final takeoff weight of the aircraft can then be found using the equation:

$$W_0 = \frac{W_{\text{Crew}} + W_{\text{Passengers}}}{1 - \frac{W_{\text{f}}}{W_0} - \frac{W_{\text{e}}}{W_0} - \frac{W_{\text{Bat}}}{W_0}} \tag{10}$$

The values used for the equations are shown in Table 2 under the specifications listed for our aircraft. From our preliminary weight estimation, we found our initial estimated takeoff weight to be 62,000 lb.

B. Key Constraints and Constraint Equations

We will have six performance constraints based on, stall speed, takeoff, landing, climb, cruise, and ceiling. In this subsection, we will state the constraints according to the RFP along with the related equations.

1) Stall speed

The constraint equation related to stall speed is:

$$W = L$$

which can be rewritten as

$$W = \frac{1}{2}\rho V_{\text{Stall}}^2 C_{\text{L}_{\max}} S_{\text{w}} \tag{11}$$

2) Takeoff

Our original takeoff distance was based on FAR 25 takeoff parameters and the equation below:

$$\frac{BFL}{37.5} = \frac{W_0/S_{\text{w}}}{(\rho/\rho_{\text{SL}}) \cdot C_{\text{L}_{\max,\text{TO}}} \cdot T_0/W_0} \tag{12}$$

However, this is defined for a takeoff obstacle of 35 ft whereas the RFP requires an obstacle height of 50 ft. Therefore, we must use a different set of equations. Roskam has a constraint equation for sizing military takeoff ground-run requirements which is based on an obstacle height of 50 ft ([7], Eqn 3.9). Hence, we will be sizing our takeoff requirements based on this equation:

$$S_{\text{TOG}} = \frac{k_1(W_0/S_{\text{w}})}{\rho \left(C_{\text{L}_{\max,\text{TO}}}(k_2(P_0/W_0) - \mu_{\text{G}}) - 0.72C_{\text{D}_{\text{O}}} \right)} \tag{13}$$

where S_{TOG} is the takeoff groundrun.

3) Landing

According to the FAR 25, the relevant equation is:

$$S_{\text{land}} = \frac{1}{0.6}\left(80\frac{W_{\text{L}}/S_{\text{w}}}{((\rho/\rho_{\text{SL}})C_{\text{L}_{\text{max,L}}})} + S_{\text{a}}\right) \tag{14}$$

where S_{a} is the obstacle clearance distance, S_{land} is the landing field length and W_{L} is the landing weight.

4) Climb

The constraint equation for climb is:

$$\frac{T_0}{W_0} = \frac{k_{\text{s}}^2 C_{\text{D}_0}}{C_{\text{L}_{\text{max,CL}}}} + k\frac{C_{\text{L}_{\text{max,CL}}}}{k_{\text{s}}^2} + G \tag{15}$$

where k is:

$$k = \frac{1}{\pi e AR_{\text{w}}} \tag{16}$$

5) Cruise

For a propeller-powered aircraft the constraint equation for power required during cruise is:

$$P = TV = \frac{1}{2}\rho V^2 S_{\text{w}} C_{\text{D}} V \tag{17}$$

6) Ceiling

There are two ceiling constraints: absolute and service. The FAR does not mention a service ceiling constraint to be met; therefore, we will only be sizing based on the absolute ceiling constraint. The constraint equation for the ceiling parameter is:

$$\left(\frac{T}{W}\right)_{\text{min}} = 2\sqrt{kC_{\text{D}_0}} \tag{18}$$

where k is Eqn 16.

C. Required Values to Transform Constraint Equations

In this subsection, we will transform the constraint equations to be in terms of power loading (W_0/P_0), and wing loading (W_0/S_{ref}). The density of air at sea level, ρ_{SL}, is 0.00237 slugs/ft^3. Since the airplane we are designing is a propeller aircraft, we will need to convert $\frac{T}{W_0}$ to power ratio $\frac{P}{W_0}$ using the equation:

$$\frac{T}{W_0} = \frac{550\eta_{\text{p}}}{V}\frac{P}{W_0} \tag{19}$$

where the propulsive efficiency, η_{p}, is 0.8 ([3], p. 36), and the 550 value is to convert our units to hp/lb.

1) Stall speed

Starting with Eqn 11:

$$W_0 = \frac{1}{2}\rho V_{\text{Stall}}^2 C_{\text{L}_{\text{max}}} S_{\text{w}}$$

Rearranging Eqn 11, we get:

$$\frac{W_0}{S_{\text{w}}} = \frac{1}{2}\rho V_{\text{Stall}}^2 C_{\text{L}_{\text{max}}} \tag{20}$$

which is the stall speed constraint in terms of wing loading.

According to Raymer ([3], p. 125), we can estimate the approach speed as being 1.3 times V_{stall}. Since the approach speed requirement in the RFP is 141 knots or roughly 238 ft/s, we then use a value of 182 ft/s for V_{stall}. Stall is most likely during landing as that is when the aircraft is flying the slowest. Therefore, we use the density conditions for our worse case scenario during landing at an altitude of 5000 ft which is 0.002048 slug/ft$_3$.

Placing everything back into Eqn 20 we get:

$$\frac{W_0}{S_w} = \frac{1}{2} \cdot 0.002048 \cdot 182^2 \cdot 1.55$$

2) Takeoff

Starting with Eqn 13:

$$S_{TOG} = \frac{k_1(W_0/S_w)}{\rho\left(C_{L_{max,TO}}(k_2(P_0/W_0) - \mu_G) - 0.72C_{D_O}\right)}$$

Rearranging for power loading, we get:

$$\frac{W_0}{P_0} = \left(\frac{1}{k_2}\left(\frac{\frac{k_1(W_0/S_w)}{S_{TOG}\rho} + 0.72C_{D_O}}{C_{L_{max,TO}}} + \mu_G\right)\right)^{-1} \tag{21}$$

where k_1 is 0.0376 ([7], p. 102), μ_G = 0.025 ([7], Table 3.2), and:

$$k_2 = l_p\left(\frac{\rho}{\rho_{SL}}(ND_P^2/P_0)\right)^{1/3} \tag{22}$$

Using Eqn 22, we then rewrite Eqn 21 as:

$$\frac{W_0}{P_0} = \left(\frac{1}{l_p\left(\frac{\rho}{\rho_{SL}}(N \cdot D_P^2/P_0)\right)^{1/3}}\left(\frac{\frac{0.0376(W_0/S_w)}{S_{TOG}\cdot\rho} + 0.72C_{D_O}}{C_{L_{max,TO}}} + 0.025\right)\right)^{-1}$$

Since our aircraft will have variable pitch propellers, l_p is 5.75 ([7], p. 102). N is the number of engines. P_{TO} is the total takeoff power which we assume is 5000 hp, and D_P is the diameter of the propellers. The value of $C_{L_{max,TO}}$ used is 2 ([7], Table 3.1). The value for C_{D_o} is from Eqn 88. As for the takeoff groundrun, S_{TOG}, we assume that it is 60% of the takeoff field length ([7], Eqn 3.5). Finally we get:

$$\frac{W_0}{P} = \left(\frac{1}{5.75\left(\frac{0.002048}{0.00237}(2 \cdot 13^2/5000)\right)^{1/3}}\left(\frac{\frac{0.0376(W_0/S_w)}{0.6\cdot4500\cdot0.002048} + 0.72 \cdot 0.0506}{2} + 0.025\right)\right)^{-1}$$

3) Landing

Beginning with Eqn 14, we substitute the value for ρ_{SL}:

$$S_{land} = \left(80\frac{W_L/S_w}{((\rho/0.00237)C_{L_{max,L}})} + S_a\right)$$

We then convert the maximum landing weight back to takeoff weight using the equation:

$$\frac{W_0}{S_w} = \frac{W_L/S_w}{W_L/W_0} \tag{23}$$

which yields:

$$S_{FL} = \left(80\frac{\frac{W_0}{S_w}\frac{W_L}{W_0}}{((\rho/0.00237)C_{L_{max,L}})} + S_a\right)$$

Rearranging the equation, we get:

$$\frac{W_0}{S_{\text{w}}} = \left(\frac{S_{\text{FL}} - S_{\text{a}}}{80}\right) \frac{C_{\text{L}_{\text{max,L}}} (\rho/0.00237)}{\frac{W_{\text{L}}}{W_0}}$$

According to the RFP, a maximum landing distance of 4,500 ft (Table 3), an obstacle clearance distance of 1,000 ft ([3], p. 133) are required. The value of ρ at sea level was used. The value of $C_{\text{L}_{\text{max, L}}}$ used is 2.6 ([7], Table 3.1). From the calculations conducted in the concept tradeoff study, the landing weight ratio is 0.994. The landing weight ratio is based on a flight consisting of takeoff, climb, 15 minute loiter and descent:

$$\frac{W_0}{S_{\text{w}}} = \left(\frac{0.6 \cdot 4500 - 1000}{80}\right) \frac{2.6(0.002048/0.00237)}{0.994}$$

4) Climb

Based on FAR 25, there are six different climb requirements which are summarized in Table 7. Note that AEO stands for "all engines operative" and OEI stands for "one engine inoperative." The $C_{\text{L}_{\text{max,CL}}}$ values are chosen based on whether the landing or takeoff flaps are extended or retracted.

Table 7   Climb Segment Values ([4], pp. 39-40)

Climb Segment	G[%]	k_{s}	Weight
Takeoff (OEI)	1.2	1.2	Max Takeoff
Transition Segment (OEI)	0.0	1.19	Max Takeoff
Second Segment (OEI)	2.4	1.2	Max Takeoff
En-route (OEI)	1.2	1.25	Max Takeoff
Balked Landing (AEO)	3.2	1.3	Max Landing
Balked Landing (OEI)	2.1	1.5	Max Landing

Beginning with Eqn 15, and bringing in Eqn 16:

$$\frac{T_0}{W_0} = \frac{k_{\text{s}}^2 C_{\text{D}_0}}{C_{\text{L}_{\text{max,CL}}}} + \frac{1}{\pi e AR_{\text{w}}} \frac{C_{\text{L}_{\text{max,CL}}}}{k_{\text{s}}^2} + G$$

We then use Eqn 19 to change it in terms of power ratio:

$$\frac{550 \cdot 0.8}{V} \frac{P_0}{W_0} = \frac{k_{\text{s}}^2 C_{\text{D}_0}}{C_{\text{L}_{\text{max,CL}}}} + \frac{1}{\pi e AR_{\text{w}}} \frac{C_{\text{L}_{\text{max,CL}}}}{k_{\text{s}}^2} + G$$

The value for V for this scenario is given by:

$$V = \sqrt{\frac{2}{\rho C_{\text{L}_{\text{max,CL}}}} \frac{W_0}{S_{\text{w}}}} \tag{24}$$

We rearrange the equation to get it in terms of power loading and substitute Eqn 24 for the value of V, which leads to:

$$\frac{W_0}{P_0} = \left(\frac{\frac{k_{\text{s}}^2 C_{\text{D}_0}}{C_{\text{L}_{\text{max,CL}}}} + \frac{1}{\pi e AR_{\text{w}}} \frac{C_{\text{L}_{\text{max,CL}}}}{k_{\text{s}}^2} + G}{\frac{550 \cdot 0.8}{\sqrt{\frac{2}{\rho C_{\text{L}_{\text{max,CL}}}} \frac{W_0}{S_{\text{w}}}}}}\right)^{-1} \tag{25}$$

Note that the value for air density changes for each climb segment as the altitude of the aircraft is increasing. For the sake of simplicity, an average value for density between an altitude of 28,000 ft and sea level was used for

all climb phases except for the balked landing climb phases. The altitude at sea level was used for the balked landing climb phases. While this may lead to slightly inaccurate constraint values for the other climb segments, this would have no effect on our design space as the active constraint is the balked landing OEI condition and the density which is used for that condition is accurate.

a. Takeoff Climb

Using Eqn 25 and factoring the climb corrections along with the values in Table 7.

$$\frac{W_0}{P_0} = \left(\frac{\left(\frac{1.2^2 C_{D_0}}{C_{L_{max,CL}}} + \frac{1}{\pi e AR_w} \frac{C_{L_{max,CL}}}{1.2^2} + 0.012 \right) \frac{2}{2-1} \frac{1}{0.8}}{\frac{550 \cdot 0.8}{\sqrt{\frac{2}{\rho C_{L_{max,CL}}} \frac{W_0}{S_w}}}} \right)^{-1}$$

In this segment, the takeoff flaps and landing gear are retracted. From Table 21, e is 0.8, and from Eqn 87, C_{D_o} is 0.0306. Since we have the takeoff flaps engaged, $C_{L_{max,CL}}$ is $C_{L_{max,TO}}$.

b. Transition Climb

Using Eqn 25 and factoring the climb corrections along with the values in Table 7.

$$\frac{W_0}{P_0} = \left(\frac{\left(\frac{1.19^2 C_{D_0}}{C_{L_{max,CL}}} + \frac{1}{\pi e AR_w} \frac{C_{L_{max,CL}}}{1.19^2} \right) \frac{2}{2-1} \frac{1}{0.8}}{\frac{550 \cdot 0.8}{\sqrt{\frac{2}{\rho C_{L_{max,CL}}} \frac{W_0}{S_w}}}} \right)^{-1}$$

In this segment, the takeoff flaps are engaged and the landing gear is down. From Table 21, e is 0.8, and from Eqn 88, C_{D_o} is 0.0506. Since we have the takeoff flaps engaged, $C_{L_{max,CL}}$ is $C_{L_{max,TO}}$.

c. Second Segment Climb

Using Eqn 25 and factoring the climb corrections along with the values in Table 7.

$$\frac{W_0}{P_0} = \left(\frac{\left(\frac{1.2^2 C_{D_0}}{C_{L_{max,CL}}} + \frac{1}{\pi e AR_w} \frac{C_{L_{max,CL}}}{1.2^2} + 0.024 \right) \frac{2}{2-1} \frac{1}{0.8}}{\frac{550 \cdot 0.8}{\sqrt{\frac{2}{\rho C_{L_{max,CL}}} \frac{W_0}{S_w}}}} \right)^{-1}$$

In this segment, the takeoff flaps are engaged and the landing gear is retracted. From Table 21, e is 0.8, and from Eqn 87, C_{D_o} is 0.0306. Since we have the takeoff flaps engaged, $C_{L_{max,CL}}$ is $C_{L_{max,TO}}$.

d. En-route Climb

Using Eqn 25 and factoring the climb corrections along with the values in Table 7.

$$\frac{W_0}{P_0} = \left(\frac{\left(\frac{1.25^2 C_{D_0}}{C_{L_{max,CL}}} + \frac{1}{\pi e AR_w} \frac{C_{L_{max,CL}}}{1.25^2} + 0.012 \right) \frac{2}{2-1} \frac{1}{0.8} \frac{1}{0.94}}{\frac{550 \cdot 0.8}{\sqrt{\frac{2}{\rho C_{L_{max,CL}}} \frac{W_0}{S_w}}}} \right)^{-1}$$

In this segment, the takeoff flaps retracted and landing gear are retracted. From Table 21, e is 0.85, and from Eqn 86, C_{D_o} is 0.0156. Since we have the takeoff flaps retracted, $C_{L_{max,CL}}$ is $C_{L_{max,Cr}}$.

e. Balked Landing Climb (AEO)

Using Eqn 25 and factoring the climb corrections along with the values in Table 7.

$$\frac{W_0}{P_0} = \left(\frac{\left(\frac{1.3^2 C_{D_0}}{C_{L_{\text{max,CL}}}} + \frac{1}{\pi e AR_{\text{w}}} \frac{C_{L_{\text{max,CL}}}}{1.3^2} + 0.032 \right) \frac{W_L}{W_0} \frac{1}{0.8}}{\frac{550 \cdot 0.8}{\sqrt{\frac{2}{\rho C_{L_{\text{max,CL}}}} \frac{W_0}{S_{\text{w}}}}}} \right)^{-1}$$

In this segment, the landing flaps are engaged and the landing gear is down. From Table 21, e is 0.75, and from Eqn 90, C_{D_o} is 0.1006. Since we have the landing flaps engaged, $C_{L_{\text{max,CL}}}$ is $C_{L_{\text{max,L}}}$. The landing weight ratio is the same value that is used in the landing constraint section.

   f. Balked Landing Climb (OEI)

Using Eqn 25 and factoring the climb corrections along with the values in Table 7.

$$\frac{W_0}{P_0} = \left(\frac{\left(\frac{1.5^2 C_{D_0}}{C_{L_{\text{max,CL}}}} + \frac{1}{\pi e AR_{\text{w}}} \frac{C_{L_{\text{max,CL}}}}{1.5^2} + 0.021 \right) \frac{2}{2-1} \frac{1}{0.8} \frac{W_L}{W_0}}{\frac{550 \cdot 0.8}{\sqrt{\frac{2}{\rho C_{L_{\text{max,CL}}}} \frac{W_0}{S_{\text{w}}}}}} \right)^{-1}$$

In this segment, the approach flaps are engaged and the landing gear is down. From Table 21, e is 0.75, and C_{D_o} is the average between landing and takeoff with gear down, which is 0.0756. Since we have the approach flaps engaged, $C_{L_{\text{max,CL}}}$ is $C_{L_{\text{max,L}}}$. The landing weight ratio is the same value that is used in the landing constraint.

5) Cruise

Referring to Eqn 17:

$$P_0 = TV = \frac{1}{2}\rho V^2 S_{\text{w}} C_D V_{\text{cruise}}$$

We can then incorporate a conversion from lb-ft/s to horsepower, the drag polar equation 83, and the propeller efficiency to get:

$$P_0 = \frac{qV_{\text{Cruise}}SC_D}{550\eta_{\text{p}}} = \frac{qV_{\text{Cruise}}S_{\text{w}} \left(C_{D_0} + \frac{C_L^2}{\pi e AR} \right)}{550\eta_{\text{p}}} \tag{26}$$

Incorporating the takeoff weight W of the aircraft, replacing C_L with it's constituent components, and dividing both sides by the weight leads to:

$$\frac{P_0}{W_0} = \frac{q \cdot V_{\text{Cruise}} \left(C_{D_0} + \frac{(W_0/S_{\text{w}})^2}{q^2 \pi e AR} \right)}{550\eta_{\text{p}}(W_0/S_{\text{w}})} \tag{27}$$

We can apply corrections for the takeoff power-to-weight ratio and wing loading:

$$\frac{P_0}{W_0} = \left(\frac{q \cdot V_{\text{Cruise}} \left(C_{D_0} + \frac{(W_0/S_{\text{w}})^2(W_{\text{Cruise}}/W_0)^2}{q^2 \pi e AR_{\text{w}}} \right)}{550\eta_{\text{p}}(W_0/S_{\text{w}})} \right) \left(\frac{P_{\text{TO}}}{P_{\text{Cruise}}} \right) \tag{28}$$

Finally we invert Eqn 28 to get it in terms of power loading:

$$\frac{W_0}{P_0} = \left(\left(\frac{q \cdot V_{\text{Cruise}} \left(C_{D_0} + \frac{(W_0/S_{\text{w}})^2(W_{\text{Cruise}}/W_0)^2}{q^2 \pi e AR_{\text{w}}} \right)}{550\eta_{\text{p}}(W_0/S_{\text{w}})} \right) \left(\frac{P_{\text{TO}}}{P_{\text{Cruise}}} \right) \right)^{-1} \tag{29}$$

The value for C_{D_0} can be determined using Eqn 86 and the value for e can be determined from Table 21 since the

wing is in the clean configuration during cruise. Assuming that the takeoff power is 90% of our rated power, and the cruise power is 80% of the rated power, then, $\frac{P_{\text{TO}}}{P_{\text{Cruise}}}$ is equal to 1.125. The cruise weight ratio is obtained from the calculations in the concept trade off study which is 0.932. The dynamic pressure, q, is determined from a density at FL280 and the cruise speed.

6) Ceiling

Eqn 18 represents the ceiling constraint equation:

$$\left(\frac{T_0}{W_0}\right)_{\min} = 2\sqrt{kC_{\text{D}_0}}$$

We then use Eqn 19 and rearrange it to be in terms of power-to-weight ratio:

$$\left(\frac{P_0}{W}\right)_{\min} = 2\sqrt{kC_{\text{D}_0}}\frac{V}{550\eta_{\text{p}}}$$

Here V is:

$$V = \sqrt{\frac{2}{\rho C_L}\frac{W_0}{S_{\text{w}}}} \tag{30}$$

where C_L is the coefficient of lift of the wing in the clean configuration while L/D is maxed. From Figure 20, we can see this is roughly 0.75.

Finally, we substitute k from Eqn 16, V from Eqn 30 we invert it to obtain the ceiling constraint in terms of power loading:

$$\left(\frac{W_0}{P}\right)_{\min} = \left(2\sqrt{\frac{C_{\text{D}_0}}{\pi e AR_{\text{w}}}}\frac{\sqrt{\frac{2}{\rho 0.75}\frac{W_0}{S_{\text{w}}}}}{550\eta_{\text{p}}}\right)^{-1} \tag{31}$$

For this case, the value for C_{D_0} will be for the clean configuration obtained from Eqn 86, and from Table 21 the value for e is 0.85.

D. Plot of Design Constraints

By plotting out all the constraint equations, we get the graph shown in Figure 8.
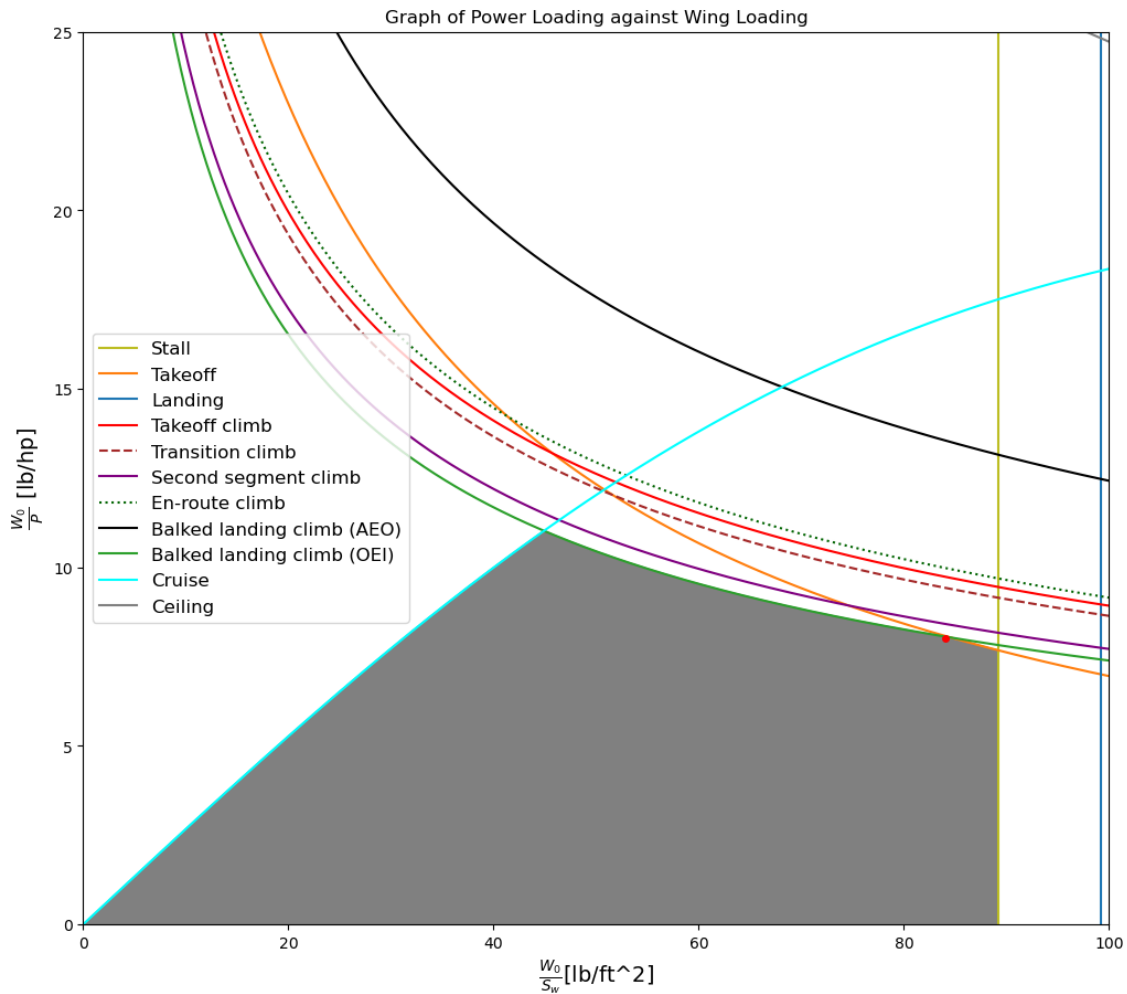
Fig. 8   Power loading against wing loading graph

The shaded area in Figure 8 represents our feasible design space. The red point is our design point and the rationale behind it will elaborated in the later subsections. We found that the active constraint for the power loading is the OEI balked landing climb condition and for the wing loading it is the stall speed. Note that the ceiling constraint is barely seen in the top right corner of Figure 8.

E. Wing Loading and Total Propulsive Power Loading

Before we can pick a suitable wing loading and power loading value we will also need to consider our powertrain architecture. We eventually decided to move forward with a parallel architecture and the reasoning for said decision will be elaborated in the Propulsion System section later. To fulfil our design constraint requirements, we also have to select a wing loading and power loading in the shaded area for each component shown in Figure 31. Based on these graphs,

we can see that the optimal value for power loading and wing loading are in different locations. Picking the higher wing loading value results in a less than optimal value for power loading and vice versa.

Ultimately, we decided on a compromise between both values. Increasing the wing loading allows for a lighter wing, however that decreases our power loading and leads to higher required takeoff power. By testing different design points, we found that a power loading value of 8 lb/hp and wing loading value of 84 lb/ft^2 were the optimal values for our design.

With the selected wing loading value, we can also determine the power loading values for each component which are shown in Table 8.

Table 8   Power loading of components for parallel architecture

Component	Fuel	Gas Turbine	Gearbox	Battery	Power Management System	Motor /Generator	Propulsion 1
Power Loading [lb/hp]	4	11	7	17	17	18	8

F. Improved Weight Estimate

Now that we have our final power loading and wing loading values, we can refine the original weight estimate to better reflect the actual weight of the final aircraft. Breaking down the takeoff weight of our aircraft, we get the equation:

$$W_0 = W_{\text{Crew}} + W_{\text{Passengers}} + W_{\text{f}} + W_{\text{bat}} + W_{\text{e}} \tag{32}$$

where the empty weight, W_{e}, for an aircraft is

$$W_{\text{e}} = W_{\text{e}'} + W_{\text{w}} + W_{\text{PT}} \tag{33}$$

Here, $W_{\text{e}'}$ represents 'everything else' weight, W_{w} is the wing weight and W_{PT} is the weight of the powertrain. We begin by finding reference $W_{\text{e}'}$ values of other conventional turboprop aircraft. This can be done by subtracting the wing weight and power plant weight from their empty weights. The power plant weight includes the engine weight and the propeller weight. Since the information on propeller weights were limited, we took the propeller weights that we were able to obtain and plotted them against engine weights. The relationship between the propeller weight and engine weight was found to be:

$$W_{\text{prop}} = -6 \cdot 10^{-5} W_{\text{eng}}^2 + 0.4061 W_{\text{eng}} + 14.959. \tag{34}$$

We then estimated the wing weight by multiplying the wing area with 10 lb/ft^2 for transport aircraft([3], Table 15.2). With the data found, we then plot $\frac{W_{\text{e}'}}{W_0}$ against W_0 and obtain an equation in the form of:

$$\frac{W_{\text{e}'}}{W_0} = A W_0^C \tag{35}$$

From our analysis as shown in Figure 9, we found the regression constants A to be 2.0834 and C to be -0.162.

To find W_{w} for our aircraft, we use the wing loading value determined in the previous section to estimate the
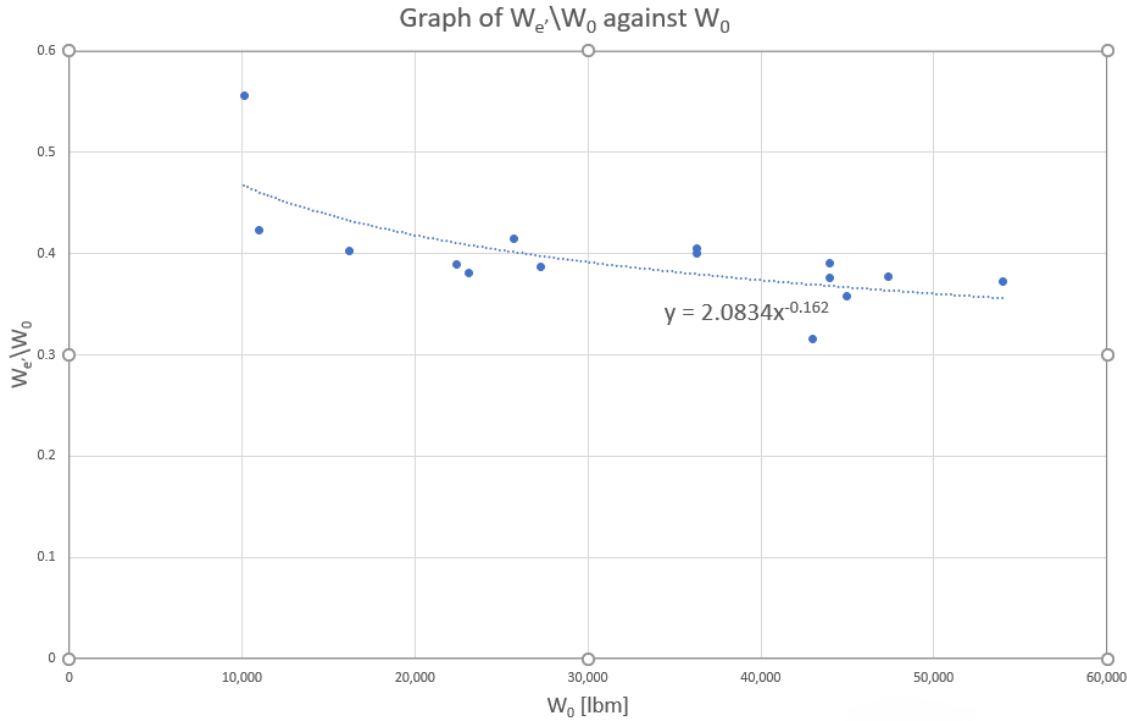
Fig. 9   'Everything else' weight estimation graph

reference area of our aircraft's wing. We then multiply that value by 10 lb/ft^2 to get the weight of the wings ([3], Table 15.2).

With the power loading values of the components, we can then find the power required for each stage of the powertrain. Taking P_{s1} as our rated takeoff shaft-horsepower, we calculate the power requirement for our aircraft, and from there, determine an engine weight, W_{eng}, that can satisfy our requirements. The weight of the propulsion group for each engine, W_{pg}, which includes the engine, propeller, and other components required for an engine installation, can then be found using the following relation([4], p. 79):

$$W_{pg} = k_{pg} \left(W_{eng} + 0.24P_0 \right) \tag{36}$$

where k_{pg} is 1.35 for a multi-engine propeller aircraft ([4], p. 80)

For the weight of the electric motor, we estimate this using an electric motor from Siemens, with a power-to-weight ratio of 5.2 kW/kg [43], which is equal to 3.16 hp/lb. Using the ideal power loading for P_{e1} from Table 8, we can estimate the power required for the electric motor. This value is then divided by 3.16 to estimate the weight of our electric motor, W_{em}.

We could not find much information regarding the weight of the power management system, W_{pms}, therefore, we used a value of 397 lb which was provided by de Vries ([44], p. 319). Finally, we add up W_{pg}, W_{pms} and W_{em} to obtain W_{PT}. We then sum up the values for $W_{e'}$, W_W and W_{PT} to get the updated W_e value for our aircraft.

Next, we use the range equation shown below [44] to estimate the battery and fuel weight:

$$R = \eta_3 \frac{e_f}{g} \left(\frac{L}{D}\right) \left(\eta_{P1} + \eta_{P2} \frac{\Phi}{1-\Phi}\right) \ln \left[\frac{W_e + W_{\text{payload}} + \frac{g}{e_{\text{bat}}} E_{0,\text{tot}} \left(\Phi + \frac{e_{\text{bat}}}{e_f}(1-\Phi)\right)}{W_e + W_{\text{payload}} + \frac{g}{e_{\text{bat}}} \Phi E_{0,\text{tot}}}\right] \tag{37}$$

where e_f is the specific energy of fuel, and e_{bat} is the specific energy of the battery in J/kg. For these values, we will be using 12,000 Wh/kg [39] and 750 Wh/kg respectively. This 750 Wh/kg value represents an average between two values we found, 1,000 Wh/kg [39] and 500 Wh/kg [44]. η_1 is η_{GT}, η_2 is η_{EM} and η_3 is η_{P} ([44], p. 295). The values for range, R and the lift-to-drag ratio, L/D will be the values we used for our concept as shown in Figure 2.

Rearranging Eqn 37, we get:

$$e^{\frac{R}{A}} \cdot (W_e + W_{\text{Payload}}) - (W_e + W_{\text{Payload}}) = \frac{g * E_{0,\text{tot}}}{e_{\text{bat}}} \cdot \left(B - \Phi e^{\frac{R}{A}}\right)$$

where

$$A = \eta_3 \frac{e_f}{g} \left(\frac{L}{D}\right) \left(\eta_{P1} + \eta_{P2} \frac{\Phi}{1-\Phi}\right)$$

$$B = \Phi + \frac{e_{\text{bat}}}{e_f}(1-\Phi)$$

Isolating $E_{0,\text{tot}}$, we then obtain:

$$E_{0,\text{tot}} = \frac{\left(e^{\frac{R}{A}} \cdot (W_e + W_{\text{Payload}}) - (W_e + W_{\text{Payload}})\right) e_{\text{bat}}}{g \left(B - \Phi e^{\frac{R}{A}}\right)} \tag{38}$$

Eqn 38 allows us to solve for the total energy needed for our aircraft. The energy supplied by the fuel, $E_{0,f}$ is then given by the equation:

$$E_{0,f} = (1 - \Phi)E_{0,\text{tot}} \tag{39}$$

and the energy supplied by our battery, $E_{0,\text{bat}}$ is given by the equation:

$$E_{0,\text{bat}} = \Phi E_{0,\text{tot}} \tag{40}$$

Finally, the weight of our fuel can be found with the equation:

$$W_f = \frac{g}{e_f} E_{0,f} \tag{41}$$

and the weight of our battery can be found with the equation:

$$W_{\text{bat}} = \frac{g}{e_{\text{bat}}} E_{0,\text{bat}} \tag{42}$$

Note that Eqn 37 was derived for metric units. Therefore, we will convert our values to metric for the battery and fuel weight calculation and the results will be converted back into imperial units.

With all the weight values found in Eqn 32, a new estimate for our takeoff weight can then be calculated. We then repeat the process from the start since the equations are affected by the takeoff weight. Eventually, the values will converge and give us our improved final estimate for the takeoff weight of our aircraft.

G. Dimensional Values of W, P, and S

From the procedures shown in the previous subsections, we found the updated takeoff weight of our aircraft to be 62,000 lb, with a takeoff power of 7,750 hp and a wing area of 730 ft^2.

H. Power vs. Area Graph

The power vs area graph shown in Figure 10 was obtained by taking our takeoff weights and dividing them with our constraint values.
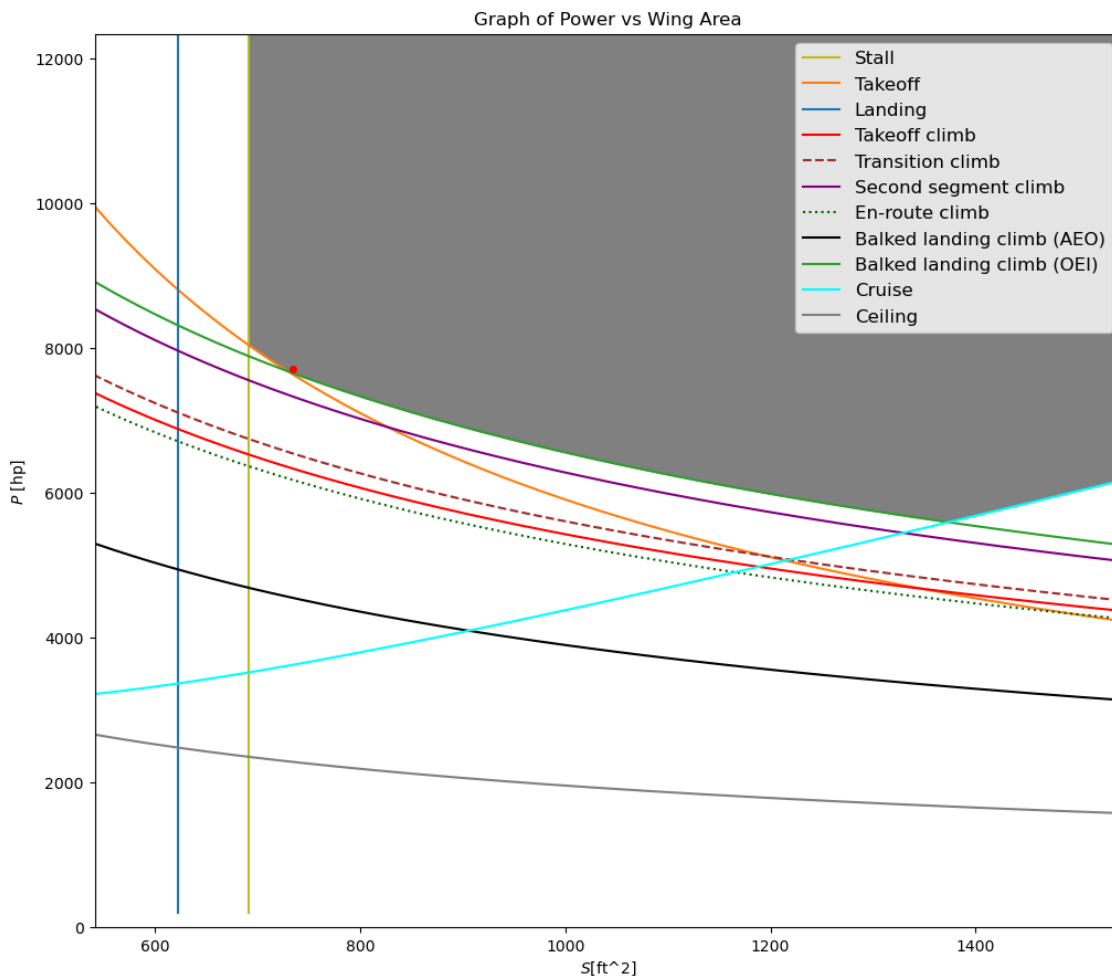
Fig. 10   Power against wing area graph

V. Interior Layout

A. Fuselage Configuration

1. Crew, Payload, and Operational Items

From the RFP in Table 3, we define requirements for crew and payload as in Table 9:

Table 9   Crew, Payload, and Operational Items

Description	Weight [lb]	*Volume [ft^3]
2 Cockpit Crew	380	-
1 Cabin Crew	190	-
50 Passengers	10,000	-
Crew Luggage	90	12
Passenger Luggage	2,000	250

We assume that the total luggage volume required to be carried is 262 ft^3, and all of it will be carried in containers aft of the cabin area, separated by a bulkhead. This is a safe, albeit unrealistic assumption, since some passengers are bound to use overhead storage instead. In order to fulfill these volume requirements, we have selected the following containers and configurations as shown in Table 10. W represents width, H represents height and D represents depth.

Table 10   Cargo Containers

Container	AS1825 Volume [ft^3]	Dimensions W x H x D [ft]
LD-3	159 [45]	79.0 x 64.0 x 60.4 [4]
LD-2	124 [45]	61.5 x 64.0 x 60.4 [4]

Using an arrangement with one of each container, we can meet a carrying volume of around 283 ft^3 of cargo capacity. Of course, this is a conservative estimate of total capacity as it does not account for overhead storage in the cabin section.

2. Size and Shape

Our fuselage cross section shape will be roughly circular in order to minimize the weight required to withstand pressurization. The bottom of the fuselage around the main landing gear is slightly larger as to accommodate the deployment equipment and tire volume. The seating we have selected to accommodate 50 passengers is four-abreast with one center aisle, which results in 13 total rows (12 full-seating rows, and one row with 2 seats). The sizing of the fuselage diameter is largely dependent on the seating width and the required inner diameter of the fuselage. The structural depth, t [inch], of the fuselage is determined using this equation ([6], p. 124):

$$t = (0.02d_f + 1) + 0.750 \tag{43}$$

Where d_f is the fuselage diameter and the additional 0.750 inches of additional thickness accounts for fuselage deflection, seat width tolerances, and seat track location tolerances ([4], p. 54)

The inner diameter d_{fi} is defined by this equation:

$$d_{fi} = d_f - 2t \tag{44}$$

Where the inner diameter needs to accommodate the total width of the row, which consists of four seat widths, six 2-inch armrests (3 for every 2 adjoined seats), and the 18-inch aisle width as per the RFP in Table 3. Solving these equations

simultaneously with a total row width in mind results in the following for fuselage diameters:

Table 11   Seating Width and Fuselage Diameters

Seat Width [in]	Structural Depth, t [in]	Fuselage Diameter, d_f [ft]
(Minimum) 17.2	3.88	8.88
17.5	3.91	8.98
(Target) 18	3.95	9.16

Considering these dimensions, we have decided to make the fuselage 9.1 ft in diameter as to accommodate the 17.5 inch seat widths. There is also some extra room to account for some changes to seat-back widths being larger than expected. We will also note that the structural depth appears rather large through Roskam's method as Raymer cites a value of around 4 inch for jumbo jets, which is not our plane class ([3], p. 267). There may be more internal diameter than estimated, or the outer diameter can be smaller. Future studies can be conducted on this parameter to see how it can be optimized.

3. Cabin and Cargo Hold Sizing

We also need to determine the length of the fuselage. There are 13 total rows of seats which have a pitch of 30 inches as stated in the RFP from Table 3. This leads to a length for the seating arrangement of 32.5 ft. Additionally, the FAR 25.807 requires at least 2 Type 1 exits per-side of the fuselage [46], with an access width 3.0 feet each [6] for a total of 6 feet in length. The front-most exit on the port-side will double as a passenger ingress point for the aircraft.

There needs to be space for the depth of the two storage containers, which adds an additional 10.1 ft. The thickness of any interior bulkheads will be defined by the materials used and pressurization, so for now we assume they are around 0.5-1 inch thick [47] adding an additional 0.1667 ft for 2 bulkheads dividing the cockpit, cabin, and cargo areas.

Taking an average of the dimensions of these compartments from other regional turboprops ([6], Table 3.6), we can estimate our galleys to have an area of 35 x 24 inch^2 and lavatories to have an area of 50 x 36 inch^2. Raymer cites lavatory sizes of 40 x 40 inch^2 ([3] , p. 267), so we will take a value of 45 x 38 inch^2 or 3.75 x 3.17 ft^2 for the lavatory.

Table 12   Fuselage-wise Length of Segments Aft of Cockpit

Item	Length [ft]
13 Seat Rows	32.5
1 Lavatory	3.75
1 Galley	2.92
LD-2 and LD-3 Cargo Containers	10.1
2 Bulkheads	0.167
2 FAR 25 Type 1 Exits on Each Side	6.0

4. Cockpit Sizing

To complete the sizing for the fuselage, we now need the general dimensions of the cockpit. Referencing diagrams given for the cockpits of the Sud Caravelle ([6], Figure 2.22), Fokker F-28, and Boeing 707 ([6], Figure 2.24), the cockpit lengths from the tip of the nose cone to the beginning of the cabin range from around 3.5-4.5 meters. Martins cites a cockpit length of 110-150 inch ([4], p. 57) depending on the size of the aircraft. Finally, Raymer cites a cockpit length of 100 inches for a two-crew-member cockpit ([3], p. 265). These result in a cockpit length range of around 8.33-14.76 ft.

For the pilot, Raymer diagrams a distance of around 50 inches ([3], p. 264) from seat-base to foot rest for a 95th percentile male pilot while Roskam diagrams around 36 inches ([6], p. 8). We will assume 50 inches. We also are recommended by Roskam to scale cockpit dimensions by 0.85 ([6], p. 4) to account for female stature, which results in a pilot length of about 3.54 ft. The cockpit space behind the pilot is taken up by radio rack space, other electronics, and potentially a third navigator crew person, filling up around 2.62 ft ([6], Figure 2.22, Figure 2.24). We do not have a third cockpit crew member, so we will assume this is a safe estimate. The length of the nose cone and any cockpit instruments forward of the pilot is estimated to be around 1.65 meters, or 5.41 ft ([6], Figure 2.22, Figure 2.24). Adding these cockpit dimensions results in a cockpit length of 11.57 ft, which is within the range predicted earlier.

The volume of the space forward of the pilot is determined from the dimensions of any cockpit instruments and nose cone components. Table 13 has the dimensions and quantity of some cockpit instruments. Note that these values found do seem to be a bit large and further research will be needed to validate these dimensions.

Table 13   Cockpit Instrument Dimensions [5]

Instrument	Dimensions L x W x H [in]	Quantity	Weight [lb]
Airspeed Indicator	18 x 12 x 12	1	8
Altimeter	15 x 10 x 10	1	5
Magnetic Direction Indicator	18 x 12 x 12	1	10
Tachometer	15 x 10 x 10	2	4
Oil Pressure Indicator	15 x 10 x 10	2	3
Temperature Indicator	15 x 10 x 10	2	3
Engine Oil Temperature Indicator	15 x 10 x 10	2	3
Fuel Flow Rate Indicator	15 x 10 x 10	2	5
Fuel Gage Indicator	15 x 10 x 10	2	5

From this we can estimate the instrument panel to be about 18 inches or 1.5 ft in length, leaving 3.91 ft remaining for the nose cone instruments.

Aside from general sizing of the cockpit, we want to establish visibility parameters for the pilot. Approximate FAR 25 certified visibility angles for the cockpit are referenced from diagrams in Roskam, with 15 degrees downwards and 20 degrees of upwards visibility over the nose ([6], Figure 2.16). Additionally, for 2 pilots, the port-side pilot should

have 135 degrees of port-side visibility and 30 degrees of starboard visibility ([6], Figure 2.16). Diagrams for other aircraft generally have the pilots around 1 meter apart ([6], Figure 2.22, Figure 2.24), so we will also space our pilots at 3 ft in distance from each other.

5. Floor Height

To determine the cabin floor height, we will consider the standing height and the sitting head-room for the passengers as the RFP asks for these to be similar to competitive aircraft. The relevant values for an economy sized passenger compartment are tabulated below:

Table 14   Economy Passenger Compartment ([6], p. 267)

Description	Height
Headroom [ft]	5.42
Aisle Height [ft]	6.33

If we use this value for aisle height, it will be similar to the cabin height of the Dash 8 Q400 at 6.39 ft [25]. Thus we size the floor by placing it at 6.33 ft from the ceiling of the interior diameter. We can place the bottom of the overhead bins 5.42 ft away from the floor.

We also determine the height of the seats. From Roskam, the average values for economy class seating gets us the values in Table 15 if the cabin floor is used as the reference height:

Table 15   Seat Heights ([6], Table 3.1, Figure 3.28)

Description of Dimension	Value [in]
Top of Seat-back	39
Bottom of Seat Frame	8.5
Top of Seat Cushion	17.75

6. Summary of Fuselage Sizing

Finally, we can summarize the fuselage dimensions as shown in Table 16.

Table 16   Fuselage Dimensions

Description	Value
Fuselage Diameter, d_f [ft]	9.10
Fuselage Length l_f [ft]	83.00
Cockpit Length l_c [ft]	11.57
Structural Depth [in]	3.90
Fuselage Inner Diameter d_{fi} [ft]	8.44
Fuselage Cone Length l_{fc} [ft]	28.33
Fuselage Cone Angle θ_{fc} [deg]	17.81
l_f/d_f	9.12
l_{fc}/d_f	3.11

B. Fuselage Layout

Cross-sections and layouts of the cabin, cargo, and cockpit are in Figures 11, 12, 13, 14 and 15.
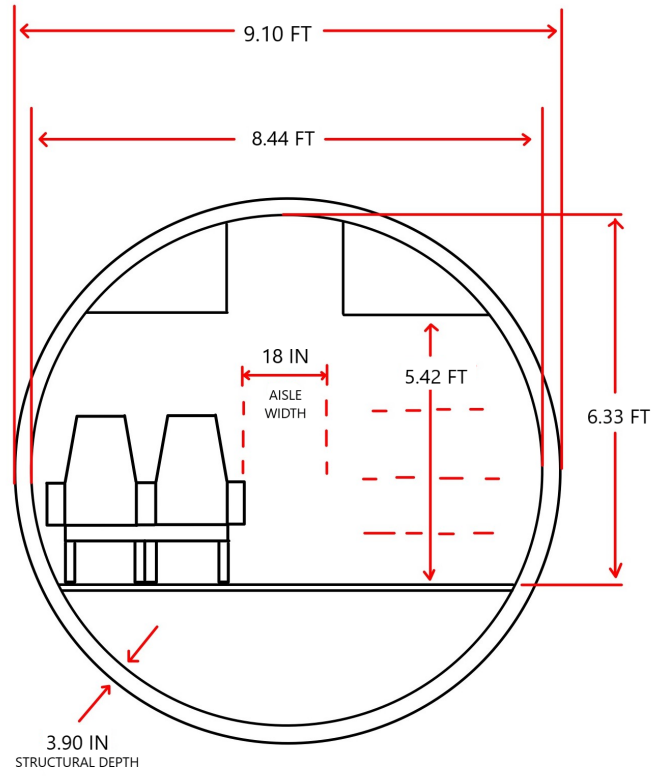
DIMENSIONS IN INCHES UNLESS STATED OTHERWISE
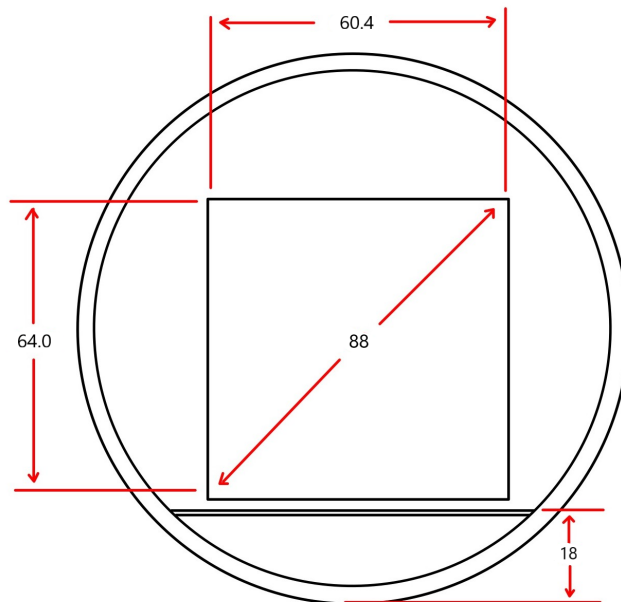
Fig. 11   Cabin and cargo cross-sections

DIMENSIONS IN FEET UNLESS STATED OTHERWISE
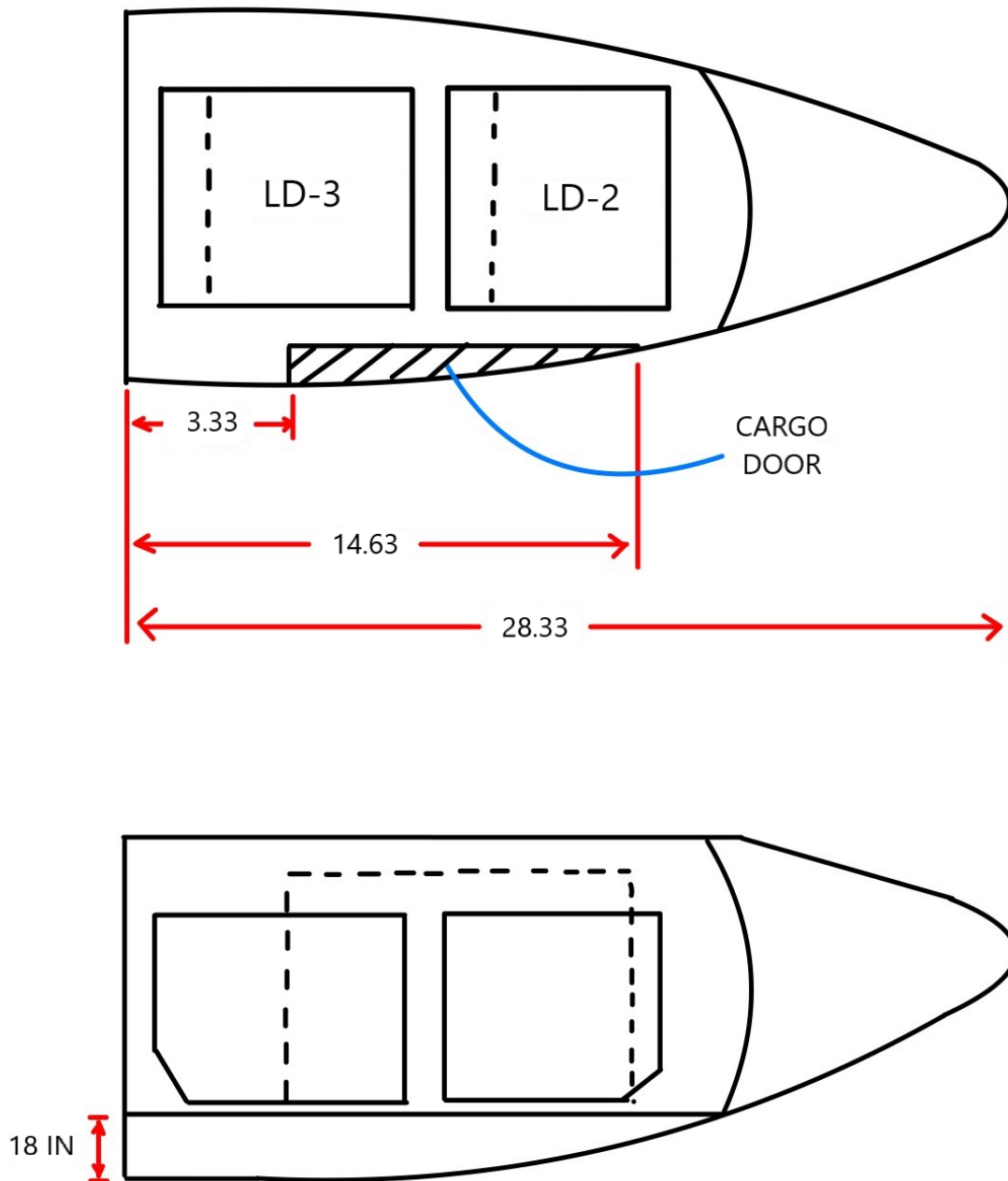
Fig. 12   Cargo layout
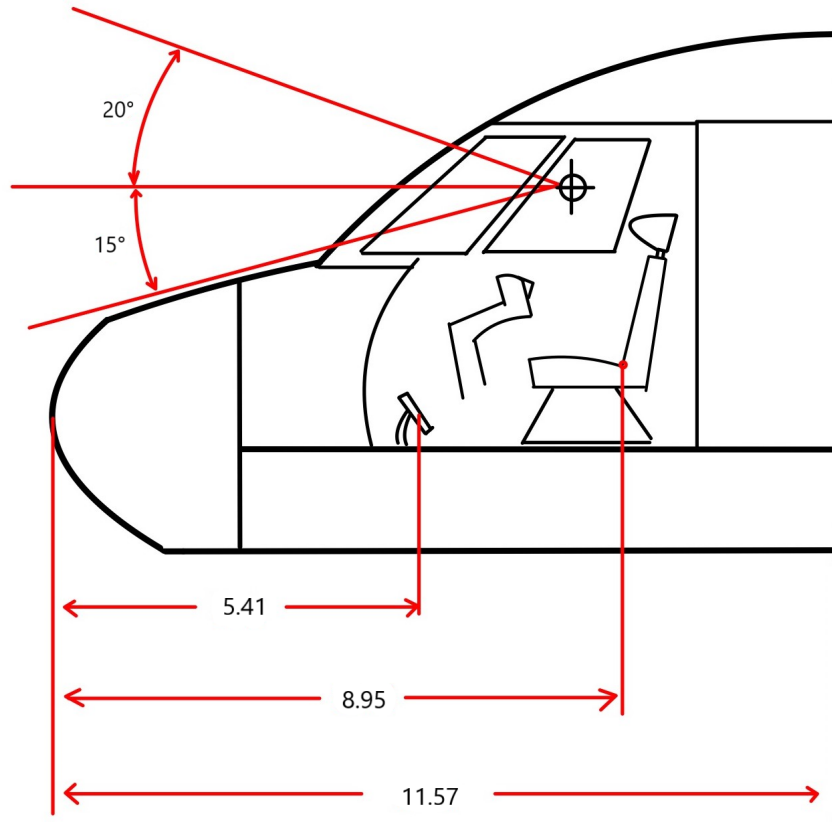
DIMENSIONS IN FEET UNLESS STATED OTHERWISE

Fig. 13   Cockpit layout

TYPE 1 EXITS

2.92   4.00   30 IN SEAT-PITCH   3.00

GALLEY

2

FOLDING
CREW-SEAT

LAVATORY

3.17

₵

3.75

2.00

42.42

TYPE 1 EXITS

DIMENSIONS IN FEET UNLESS STATED OTHERWISE
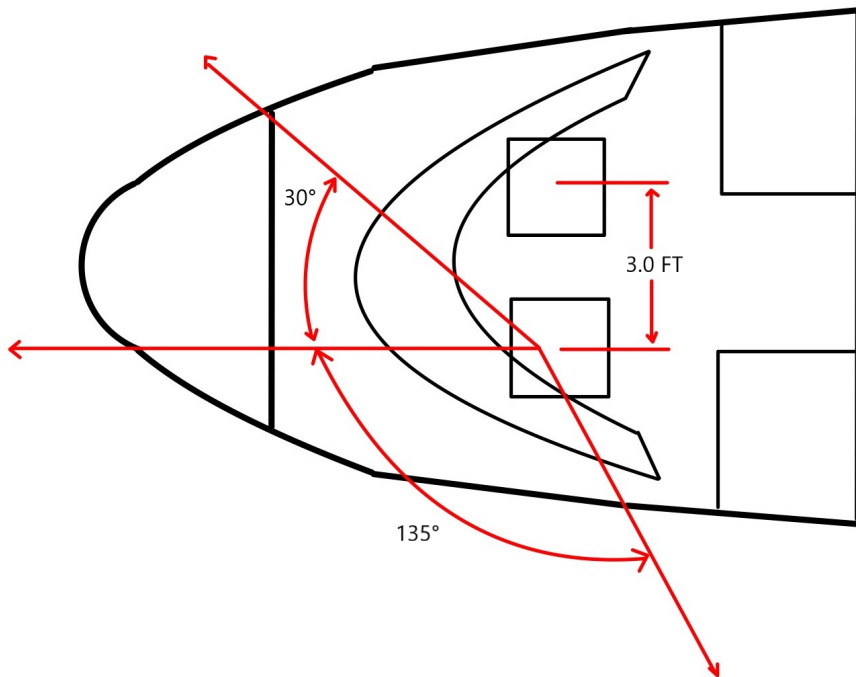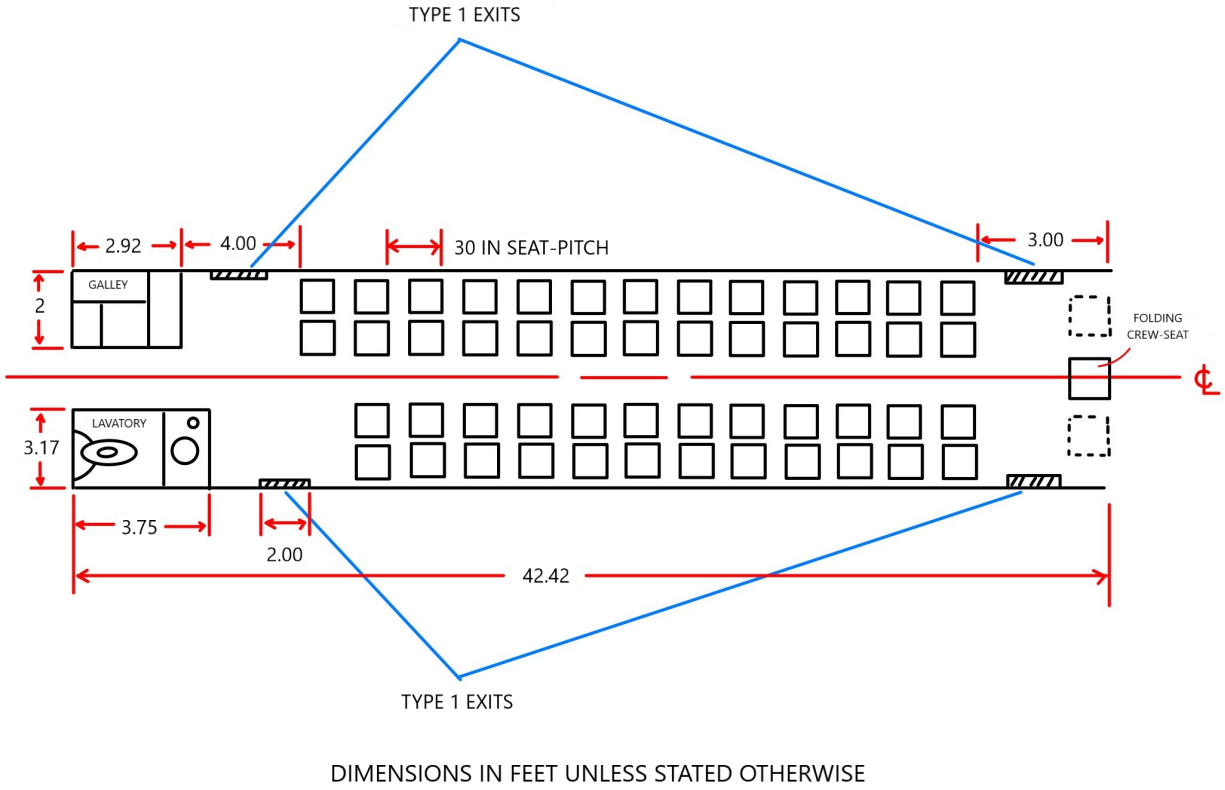
Fig. 14   Passenger cabin layout and door locations

$l_{fc} = 28.33$

$d_f = 9.10$

d_f

$\theta_{fc} = 17.81°$

$l_c = 11.57$

54.67

$l_f = 83.0$

DIMENSIONS IN FEET UNLESS STATED OTHERWISE
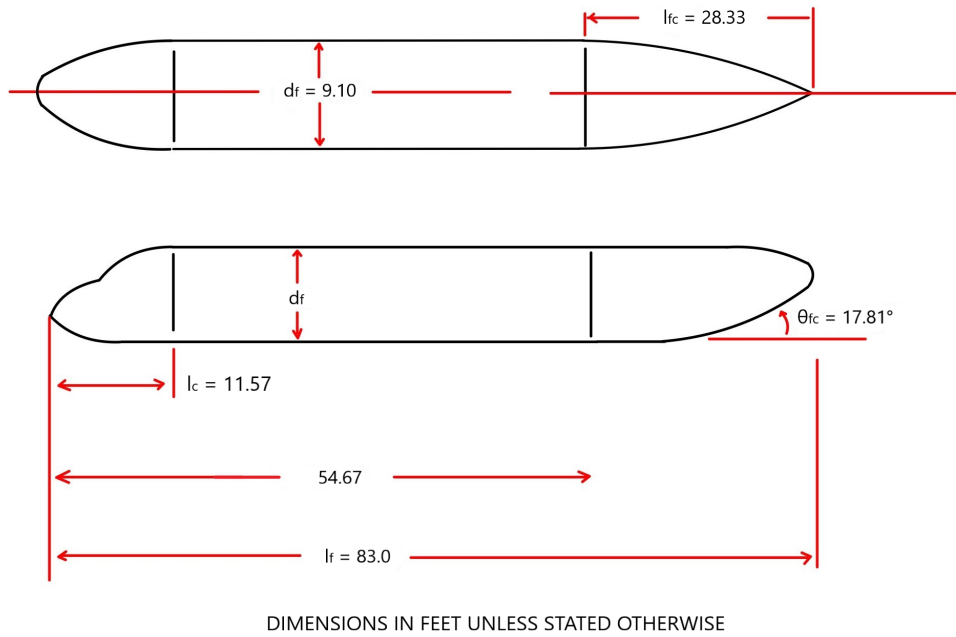
Fig. 15   Fuselage center-line diagram

C. Battery System

Batteries have three main designs: pouch cell, cylindrical cell and prismatic cell. The pouch and prismatic cell designs are similar in cell size and shape representing a thin box. The cylindrical cells have a larger cell specific energy than the pouch and prismatic cells; however, the trend in advancing technology shows that the prismatic and pouch cells are predicted to become more energy dense than cylindrical cells. System level specific energy has similar characteristics where cylindrical systems are more energy dense than prismatic or pouch systems; however, the cylindrical system are predicted to become more energy dense than prismatic or pouch systems [48]. Therefore, cylindrical cells will be used in EcoProp. These cylindrical cells will be packed based on the honeycomb design in Figure 16 because battery density is maximized [2].
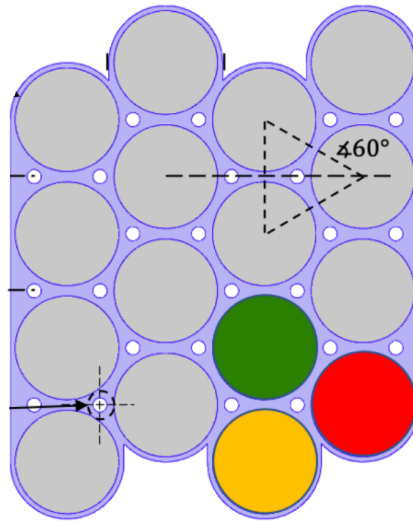
Fig. 16   Honeycomb Battery Pack [2]

VI. Weights and Center of Gravity

A. Weight Groups

A combination of equations from Roskam and Raymer were employed to estimate our component weights as shown below.

1) Wing weight equation ([3], Eqn 15.25)

$$W_{\mathrm{w}} = 0.0051 \left(W_{\mathrm{dg}} N_{\mathrm{z}}\right)^{0.557} S_{\mathrm{w}}^{0.649} AR^{0.5} \left(t/c\right)_{\mathrm{root}}^{-0.4} (1+\lambda)^{0.1} (\cos \Lambda)^{-1.0} S_{\mathrm{csw}}^{0.1} \qquad (45)$$

where W_{dg} is the gross design weight, N_{z} is the ultimate load factor, $(t/c)_{\mathrm{root}}$ is the nondimensional wing thickness at the root, λ is the wing taper ratio, Λ is the wing sweep and S_{csw} is the wing control surface area.

2) Horizontal tail weight equation ([3], Eqn 15.26)

$$W_{\mathrm{ht}} = 0.0379 K_{\mathrm{uht}}(1 + F_{\mathrm{w}}/B_{\mathrm{h}})^{-0.25} W_{\mathrm{dg}}^{0.639} N_{\mathrm{z}}^{0.10} S_{\mathrm{ht}}^{0.75} L_{\mathrm{vt}}^{-1.0} K_{\mathrm{y}}^{0.704} (\cos \Lambda_{\mathrm{ht}})^{-1.0} AR_{\mathrm{h}}^{0.166}(1 + S_{\mathrm{e}}/S_{\mathrm{ht}})^{0.1} \qquad (46)$$

where K_{uht} is 1 for a non all-moving horizontal tail ([3], p. 577), F_w is the fuselage width at horizontal tail intersection, B_h is the horizontal tail span, S_{ht} is the horizontal tail area, L_{vt} wing quarter MAC to tail quarter MAC, K_y is the aircraft pitching radius of gyration which can be approximated as $0.3L_{vt}$ ([3], p. 577), Λ_{ht} is the horizontal tail sweep angle, AR_h is the horizontal tail aspect ratio and S_e is the elevator area.

3) Vertical tail weight equation ([3], Eqn 15.27)

$$W_{vt} = 0.0026(1 + H_t/H_v)^{0.225} W_{dg}^{0.556} N_z^{0.536} L_{vt}^{-0.5} S_{vt}^{0.5} K_z^{0.875} (\cos \Lambda_{vt})^{-1} A_v^{0.35} (t/c)_{root}^{-0.5} \tag{47}$$

where H_t/H_v is 1 for a T-tail ([3], p. 577), S_{vt} is the vertical tail area, K_z is the aircraft yawing radius of gyration which can be approximated by L_{vt} ([3], p. 577), Λ_{vt} is the vertical tail sweep angle, AR_v is the vertical tail aspect ratio.

4) Fuselage weight equation ([3], Eqn 15.28)

$$W_{fus} = 0.3280 K_{door} K_{Lg} (W_{dg} N_z)^{0.5} L^{0.25} S_f^{0.302} (1 + K_{ws})^{0.04} (L/t)^{0.10} \tag{48}$$

where K_{door} is 1.06 for one side cargo door ([3], p. 577), K_{Lg} is 1.12 for fuselage mounted landing gear ([3], p. 577), l_f is the fuselage length, S_f is the fuselage wetted area, L is the fuselage structural length. K_{ws} is given by the equation ([3], p. 577):

$$K_{ws} = 0.75[(1 + 2\lambda)/(1 + \lambda)](B_w/L) \tan \Lambda \tag{49}$$

where B_w is the wing span.

5) Main landing gear weight equation ([3], Eqn 15.29)

$$W_{mlg} = 0.0106 K_{mp} W_L^{0.888} N_l^{0.25} l_m^{0.4} N_{mw}^{0.321} N_{mss}^{-0.5} V_{Stall}^{0.1} \tag{50}$$

where K_{mp} is 1 for non kneeling gear ([3], p. 577), N_l is the ultimate landing load factor, l_m is the length of the extended main landing gear in inches, N_{mw} is the number of main wheels and N_{mss} is the number of main gear shock struts.

6) Nose landing gear weight equation ([3], Eqn 15.30)

$$W_{nlg} = 0.032 K_{np} W_L^{0.646} N_l^{0.2} l_n^{0.5} N_{nw}^{0.45} \tag{51}$$

where K_{np} is 1 for non kneeling gear ([3], p. 577), where l_n is the length of the extended nose gear length in inches and N_{nw} is the number of nose wheels.

7) Nacelle group weight equation ([3], Eqn 15.31)

This weight includes air induction and pylon

$$W_{ng} = 0.6724 K_{ng} N_{Lt}^{0.10} N_w^{0.294} N_z^{0.119} W_{ec}^{0.611} N^{0.984} S_n^{0.224} \tag{52}$$

where K_{ng} is 1 ([3], p. 577) for a non pylon mounted engine, N_{Lt} is the nacelle length, N_w is the nacelle width,

S_n is the nacelle wetted area.

$$W_{ec} = 2.331 W_{en}^{0.901} K_p K_{tr} \tag{53}$$

where W_{en} is the engine weight, K_p is 1.4 for an engine with a propeller ([3], p. 577) and K_{tr} is 1 for a non jet with thrust reverser ([3], p. 577)

8) Engine controls weight equation ([3], Eqn 15.32)

$$W_{eCon} = 5.0N + 0.80 L_{ec} \tag{54}$$

where L_{ec} is the routing distance from engine front to cockpit.

9) Starter weight equation ([3], Eqn 15.33)

$$W_{start} = 49.19 \left(\frac{N \cdot W_{en}}{1000} \right)^{0.541} \tag{55}$$

10) Fuel system weight equation ([3], Eqn 15.34)

$$W_{fs} = 2.405 V_t^{0.606} \left(1 + V_i/V_t \right)^{-1.0} \left(1 + V_p/V_t \right) N_t^{0.5} \tag{56}$$

where V_t is the total volume of fuel in gal, V_i is the integral tanks volume in gal, V_p is self sealing tanks volume in gal, and N_t is the number of fuel tanks.

11) Flight controls weight equation ([49], Eqn 7.7)

$$W_{fc} = K_{fc} W_0^{\frac{2}{3}} \cdot 1.2 \tag{57}$$

where K_{fc} is 0.64 for airplanes with powered flight controls ([49], p. 99) and the factor of 1.2 is to account for leading edge devices ([49], p. 99).

12) Installed APU weight equation ([3], Eqn 15.36)

$$W_{APUin} = 2.2 W_{APU} \tag{58}$$

where W_{APU} is uninstalled APU weight.

13) Instruments weight equation ([3], Eqn 15.37)

$$W_{inst} = 4.509 K_p K_{tp} N_c^{0.541} N \left(l_f + B_w \right)^{0.5} \tag{59}$$

where K_p is 1.4 for an engine with a propeller ([3], p. 577), K_{tp} is 0.793 for a turboprop ([3], p. 577), N_c is the number of crew.

14) Hydraulics weight equation ([3], Eqn 15.38)

$$W_{hyd} = 0.2673 N_f \left(l_f + B_w \right)^{0.937} \tag{60}$$

15) Electrical weight equation ([3], Eqn 15.39)

$$W_{Ele} = 7.291 R_{kva}^{0.782} L_a^{0.346} N_{gen}^{0.10} \tag{61}$$

where R_{kva} is the system electrical rating in kVA, L_a is the electrical routing distance from generators to avionics to cockpit and N_{gen} is the number of generators.

16) Avionics weight equation ([3], Eqn 15.40)

$$W_{\text{avio}} = 1.73 W_{\text{uav}}^{0.983} \tag{62}$$

where W_{uav} is the unistalled avionics weight.

17) Furnishings weight equation ([49], Eqn 7.45)

$$W_{\text{fur}} = 0.211 (W_0 - W_{\text{f}})^{0.91} \tag{63}$$

18) Air conditioning weight equation ([3], Eqn 15.42)

$$W_{\text{ac}} = 62.36 N_{\text{pers}}^{0.25} \left(V_{\text{pr}}/1000 \right)^{0.604} W_{\text{uav}}^{0.10} \tag{64}$$

where N_{pers} is the number of crew and passengers, V_{pr} is the volume of the pressurized section in ft^3.

19) Anti-ice weight equation ([3], Eqn 15.25)

$$W_{\text{dIce}} = 0.002 W_{\text{dg}} \tag{65}$$

20) Propeller weight equation ([49], Eqn 6.14)

$$W_{\text{prop}} = K_{\text{prop2}} (D_{\text{p}}, P_{0,\text{Prop}} (N_{\text{bl}}^{0.5}))^{0.782} \tag{66}$$

where K_{prop2} is 0.108 for turboprops ([49] p. 90), $P_{0,\text{Prop}}$ is the required takeoff power per propeller in hp and N_{bl} is the number of propeller blades.

21) Payload weight, Cockpit crew weight

The initial payload weight was obtained from Table 2. We decided to separate the cockpit crew weight from the payload weight because the cockpit crew is located much further forward than the majority of the payload, which can have significant impact on the CG. The cockpit crew weight is the weight of the two pilots and their luggage.

22) Battery, Powertrain, Fuel weight

These weights were obtained from the improved weight estimate procedure in the Preliminary Sizing section.

A summary of these results are shown in Table 17.

B. Center of Gravity Estimations

The CG for each of the components were estimated using Raymer and the OpenVSP model. The location of the wing, horizontal tail, and veritcal tail CG were estimated to be at 40% of their respective mean aerodynamic chords ([3], Table 15.2). Therefore, the CG location for the wing, horizontal tail, and vertical tail can be found using the equation ([4], Eqn 7.4):

$$x = x_{\text{RLE}} + \bar{Y} \tan (\Lambda) + 0.4 \bar{c} \tag{67}$$

where x_{RLE} is the distance of the root chord leading edge from the nose, $\bar{Y}$ is the spanwise location of the mean aerodynamic chord from the centerline found in Eqn 70, and Λ is the sweep angle.

The estimated location of the CG for the fuselage is 40-50% of the fuselage length ([3], Table 15.2). We chose the

average value of 45%. The estimated CG location of the main landing gear, nose landing gear, powertrain, propeller, payload, cockpit crew, battery, and fuel were evaluated at each of their respective centroids ([3], Table 15.2), obtained from the OpenVSP model. For the nacelle, the CG is located at 40% of their nacelle's total length ([49], p. 114). For the remainder of the components, we based the estimated CG location on "All-else empty," which is 40-45% of the fuselage length ([3], Table 15.2). A summary of the CG for each weight component can be found in Table 17.

Table 17   Component Weights (Aircraft Nose Reference Point)

Component	Weight [lb]	Estimated CG [ft]
Wing	7,000	36.58
Horizontal Tail	470	79
Vertical Tail	550	69
Fuselage	11,000	37.35
Main Landing Gear	2,200	45
Nose Landing Gear	360	5.54
Nacelle	1,200	33.9
Engine Controls	42	37.35
Starter	92	37.35
Fuel System	160	37.35
Flight Control	1,200	36.58
Installed APU	660	80
Instruments	240	37.35
Hydraulics	100	37.35
Electrical	3,100	37.35
Avionics	1,500	4
Furnishings	4,600	37.35
Air conditioning	570	37.35
Anti-ice	120	37.35
Propeller	2,500	27.99
Payload	12,220	37.4
Cockpit Crew	440	8
Battery	6,700	38.25
Powertrain	4,100	30.57
Fuel	3,700	36.58
Total Weight	64,824	36.43

The CG for our aircraft is subject to change depending on the weight scenario. The "fully loaded" weight scenario has the all the cargo placed in the passenger area. The "fully loaded 2" weight scenario has half of the cargo in the passenger area and the other half in the cargo compartment. The "fully loaded 3" scenario has all the cargo in the cargo compartment. The "out of fuel" weight scenario is for the fully loaded case without the weight of the fuel. The "no payload" scenario is the fully loaded case without the weight of the payload. The "crew only" scenario is the full loaded case without the payload, and the fuel. The "empty" scenario is the weight of the aircraft without the payload, the

fuel, or the cockpit crew. The weight scenarios and their new CG locations can be found in Table 18. Figure 17 is a visualization of how the CG shifts for different scenarios.

Table 18   Center of Gravity Envelope

Weight Scenario	Gross Weight [lb]	Estimated CG [ft]	SM [%]
Empty	48,155	36.59	11.57
Crew Only	48,625	36.31	15.11
No payload	52,262	36.34	14.66
Out of fuel	60,815	36.54	12.3
Fully loaded	64,482	35.32	12.1
Fully loaded 2	64,482	36.92	7.25
Fully loaded 3	64,482	37.53	2.39
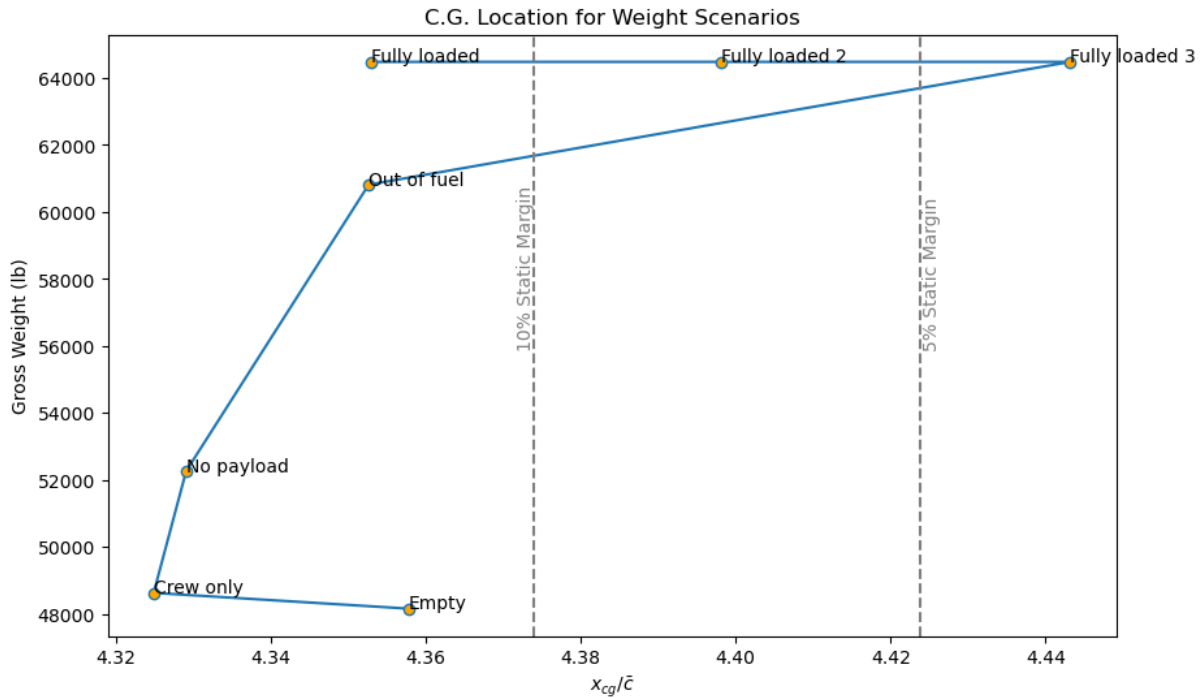
Fig. 17   CG excursion plot

The location of the CG was consistently in front of our landing gear, so our aircraft should not tip over.

VII. Stability and Control

A. Mean Aerodynamic Chord

The following formula was used to determine the mean aerodynamic chord, $\bar{c}$ ([4], Eqn 8.6):

$$\bar{c} = \frac{2}{3} c_{\text{root}} \frac{1 + \lambda + \lambda^2}{1 + \lambda} \tag{68}$$

where c_{root} is the root chord of the wing and the taper ratio, λ, is obtained by Eqn 69.

$$\lambda = \frac{c_{tip}}{c_{root}} \qquad (69)$$

where c_{tip} is the tip chord of the wing.

The spanwise location of the mean aerodynamic chord is ([4], Eqn 8.7):

$$\bar{Y} = \frac{b}{6}\left(\frac{1+2\lambda}{1+\lambda}\right) \qquad (70)$$

where b is the span.

B. Empennage Sizing

The horizontal tail was sized based on the formula ([4], Eqn 8.2):

$$c_{HT} = \frac{L_{HT}S_{HT}}{\bar{c}_W S_W} \qquad (71)$$

where $\bar{c}_W$ is the mean aerodynamic chord of the wing, L_{HT} is the horizontal tail moment arm and c_{HT} is a constant of 0.9 ([3], Table 6.4). The vertical tail was sized based on the formula ([4], Eqn 8.1):

$$c_{VT} = \frac{L_{VT}S_{VT}}{b_W S_W} \qquad (72)$$

where L_{VT} is the vertical tail moment arm, b_W is the span of the wing and c_{VT} is a constant of 0.08 ([3], Table 6.4). Each of the tail volume coefficients (c_{HT} and c_{VT}) were multiplied by a factor of 0.95 to account for the end-plate effect on the vertical tail and the clean-air effect on the horizontal tail for a T-tail design [3]. Figure 18 shows the vertical and horizontal tail of our aircraft.

The vertical and horizontal tail parameters such as their dihedral angle, angle of incidence, sweep angle, aspect ratio and taper ratio are sized based on historical data of Regional Turboprops put together by Roskam([50], Table 8.13,Table 8.14).

The elevator and rudder are sized based on Raymer's non-dimensional estimates of 0.25 and 0.32 to their respective chord lengths ([3], Table 6.5).

C. OEI Rudder Sizing

To size the rudder for the OEI condition, we determined the critical engine-out yawing moment, N_{crit} using the equation:

$$N_{t_{crit}} = T_{TO_e} y_t \qquad (73)$$

where y_t is distance of the engine from the CG's longitudinal axis and T_{TO} is the engine thrust for one engine at takeoff. The drag-induced yawing moment for a variable-pitch propeller is:

$$N_D = 0.10 N_{t_{crit}} \qquad (74)$$

The minimum control speed, V_{mc} is 1.2 times the stall speed, which is equal to 218 ft/s. The side force generated by a rudder deflection of 25 degrees is calculated by using AVL to model the vertical tail as a half-wing. The lift force calculated from AVL is the side force which will be used to calculate the vertical tail yawing moment. This vertical tail yawing moment can be calculated by multiplying the side force by the distance of the vertical tail AC from the CG. To fulfill the OEI condition for the rudder sizing, the yawing moment from the vertical tail must be greater than sum of N_{crit} and N_D. We determined that the vertical tail moment is greater than the moment of the critical engine-out yawing moment plus the drag-induced yawing moment. Therefore, the sizing of the rudder is appropriate to maintain control at the OEI condition.

D. Empennage Layout

The final design of the empennage is shown in Figure 18 while the specifications for the horizontal and vertical tail are shown in Table 19 and 20. The highlighted portions of the empennage are the control surfaces. The vertical tail uses the NACA 0009 airfoil and the horizontal tail uses the NACA 0012 airfoil.
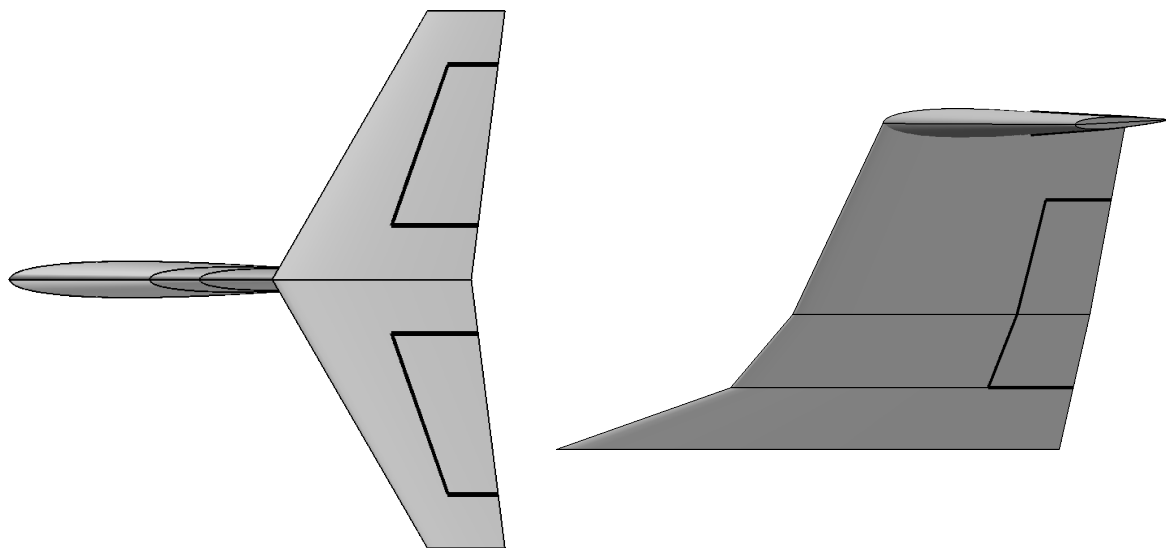
Fig. 18   Empennage diagram

Table 19   Horizontal Tail Specifications

Horizontal Tail Specifications	Parameter
Area [ft^2]	170
Span [ft]	25.7
Taper Ratio	0.39
Sweep Angle [degrees]	30.0
Dihedral Angle [degrees]	0
Elevator Area (Approx.)[ft^2]	28.4

Table 20   Vertical Tail Specifications

Vertical Tail Specifications	Parameter
Area [ft^2]	150
Span [ft]	12.5
Taper Ratio	0.59
Sweep Angle [degrees]	25.3
Rudder Area (Approx.)[ft^2]	25.0

E. Wing Control Surfaces

The control surfaces on the wing are highlighted in black on Figure 19. The control surfaces were sized according to historical data of jet transport aircraft by Raymer, which is 35% of the wing's chord([3], Figure 6.3).
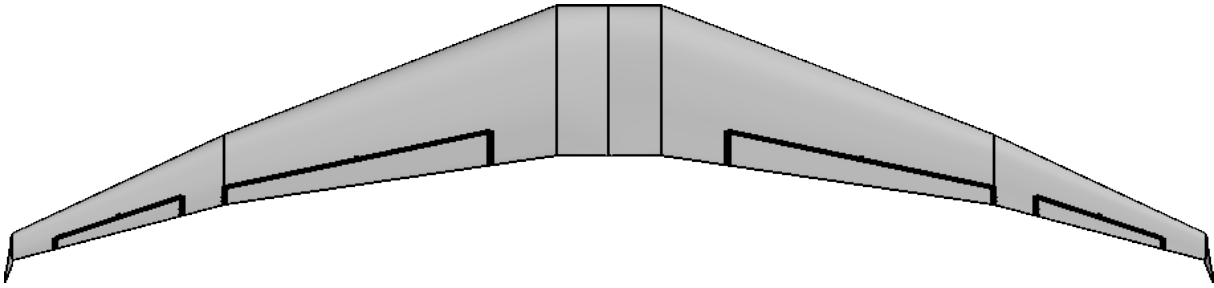
Fig. 19   Lifting surfaces and control surfaces

F. Neutral Point Calculations

To calculate the neutral point, we start with the pitch stability derivative using the equation ([4], Eqn 8.10):

$$\frac{\partial C_{m_{cg}}}{\partial \alpha} = \frac{x_{cg}}{\bar{c}_w}\frac{\partial C_{L_w}}{\partial \alpha} + \frac{\partial C_{m_{w,ac}}}{\partial \alpha} - \frac{l_h S_{HT}}{\bar{c}S_w}\frac{\partial C_{L_h}}{\partial \alpha} + \frac{\partial C_{m_{fus}}}{\partial \alpha} \tag{75}$$

where l_h is the distance of the aerodynamic center of the horizontal tail to the CG of the aircraft. We also know that the pitching moments are constant about the aerodynamic center, therefore $\frac{\partial C_{m_{w,ac}}}{\partial \alpha} = 0$. Furthermore, by definition, the neutral point is the location where the CG is placed that would achieve neutral stability, which means that $\frac{\partial C_{m_{cg}}}{\partial \alpha} = 0$. Then, replacing x_{cg} with the neutral point, x_{np}, Eqn 75 becomes:

$$\frac{\partial C_{m_{cg}}}{\partial \alpha} = \frac{x_{np}}{\bar{c}}\frac{\partial C_{L_w}}{\partial \alpha} - \frac{l_h S_h}{\bar{c}S_w}\frac{\partial C_{L_h}}{\partial \alpha} + \frac{\partial C_{m_{fus}}}{\partial \alpha} = 0$$

Next, we rearrange the equation and solve for x_{np}([4], Eqn 8.11):

$$\frac{x_{np}}{\bar{c}} = \frac{l_h S_h}{\bar{c}S_w}\frac{\partial C_{L_h}}{\partial \alpha}\left(\frac{\partial C_{L_w}}{\partial \alpha}\right)^{-1} - \frac{\partial C_{m_{fus}}}{\partial C_{L_w}} \tag{76}$$

The wing lift derivative can be estimated as ([4], Eqn 8.15):

$$\frac{\partial C_{L_w}}{\partial \alpha} \approx \frac{2\pi AR}{2 + \sqrt{(AR/\eta)^2\left(1 + \tan^2\Lambda - M^2\right) + 4}} \tag{77}$$

where η is typically 0.97 ([4], p. 88). Here, Λ is the wing sweep angle and M is the cruise mach number.

The horizontal tail experiences down-wash, therefore, its lift derivative is ([4], Eqn 8.14):

$$\frac{\partial C_{L_h}}{\partial \alpha} = \frac{\partial C_{L_{h,clean}}}{\partial \alpha} \left(1 - \frac{\partial \varepsilon}{\partial \alpha}\right) \tag{78}$$

where the clean horizontal tail lift derivative is ([4], Eqn 8.19):

$$\frac{\partial C_{L_{h,clean}}}{\partial \alpha} \approx \frac{2\pi AR_h}{2 + \sqrt{(AR_h/\eta)^2 \left(1 + \tan^2 \Lambda_h - M^2\right) + 4}} \tag{79}$$

AR_h refers to the horizontal tail aspect ratio, and the down-wash is ([4], Eqn 8.16):

$$\frac{\partial \varepsilon}{\partial \alpha} \approx \frac{2}{\pi AR} \frac{\partial C_{L_w}}{\partial \alpha} \tag{80}$$

Lastly, the fuselage pitching moment is given by ([4], Eqn 8.17):

$$\frac{\partial C_{m_{fus}}}{\partial C_L} = \frac{K_f d_f^2 l_f}{S_w \bar{c}} \left(\frac{\partial C_{L_w}}{\partial \alpha}\right)^{-1} \tag{81}$$

where d_f is the width of the fuselage, l_f is the length of the fuselage, and K_f is an empirical factor which varies with the wing quarter chord position on the fuselage ([4], p. 89). For our calculations, the value for K_f used is 0.487 ([4], p. 89).

Based on the calculations above, we found that the neutral point, x_{np} is estimated to be 3.9 ft aft of the wing aerodynamic center (37.56 ft aft of the nose).

G. Static Margin

The static margin can be calculated with using the equation ([3], Eqn 16.11):

$$SM = \frac{x_{np} - x_{cg}}{\bar{c}} \tag{82}$$

where x_{np} is the location of the neutral point and x_{cg} is the location of the CG.

A positive static margin indicates that the aircraft has static longitudinal stability. Our target static margin is between 5-10% to have longitudinal stability while still maintaining some maneuverability. We determined that the static margin for our aircraft is 9.1% when the aircraft weight is fully loaded. The static margin for the different weight scenarios can be found in Table 18. Note that we can shift the other flight conditions to havea static margin betwen 5% and 10% by simply moving the batteries.

VIII. Aerodynamics

A. Preliminary Drag Polar

In order to create the power loading against wing loading graph we will need values for the zero drag lift coefficients. In this section we will detail the steps taken to create the preliminary drag polar graph for our concept aircraft. We begin with the drag polar equation which is given as:

$$C_D = C_{D_o} + \frac{C_L^2}{\pi e AR_w} \tag{83}$$

where C_{D_o} is the zero-lift drag coefficient, e is the spanwise efficiency factor, and AR_w is from Table 2.

We will need to plot out Eqn 83 to get our preliminary drag polar graph. Before we can do that, an estimate for the parasite drag coefficient will have to be obtained. This can be done with the following equation:

$$C_{D_o} = C_f \frac{S_{\text{wet}}}{S_w} \tag{84}$$

where, C_{f_c} is the skin friction coefficient, S_{wet} is the wetted area in ft^2 and S_{ref} is the wing reference area ft^2 of our design concept.

The value we use for the skin friction coefficient is 0.0026 ([3], Table 12.3). We will also need to estimate the wetted area which can be found using the equation ([7], Eqn 3.22):

$$S_{\text{Wet}} = 10^c W_0^d \tag{85}$$

where c and d are regression constants. For our case, c is -0.0866 and d is 0.8099 ([7], Table 3.5)

As for the reference area, we rely on historical trends to obtain a wing loading value based on our takeoff weight ([51], Figure 7.4). We can then divide our takeoff weight with the wing loading value to obtain an estimated reference area.

Since e will be different and C_{D_o} will increase by ΔC_{D_o}, the drag polar graph will change depending on the configuration of the aircraft. We will have 5 different configurations and the values used to calculate them are shown in Table 21. The equation for each configuration is:

1) Clean

$$C_D = 0.0156 + 0.0288 C_L^2 \tag{86}$$

2) Takeoff flaps, gear up

$$C_D = 0.0306 + 0.0306 C_L^2 \tag{87}$$

3) Takeoff flaps, gear down

$$C_D = 0.0506 + 0.0306 C_L^2 \tag{88}$$

4) Landing flaps, gear up

$$C_D = 0.0806 + 0.0326 C_L^2 \tag{89}$$

5) Landing flaps, gear down

$$C_D = 0.1006 + 0.0326 C_L^2 \tag{90}$$

The drag polar for the different configurations are plotted and shown below in Figure 20. The range of C_D values were based on the cruise, landing and takeoff C_L values for our aircraft.

Table 21   Values used for Drag Polar Estimation ([7], Table 3.6)

Configuration	e	ΔC_{D_o}
Clean	0.85	0
Takeoff flaps, gear up	0.8	0.015
Takeoff flaps, gear down	0.8	0.015+0.020
Landing flaps, gear up	0.75	0.065
Landing flaps, gear down	0.75	0.065+0.020
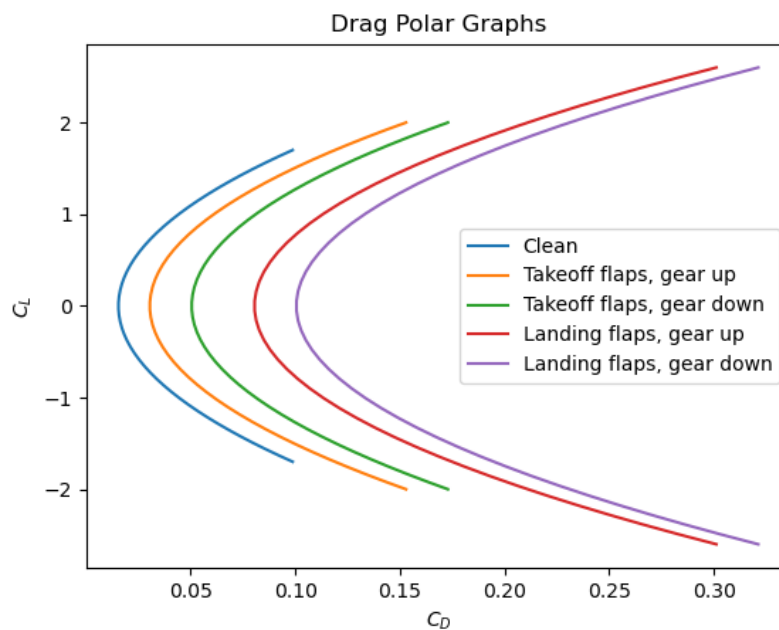
Fig. 20   Preliminary drag polar graphs

B. Wing Specifications

The wing specifications shown in Table 22 are for the wing shown in Figure 19

Table 22   Wing Specifications

Wing Specifications	Parameter
Area [ft^2]	730
Span [ft]	97
Taper Ratio	0.17
Sweep Angle [degrees]	19
Dihedral Angle [degrees]	2
MAC [ft]	10

C. Airfoil Selection

The airfoil we used for our design was based off the airfoil of the ATR-72. All configurations use a gaped airfoil design to achieve larger $C_{l_{max}}$. The ATR-72 airfoil was modified with a custom flap design.

1) Cruise Configuration

Figure 21 shows the cruise airfoil configuration.
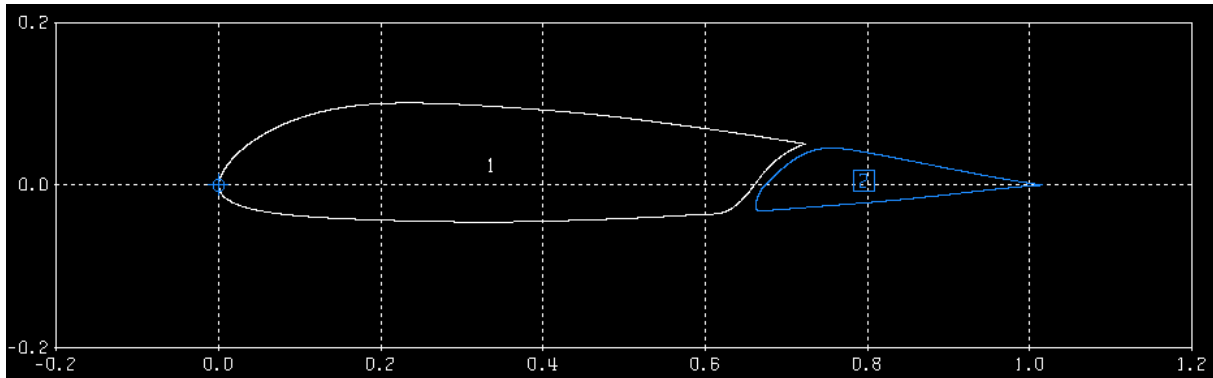
Fig. 21   Airfoil configuration during cruise (0° deflection)

2) Takeoff Configuration

Figure 22 shows the takeoff airfoil configuration.
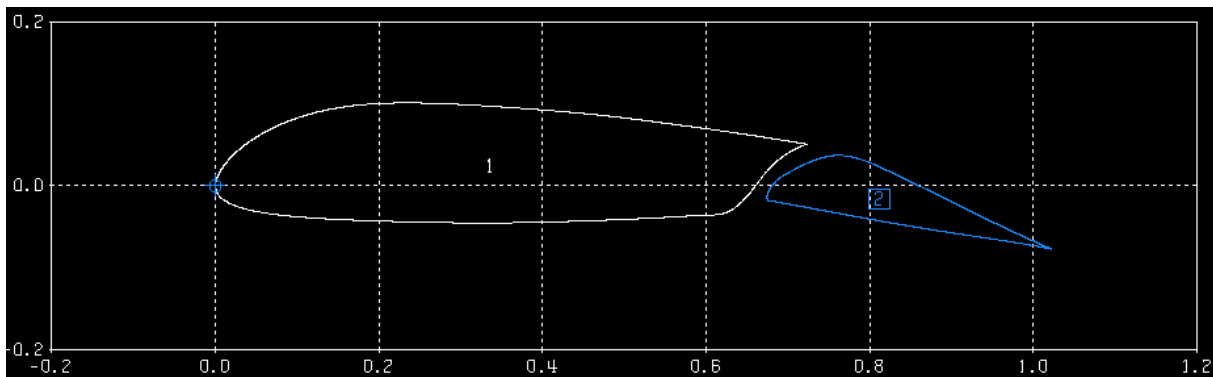
Fig. 22   Airfoil configuration during takeoff (15° deflection)

3) Landing Configuration

Figure 23 shows the landing airfoil configuration.
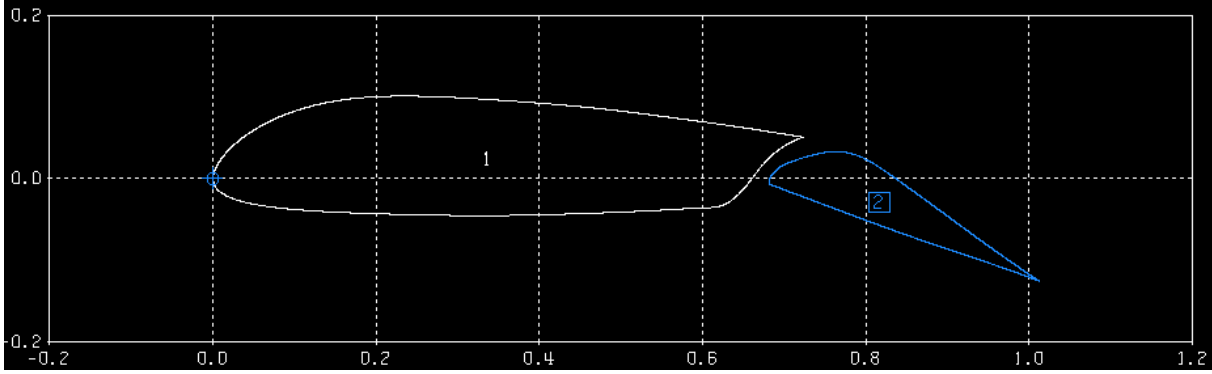
Fig. 23   Airfoil configuration during landing (25° deflection)

D. Refined Zero-Lift Drag Values

To refine the zero-lift drag value C_{D_0} we use the component build-up method described in Eqn 91. This estimates the subsonic parasite drag of each aircraft component accounting for each skin-friction drag coefficient C_{fc}, form-factor induced pressure drag FF_c, interference effects Q_c. We also account for miscellaneous drags $C_{D_{misc}}$ and leakages and protuberances $C_{D_{L\&P}}$ across the entire aircraft [3]. $S_{wet,c}$ and S_{ref} refer to the wetted area of each component and the wing reference area, respectively. For our calculations, we consider the five configurations previously used for drag polar estimation: clean, takeoff flaps with landing gear up then landing gear down, and landing flaps with landing gear up then landing gear down.

$$\left(C_{D_0}\right)_{subsonic} = \frac{\sum \left(C_{f_c} FF_c Q_c S_{wet\,c}\right)}{S_{ref}} + C_{D_{misc}} + C_{D_{L\&P}} \tag{91}$$

1) Skin-Friction C_{f_c} Values

To determine the value of C_{f_c} for each component, we first calculate the Reynolds number 92 of each component at the flight conditions using their characteristic lengths. Then, we determine a value of C_{f_c} using Eqns 94 for turbulent and 93 for laminar flow. Lastly, we take a weighted average of these two values depending on how much laminar flow we expect to attain which is based of Table 23.

$$R = \frac{\rho V \ell}{\mu} \tag{92}$$

$$C_{f_{c,lam}} = \frac{1.328}{\sqrt{R}} \tag{93}$$

$$C_{f_{c,turb}} = \frac{0.455}{(\log_{10} R_{cutoff})^{2.58}(1 + 0.144 M^2)^{0.65}} \tag{94}$$

$$38.21\left(\frac{l}{k}\right)^{1.053} \tag{95}$$

We assumed a 'smooth paint' surface roughness to determine the value of $k = 2.08E - 05$ [3]

Table 23   Predicted Attainable Laminar Flow [3]

Design	Fuselage %	Wing and Tails %
General Aviation - Smooth Metal (No Rivets or Cracks	10	35
General Aviation - Smooth Molded Composites	25	50

2) Form-Factor FF_c Values

To determine the form-factor contributions to the parasite drag, we use the following equations estimating the value of FF_c for different profiles.

Wings, tails, struts, and pylons [3] where t refers to the maximum thickness, $(x/c)_m$ refer to the chord wise location of the maximum thickness, M refers to the mach number, and Λ_m refers to the sweep angle of the maximum thickness line:

$$FF = \left[1 + \frac{0.6}{(x/c)_m}\left(\frac{t}{c}\right) + 100\left(\frac{t}{c}\right)^4\right]\left[1.34M^{0.18}\left(\cos\Lambda_m\right)^{0.28}\right] \tag{96}$$

Fuselages and smooth canopies[3] where f refers to the fineness ratio, calculated using l the length of the body, and d the diameter of the body or A_{max} the maximal cross-sectional area of the body.

$$f = \frac{\ell}{d} = \frac{\ell}{\sqrt{(4/\pi)A_{max}}} \tag{97}$$

$$f < 6, \quad FF_c = \left(0.9 + \frac{5}{f^{1.5}} + \frac{f}{400}\right) \tag{98}$$

$$f > 6, \quad FF_c = \left(1 + \frac{60}{f^3} + \frac{f}{400}\right) \tag{99}$$

Nacelles and Smooth External Stores[3]:

$$FF_c = \left(1 + \frac{0.35}{f}\right) \tag{100}$$

3) Interference Q_c Values

For the interference drag contribution, we consider the following values for Q_c. Here d refers to the diameter of the nacelle.

Table 24   Interference Drag Values [3]

Component	Q_c
Nacelle mounted on wing	1.5
Nacelle mounted less than $\frac{d}{4}$ from wing	1.3
Nacelle mounted more than d from wing	1.0
High wing wing, mid wing, or well-filleted low wing	1.0
Unfilleted low wing	1.1-1.4
Fuselage	1.0
V-tail	1.03
H-Tail	1.08
Conventional Tail	1.05

4) Miscellaneous Drags

We can calculate drag caused by fuselage up-sweep using Eqn 101, where u is the up-sweep angle of the fuselage center-line in radians and A_{max} is the maximum cross-sectional area of the fuselage [3].

$$\frac{D}{q} = 3.83u^{2.5}A_{\text{max}} \tag{101}$$

The 'base drag' caused by rearward-facing flat surfaces is calculated with Eqn 102, where A_{base} is the area of the flat-surface or the projected area of any place where the aft angle to the free stream exceeds 20 degrees [3].

$$\frac{D}{q} = \left[0.139 + 0.419\left(M - 0.161\right)^2\right] A_{\text{base}} \tag{102}$$

We consider the drag from propellers in the case where one engine becomes inoperative with the following conditions with Eqn 103 [3].

$$\frac{D}{q} = \begin{cases} 0.1\,\sigma A_{\text{disk}} & \text{feathered prop} \\[2mm] 0.8\,\sigma A_{\text{disk}} & \text{stopped prop} \\[2mm] 0.3\,A_{\text{inlet}} & \text{windmilling jet} \end{cases} \tag{103}$$

$$\sigma = \frac{A_{\text{blade}}}{A_{\text{disk}}} \tag{104}$$

We divide these $\frac{D}{q}$ 'drag areas' by the wing reference area to obtain values for the drag coefficients.

We include the drag from other miscellaneous components on the aircraft. The most relevant features to our design are tabulated below as a truncated version of the table provided by Raymer [3].

Table 25   Interference Drag Coefficients [3]

Feature	Values
Flat Plate Perpendicular to Flow	1.28
Bullet Shape Blunt Back	0.30
Air Scoops	1.2-2.0
Control Horn	0.3-0.8
Speed Brake (Wing Mounted)	1.60
Windshield (Smoothly Faired)	0.07
Windshield (Sharp Edged)	0.15
Regular Wheel and Tire	0.25
Second Wheel and Tire in Tandem	0.15
Streamlined Wheel and Tire	0.18
Streamlined Strut	0.05
Round Strut or Wire	0.30-1.17

5) Leakage and Protuberance Drags

Lastly, we can take an additional 5% of the total parasite drag to account for holes, gaps, and small protruding features [3]. We do not account for tran-sonic or supersonic parasite drags because our aircraft does not fly in those regimes.

From this process, we determine the new zero-lift drag coefficients for our 5 configurations as shown in Table 26.

Table 26   Zero-Lift Drag Coefficients

Configuration	C_{D_0}
Clean	0.0203
Takeoff Flaps, Gear Up	0.0727
Takeoff Flaps, Gear Down	0.0793
Landing Flaps, Gear Up	0.1070
Landing Flaps, Gear Down	0.1135

E. Induced Drag Refinement and New Drag Polars

AVL was used to obtain the induced drag for each configuration. The drag polars were then obtained by adding the zero-lift drag values in Table 26 with the induced drag values obtained from AVL. Figure 24 shows the graph of the drag polars for different configurations.
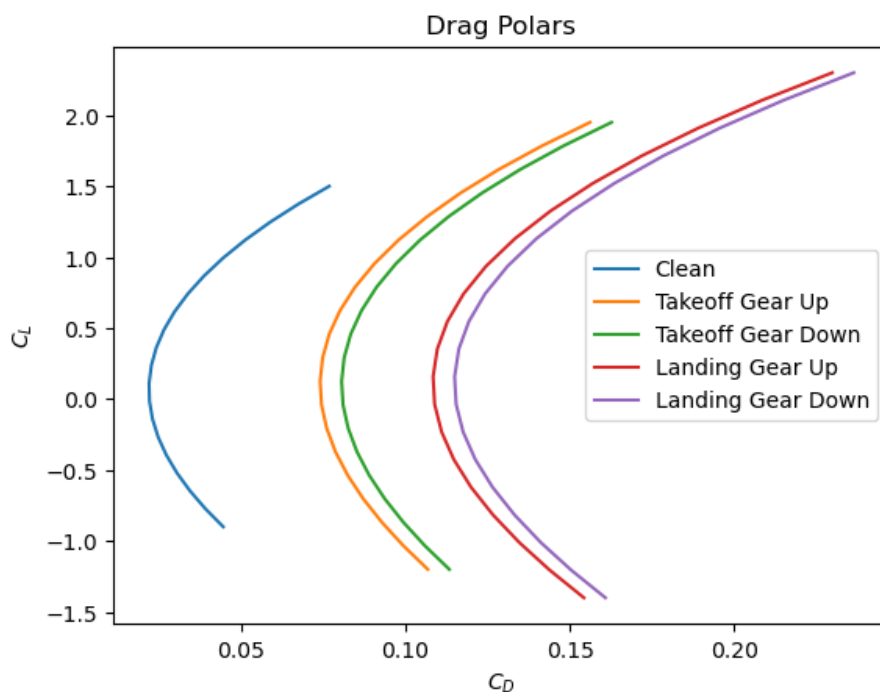
Fig. 24   Refined Drag Polars

F. Maximum Lift Coefficients of Flapped Wing Sections

All configurations and fight conditions were analysed with Multielement Airfoil Design/Analysis System (MSES). MSES was used to calculate the C_l curves to determine the maximum and minimum C_l. The flap was rotated around x/c = 0.725 and y/c = 0.01 in the undeployed configuration. This rotation point was chosen because the flap rotated nicely around it; however, the flap was sometimes translated to avoid intersecting with the main airfoil or to achieve convergence with MSES. Table 27 has the $C_{l_{max}}$ and $C_{l_{min}}$ found from MSES.

1) Cruise Configuration

The C_l curves of different deflector angles are shown in Figure 25.
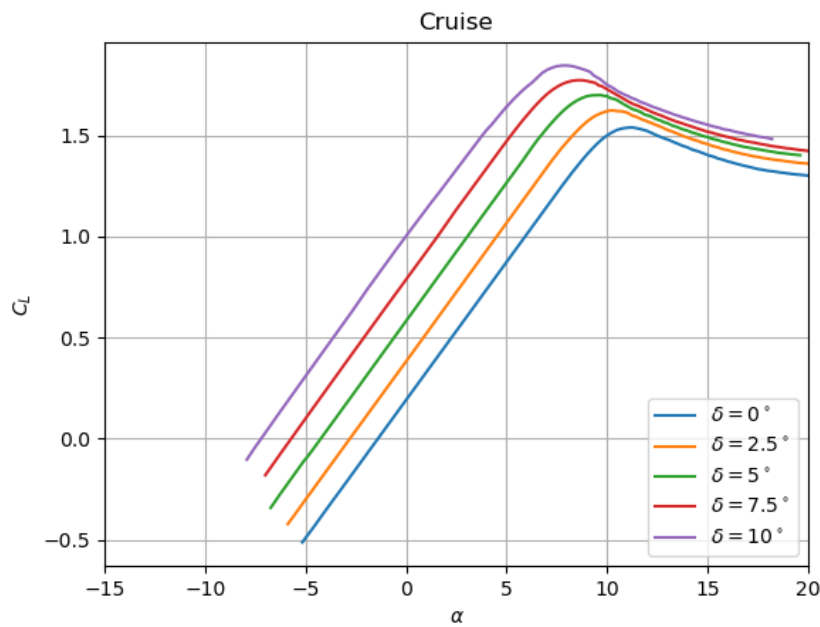
Fig. 25   Cruise C_l curves

2) Takeoff Configuration

The C_l curves of different deflector angles are shown in Figure 26.
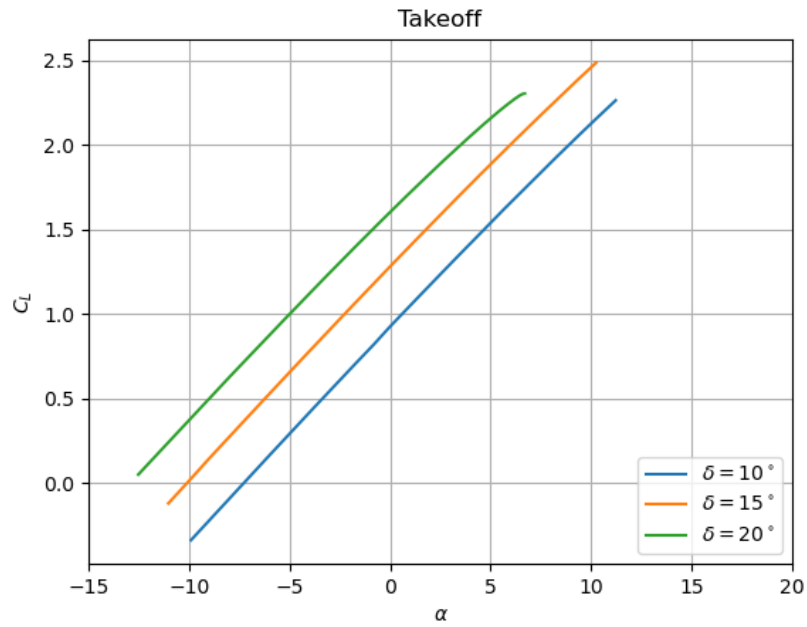
Fig. 26   Takeoff C_l curves

3) Landing Configuration

The C_l curves of different deflector angles are shown in Figure 27.
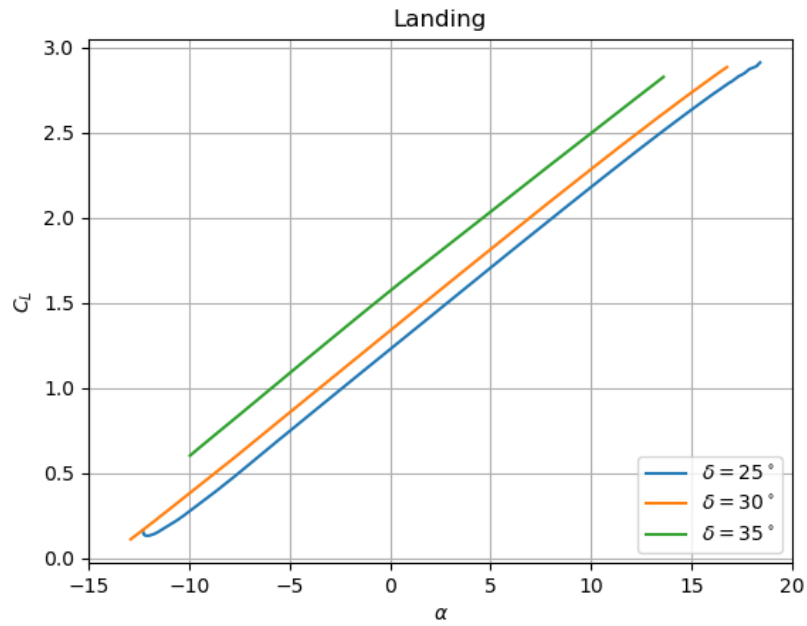
Fig. 27   Landing C_l curves

Table 27 $C_{l_{\max}}$ **and** $C_{l_{\min}}$ **for each flight condition**

Flight Condition	$C_{l_{\max}}$	$C_{l_{\min}}$
Cruise	1.55	-0.51
Takeoff	2.49	-0.12
Landing	2.89	0.11

G. Maximum Lift Coefficient of Aircraft

The $C_{L_{\max}}$ of the aircraft was found by using a combination of Athena Vortex Lattice (AVL) and MSES. We compared the C_l values obtained from AVL with those obtained from MSES and the $C_{L_{\max}}$ was obtained when the $C_{l_{\max}}$ value from AVL reached the $C_{l_{\max}}$ value obtained from MSES. The $C_{L_{\max}}$ for cruise, takeoff and landing conditions were found to be 1.55, 2.0, and 2.6 respectively.

H. Required Elevator Deflections

From the results obtained in AVL, the elevator deflection required to trim for cruise is -2.834°, for takeoff it is -18.1°and for landing it is -17.8°.

I. Static Stability Derivatives

The static stability derivatives for our aircraft were obtained through the use of AVL.

Trimmed Cruise

$$\frac{\partial C_M}{\partial \alpha} = -3.762$$

$$\frac{\partial C_N}{\partial \beta} = 0.183$$

$$\frac{\partial C_l}{\partial \beta} = -0.192$$

Trimmed Takeoff

$$\frac{\partial C_M}{\partial \alpha} = -5.275$$

$$\frac{\partial C_N}{\partial \beta} = 0.197$$

$$\frac{\partial C_l}{\partial \beta} = -0.253$$

Trimmed Landing

$$\frac{\partial C_M}{\partial \alpha} = -5.247$$

$$\frac{\partial C_N}{\partial \beta} = 0.197$$

$$\frac{\partial C_l}{\partial \beta} = -0.267$$

For longitudinal stability $\frac{\partial C_M}{\partial \alpha}$ has to be negative, and for lateral stability $\frac{\partial C_l}{\partial \beta}$ has to be negative. Lastly, for directional stability $\frac{\partial C_N}{\partial \beta}$ has to be positive. Based on the values above we can see that our aircraft satisfies all three criteria for cruise, takeoff and landing.

IX. Propulsion System

A. Sketches of Candidate Powertrain Architectures

Figure 28 shows the block diagrams for a serial powertrain architecture and Figure 29 shows a parallel powertrain architecture.
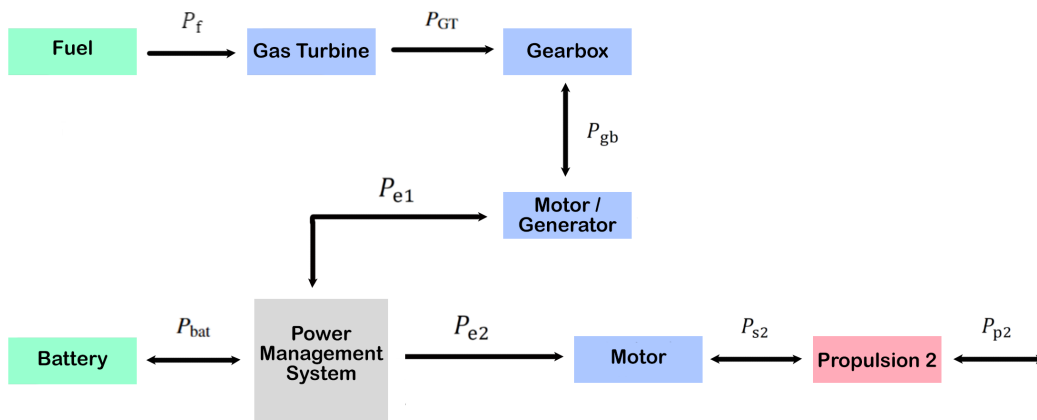
Fig. 28   Serial powertrain architecture
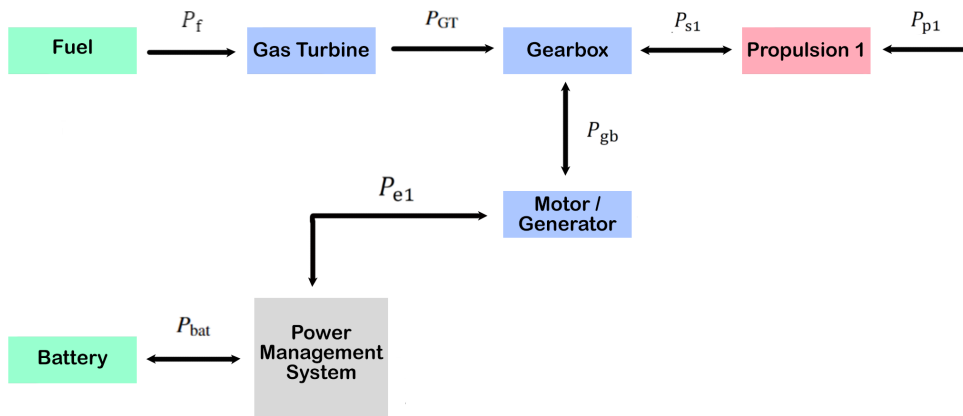
Fig. 29   Parallel powertrain architecture

B. Efficiency of Each Powertrain Component

The values for the efficiency of each powertrain component is shown in Table 28.

Table 28   Powertrain Component Efficiencies (2035 Timeframe Assumed)

Component	Efficiency
Gas Turbine Engine, η_{GT}	0.40[52]
Gearbox, η_{GB}	0.96 [53]
Electric Generator / Motor, η_{EM}	0.96 [53]
Controller / Converter, η_{CTL}	0.99[52]
Power Management and Distribution, η_{PM}	0.99 [53]
Propulsor Motor, η_{Pr}	0.96 [53]
Propeller Efficiency, η_{P}	0.8 ([3], p. 36)

C. Linear Power Balance Equations and Closing Equations

In this section, we will derive a matrix for each powertrain architecture in order to solve for the power loading conditions of each component. To find the power loading of each component, we make use of a general power balance equation which includes the efficiency of the component we are analyzing ([53], p. 12):

$$\sum P_{\text{out}} = \eta_{\text{i}} \sum P_{\text{in}} \tag{105}$$

where P_{out} is the power coming out of the component and P_{in} is the power going into the component. In order to fully solve the matrix, we also have 3 closing equations as shown below ([53], p. 11).

1) Shaft Power Ratio

This value represents the electrical shaft power in reference to the total shaft power being produced.

$$\varphi = \frac{P_{\text{elec}}}{P_{\text{elec}} + P_{\text{other}}} \tag{106}$$

2) Supplied Power Ratio

This value compares the power supplied by the batteries to the total power supplied by both the battery, P_{bat} and fuel, P_{f}.

$$\Phi = \frac{P_{\text{bat}}}{P_{\text{bat}} + P_{\text{f}}} \tag{107}$$

3) Total Propulsive Power

The total propulsive power for each architecture is equal to the sum of all the power produced by each propulsive means.

$$P_{\text{p2}} + P_{\text{p1}} = P_{\text{p}} \tag{108}$$

The supplied power ratio is based on our hybridization ratio, which can vary between 0 for a conventional gas turbine design, and 1 for a fully electric design. For our calculations, we have used our previous estimate of 20%. The efficiencies of each component and any mission segment specific parameters can be found above in Table 28. Solving for each component's power with Eqn 105 along with Eqns 107 and 108, we can divide each component power by W_0 to derive the matrices for each of the powertrain architectures which are shown in Eqns 109 and 110. Eqn 106 is not used

since both our systems only have one type of shaft power being produced.

Serial Architecture (Figure 28)

$$
\begin{bmatrix}
-\eta_{\text{GT}} & 1 & 0 & 0 & 0 & 0 & 0 & 0 \\
0 & -\eta_{\text{GB}} & 1 & 0 & 0 & 0 & 0 & 0 \\
0 & 0 & -\eta_{\text{EM1}} & 1 & 0 & 0 & 0 & 0 \\
0 & 0 & 0 & -\eta_{\text{PM}} & -\eta_{\text{PM}} & 1 & 0 & 0 \\
0 & 0 & 0 & 0 & 0 & -\eta_{\text{EM2}} & 1 & 0 \\
0 & 0 & 0 & 0 & 0 & 0 & -\eta_{\text{P2}} & 1 \\
-\Phi & 0 & 0 & 0 & (1-\Phi) & 0 & 0 & 0 \\
0 & 0 & 0 & 0 & 0 & 0 & 0 & 1
\end{bmatrix}
\cdot
\begin{bmatrix}
\frac{P_{\text{f}}}{W} \\
\frac{P_{\text{gt}}}{W} \\
\frac{P_{\text{gb}}}{W} \\
\frac{P_{\text{e1}}}{W} \\
\frac{P_{\text{bat}}}{W} \\
\frac{P_{\text{e2}}}{W} \\
\frac{P_{\text{s2}}}{W} \\
\frac{P_{\text{p2}}}{W}
\end{bmatrix}
=
\begin{bmatrix}
0 \\
0 \\
0 \\
0 \\
0 \\
0 \\
0 \\
\frac{P_{\text{p}}}{W}
\end{bmatrix}
\tag{109}
$$

Parallel Architecture (Figure 29)

$$
\begin{bmatrix}
-\eta_{\text{GT}} & 1 & 0 & 0 & 0 & 0 & 0 \\
0 & -\eta_{\text{GB}} & -\eta_{\text{GB}} & 1 & 0 & 0 & 0 \\
0 & 0 & 0 & -\eta_{\text{P1}} & 0 & 0 & 1 \\
0 & 0 & 1 & 0 & -\eta_{\text{EM1}} & 0 & 0 \\
0 & 0 & 0 & 0 & 1 & -\eta_{\text{PM}} & 0 \\
-\Phi & 0 & 0 & 0 & 0 & (1-\Phi) & 0 \\
0 & 0 & 0 & 0 & 0 & 0 & 1
\end{bmatrix}
\cdot
\begin{bmatrix}
\frac{P_{\text{f}}}{W} \\
\frac{P_{\text{gt}}}{W} \\
\frac{P_{\text{gb}}}{W} \\
\frac{P_{\text{s1}}}{W} \\
\frac{P_{\text{e1}}}{W} \\
\frac{P_{\text{bat}}}{W} \\
\frac{P_{\text{p1}}}{W}
\end{bmatrix}
=
\begin{bmatrix}
0 \\
0 \\
0 \\
0 \\
0 \\
0 \\
\frac{P_{\text{p}}}{W}
\end{bmatrix}
\tag{110}
$$

Note: There are components in each architecture that can send and receive power. Incorporating these equations in our derivations leads to slight changes in each matrix. The matrices shown above are for the case where the batteries are being discharged. For example, during take off and climb, the battery is only being discharged. However, in the case where the battery is being recharged, such as during cruise, the matrix will differ.

Figures 30 and 31 in the next subsection represent the power loading of each component for each powertrain.

D. Power Loading Diagrams
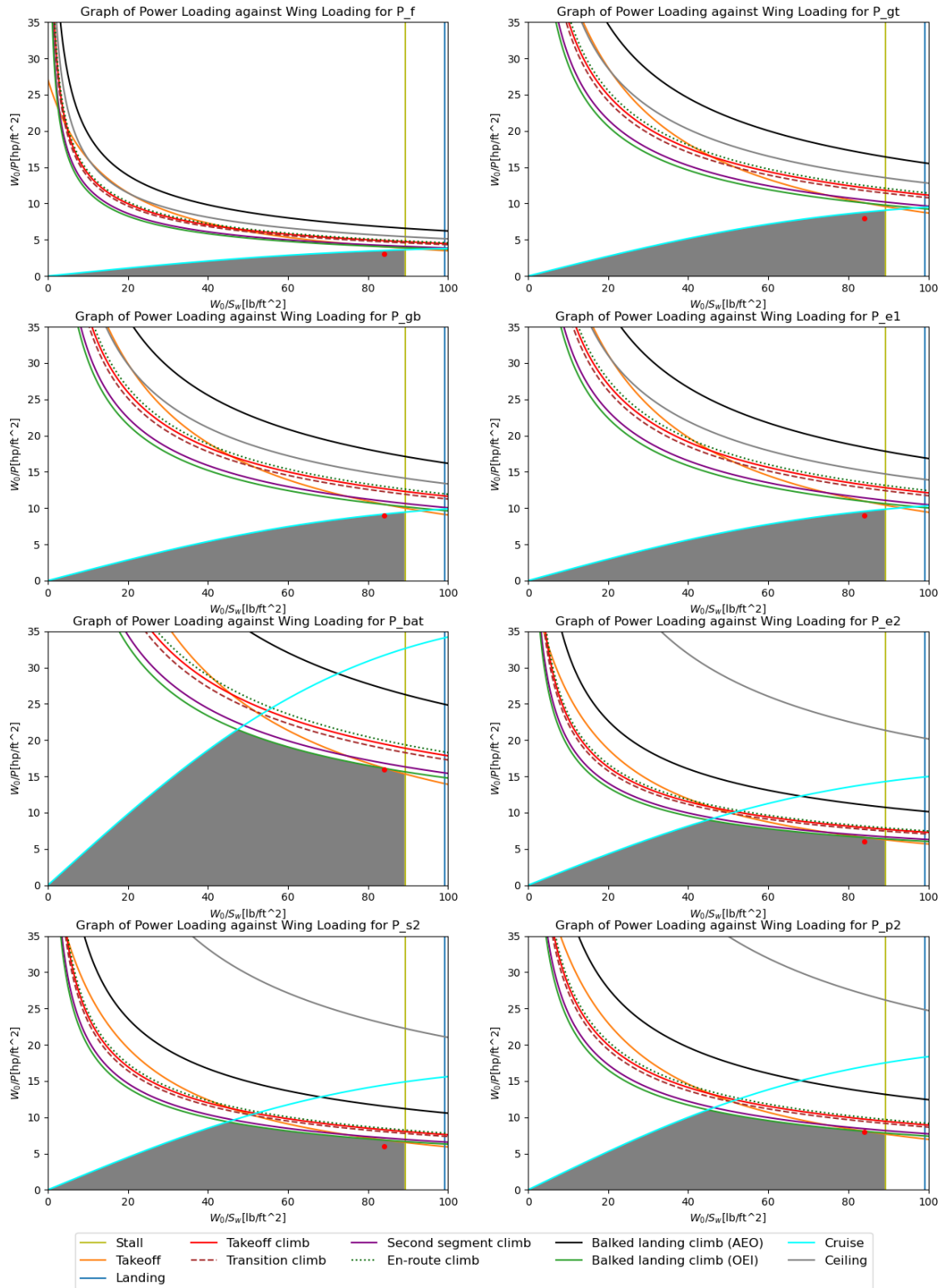
Fig. 30 Power loading graphs for serial architecture (Figure 28)
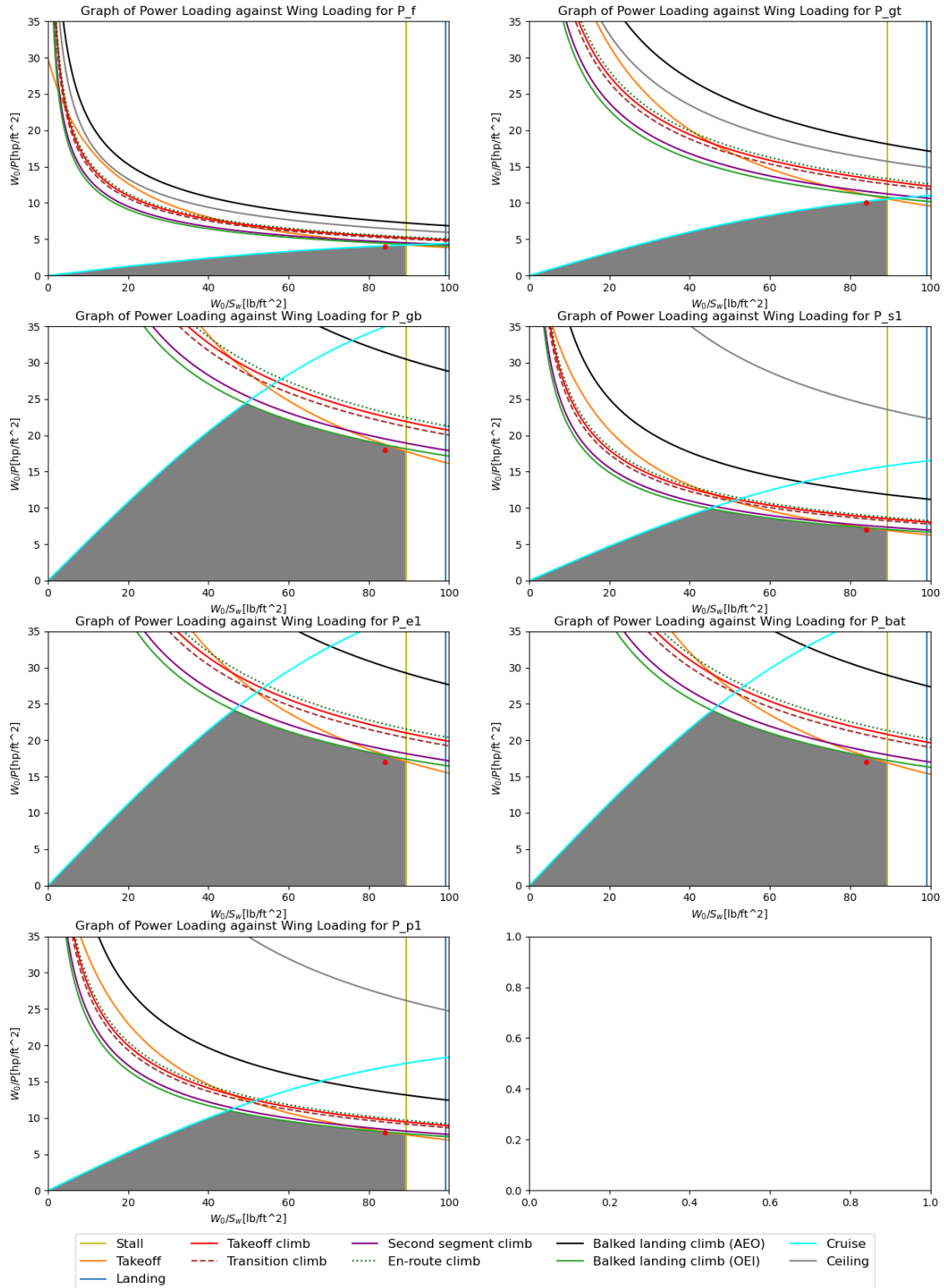
Fig. 31   Power loading graphs for parallel architecture (Figure 29)

E. Powertrain Architecture Selection

<p align="center">Table 29   (Pugh Matrix) Powertrain Comparisons</p>

Requirements	Category Weight	Serial	Parallel
Reduction in emissions vs current turboprops	5	1	1
20% reduction in block fuel use for a 500 nmi mission	5	1	1
Number of Major Components (Fewer is Better)	2	0	1
Load on Battery	2	1	0
Battery Recharging	1	0	0
Total Weight of Powertrain	4	0	1
Unweighted Totals:	–	3	4
Weighted Totals	–	12	16

Based on Table 29, we found the parallel powertrain to be the most suitable for our design. The final architecture layout can also be seen in Figure 32.

F. Architectural Schematic Pictogram
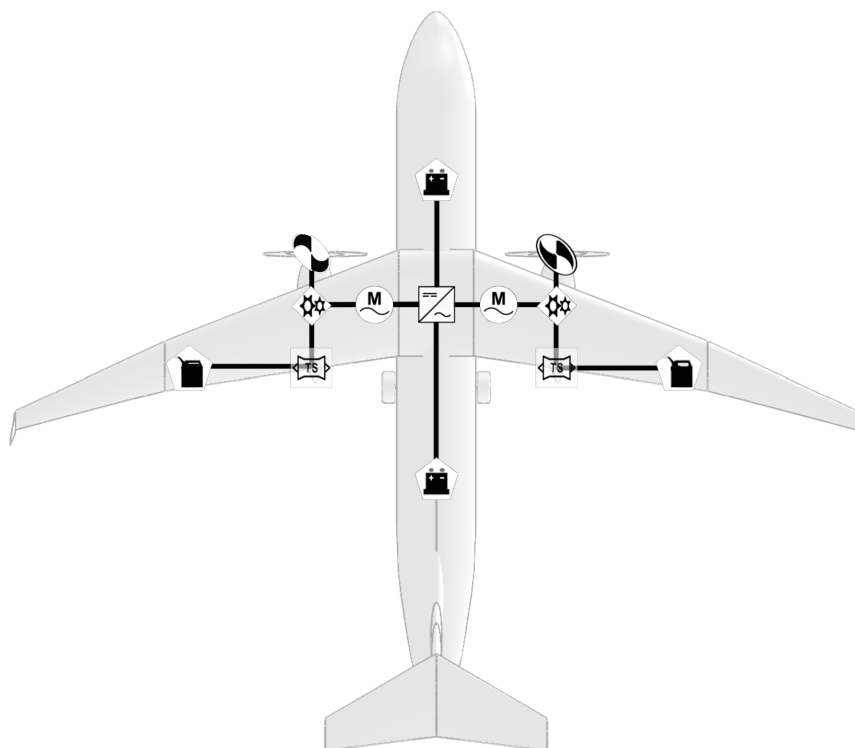
<p align="center">Fig. 32   Architectural Schematic Pictogram</p>

X. Structures

A. V-n Diagrams
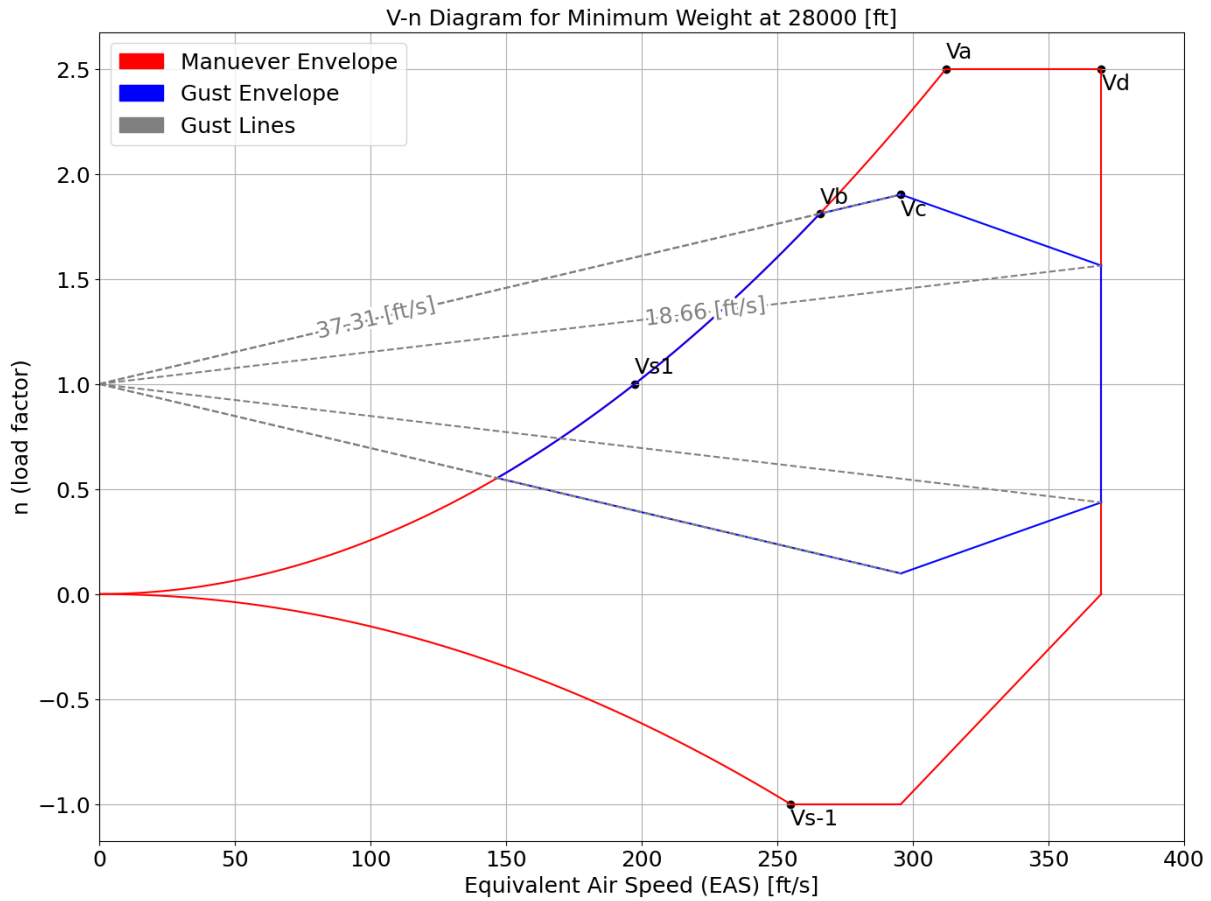
Fig. 33   V-n Diagram Minimum Weight

Table 30   Design Airspeeds and Corresponding Load Factors for Minimum Weight

	Design Airspeed (EAS) [ft/s]	Load Factor
Stalling Speed 1g, V_{S1}	197.43	1
Stalling Speed -1g, V_{S-1}	254.88	-1
Maneuvering / Cornering Speed, V_A	312.16	2.5
For Maximum Gust Intensity, V_B	265.66	1.81
Cruising, V_C	295.56	1.90
Dive, V_D	369.45	2.5
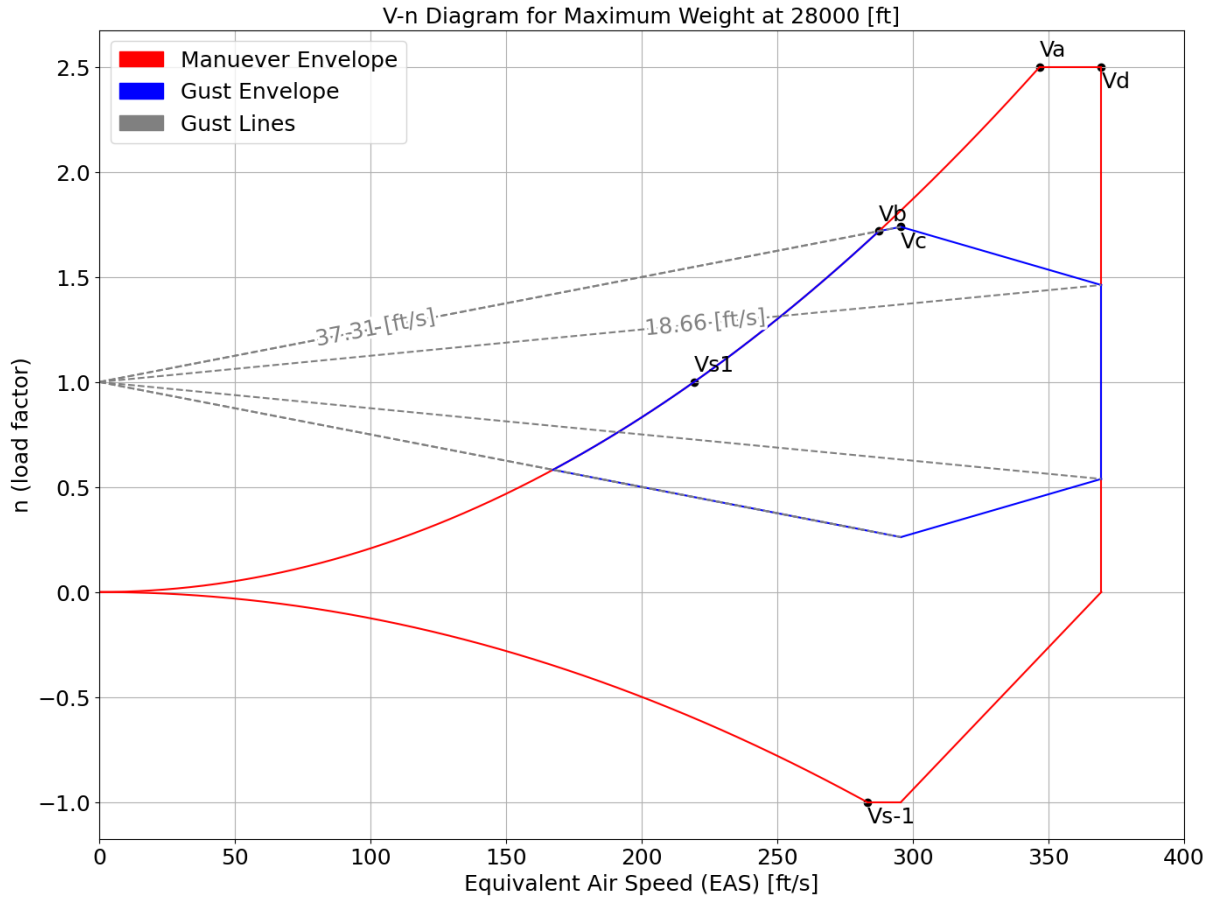
Fig. 34   V-n Diagram Maximum Weight

Table 31   Design Airspeeds and Corresponding Load Factors for Maximum Weight

	Design Airspeed (EAS) [ft/s]	Load Factor
Stalling Speed 1g, V_{S1}	219.30	1
Stalling Speed -1g, V_{S-1}	283.11	-1
Maneuvering / Cornering Speed, V_A	346.7	2.5
For Maximum Gust Intensity, V_B	287.46	1.72
Cruising, V_C	295.56	1.74
Dive, V_D	369.45	2.5

B. Material Selection and Structural Design Considerations

1) Material

Our preliminary design proposes the use of a carbon composite for the main bodies of the fuselage, wings, and tail of the aircraft as is a trend in the general aviation industry. The exact makeup and layup for this composite will depend on the forces experienced by each part of the aircraft, but potentially, a different composite material and layup might be used for each of these three sections. Additionally, on aircraft like our competitor ATR-72

and on newer aircraft like the Boeing 787, the wing and tail leading edge make use of aluminum. Finally, stronger materials like steel and titanium would be considered for particularly high stress areas such as fasteners, engine mounts, or frames.

2) Fuselage

Considering the weight of our aircraft, we will likely need a semi-monocoque design incorporating stringers and/or longerons. The frames maintain the general fuselage shape and the spacing will need to be determined by load characteristics, but we can expect a higher concentration near the wing and landing gear attachment points. The frames will be mostly circular to account for the pressurization of parts like the passenger compartment and cockpit, while they can be made less circular for areas that require more space and are pressurized such as the landing gear bay. At the moment, we propose 4 ideally uninterrupted longerons from the first frame to the last frame of the fuselage. A greater density of stringers will also run along the length of the aircraft, with some interruptions from exit doors and the rear storage door. The auxiliary power unit inlet is located on the exterior of the rear cone. Service compartments and outlets for the lavatories can be found on the bottom half of fuselage exterior.
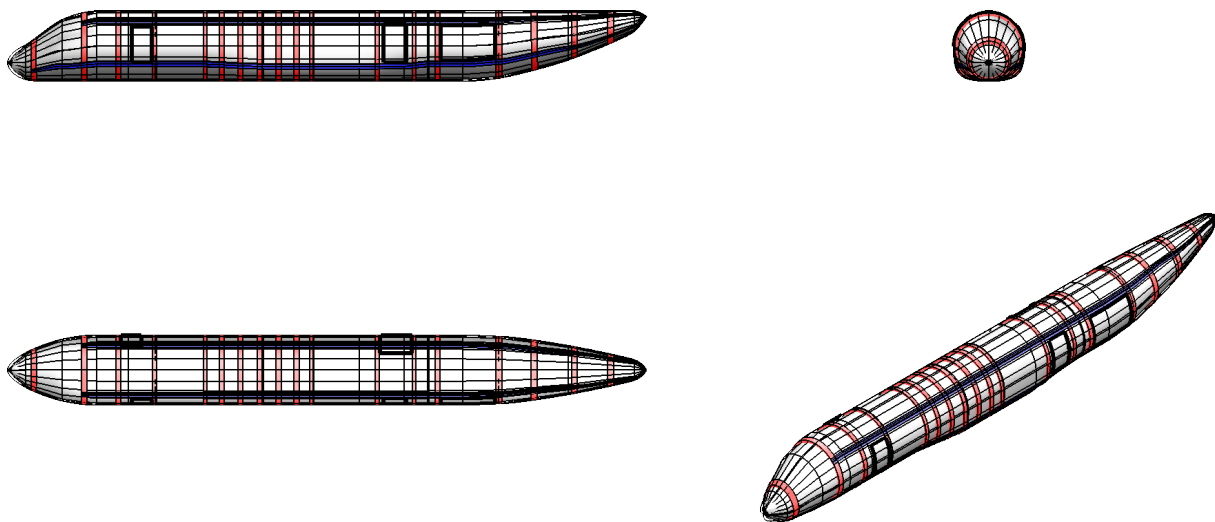
Fig. 35   Preliminary Fuselage Structural Layout

3) Wing Fuselage Attachment

We use a wing box carry through structure for our aircraft as the wing is mounted to the top of the fuselage and the volumetric concerns with such a design do not interfere with the landing gear and batteries in the lower fuselage. Additionally, it would provide volumetric storage for additional fuel.

4) Wing and Tail

We have selected the front spar to be at 28% of the chord from the leading edge, and the rear spar to be at 65% of the chord, we can have minor spars in between for additional support. However, there are volumetric

requirements for fuel storage containers, actuators, and other devices in the wings, and the support elements should be spaced to accommodate those components. Fuel storage in the wing and having our engines mounted below the wing also helps to balance the lifting load on the wing. Refueling ports are located on the bottom of each nacelle and maintenance panels for the control surfaces along with high-lift devices can be located on the upper surface of the wing above their respective component .

Because of the greater moment arm from the large T-tail, we would consider a moderately higher density of spars with spar caps to accommodate those forces. Additionally, the smaller size of the horizontal tail compared to the wing, may indicate that we only need a front and rear spar and not minor intermediary spars.
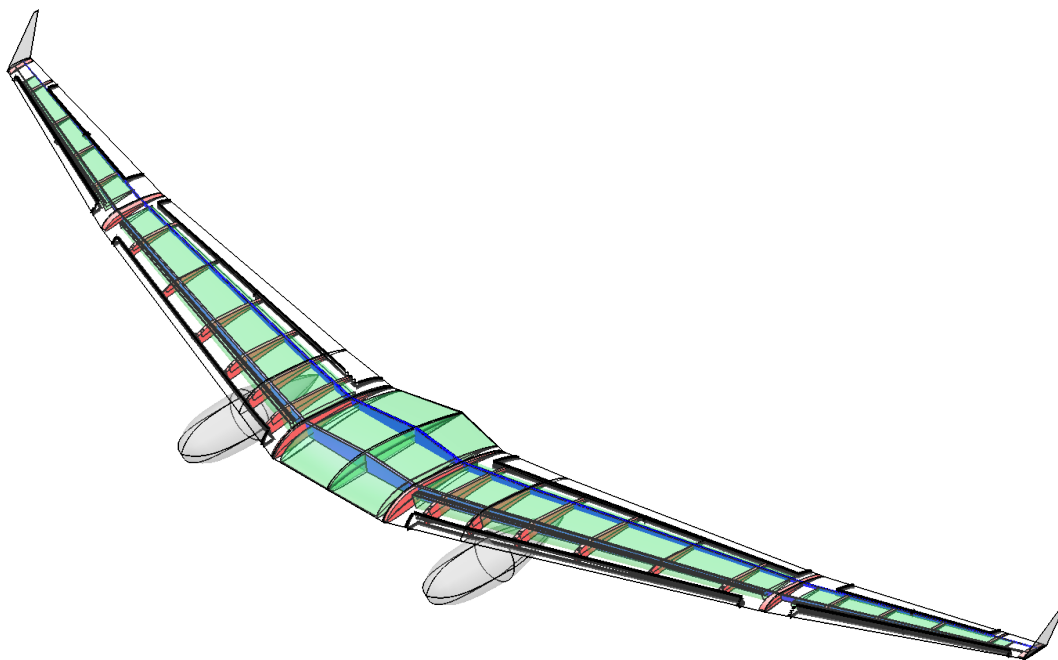
Fig. 36   Preliminary Wing Structural Layout
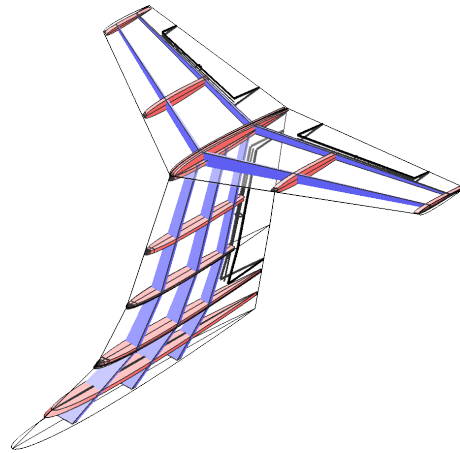
Fig. 37   Preliminary Tail Structural Layout

5) General Structural Strength

From our V-n diagrams, we can see that a possible maximum load factor of around 3.5 is possible. The aircraft structures should be able to withstand this load factor, with accounting for a safety factor of 1.5. This would be assumed under the maximum payload.
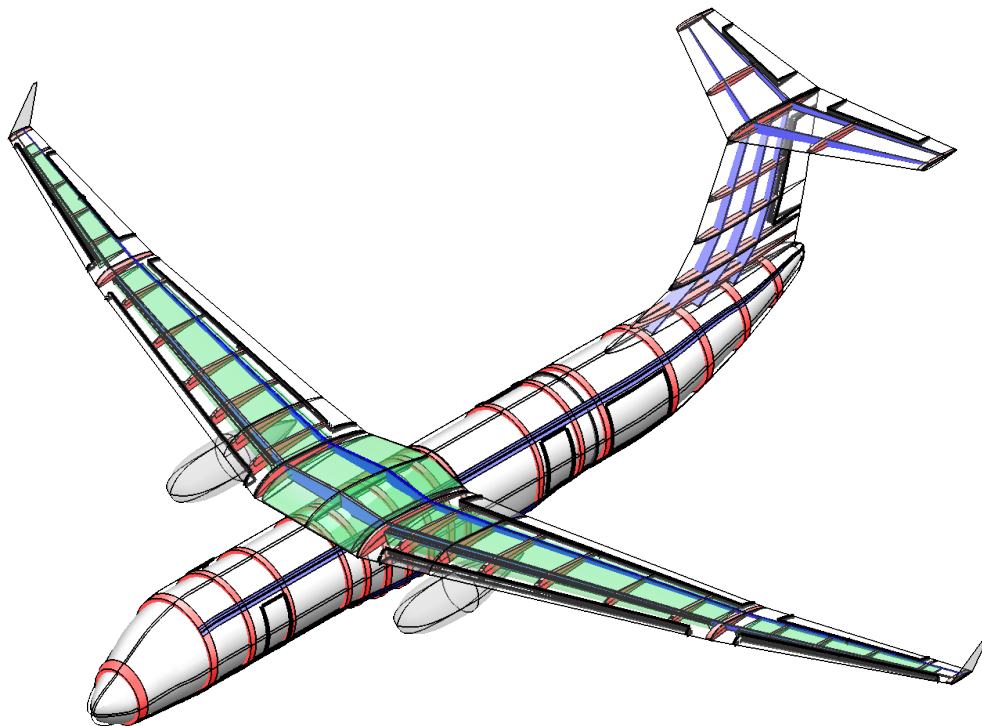
Fig. 38   Preliminary Structural Layout

XI. Landing Gear

A. Landing Gear and Fuselage Sizing

We selected a retractable landing gear configuration for our aircraft. This decision was made because our cruise speed is high enough to take advantage of the lower aerodynamic drag of this system [54] compared to a non-retractable design. Additionally, our comparable regional turboprops also use this design.

For the landing gear configuration, we select as tricycle nose wheel configuration for the good over nose visibility during ground operation, good ground steering behavior, and stability against ground loops [54].

For the disposition of the landing gear and struts we consider longitudinal and lateral criteria for aircraft tip-over and ground clearance. The notations used for Eqns 111 to 116 are Table 32 and Table 32.

Table 32   Landing Gear Calculation Nomenclature

Symbol	Description
X_{FCG}	Aircraft most-forward center of gravity
X_{ACG}	Aircraft most-aft center of gravity
W_{FM}	Lengthwise location of main landing gear strut with respect to X_{FCG}
H	Distance from X_{FCG} or X_{ACG} to bottom of main landing gear
T	Distance between outside edge of main landing gear struts
D	Ground line length
A_1	Angle between aircraft center of gravity and front nose wheel line, and nose wheel and main wheel co-linear
W_{N}	Lengthwise location of nose landing gear strut with respect to nose of fuselage
b	Wing-Span
L	Fuselage Length
Y	Vertical distance of CG with respect to fuselage roof

As a note, we make all of these measurements and calculations considering deflated struts and tires accounting for flat tires and other related non-ideal circumstances. A visual representation of these variables can be found in Figure 39

For longitudinal tip over, we presume a minimum angle θ_{TB} of 15 degrees behind vertical gear position and most aft center of gravity [54]. For lateral tip over we then want the overturn angle ψ to be lower than 63 degrees [3] and ideally lower than 55 degrees [54] when referencing the most forward center of gravity.

$$\theta_{\text{TB}} = \arctan\left(\frac{W_{\text{FM}} - (X_{\text{ACG}} - X_{\text{FCG}})}{H}\right) \tag{111}$$

$$\psi = \arctan\left(\frac{H}{D}\right) \tag{112}$$

$$A_1 = \arctan\left(\frac{\frac{T}{2}}{(X_{\text{FCG}} - W_{\text{N}}) + W_{\text{FM}}}\right) \tag{113}$$

$$\frac{D}{\sin A_1} = \frac{(X_{\text{FCG}} - W_{\text{N}}) + W_{\text{FM}}}{\sin 90°} \tag{114}$$

Next, for longitudinal ground clearance, we want angle θ_{LOF} to be at least 15 degrees measured between the bottom

of the main landing gear and the end of the fuselage [54]. We assume the forward center of gravity as the worst case scenario. For the lateral ground clearance no part of the aircraft should be below ϕ: a minimum 5 degree [54] angle measured from the bottom of the landing gear to the tip of the wing. Additionally, we account for at least 7 inches of propeller ground clearance [3].

$$\theta_{\text{LOF}} = \arctan\left(\frac{H + Y}{L - (X_{\text{FCG}} + W_{\text{FM}})}\right) \tag{115}$$

$$\phi = \arctan\left(\frac{H + 2Y}{\frac{b}{2} - \frac{T}{2}}\right) \tag{116}$$

Finally, for each of the landing gear struts we choose two wheels per strut because our aircraft is between 50,000 and 150,000 lbs and it provides redundancy in the case of flat tires [3].

The location of the main landing gear is thus defined with respect to the aircraft forward-most center of gravity and the location of the nose wheel is defined with respect to the nose of the aircraft.

Table 33   Landing Gear Location

Parameter	Dimension[ft]
W_{FM}	2.25
H	7.75
T	11.41
W_{N}	5.5

Table 34   Tip-Over and Ground Clearance Criterion

Parameter	Value [degrees]
Longitudinal Tip-Over, θ_{TB}	16.00
Lateral Tip-Over, ψ	54.00
Longitudinal Ground Clearance, θ_{LOF}	16.00
Lateral Ground Clearance, ϕ	18.79
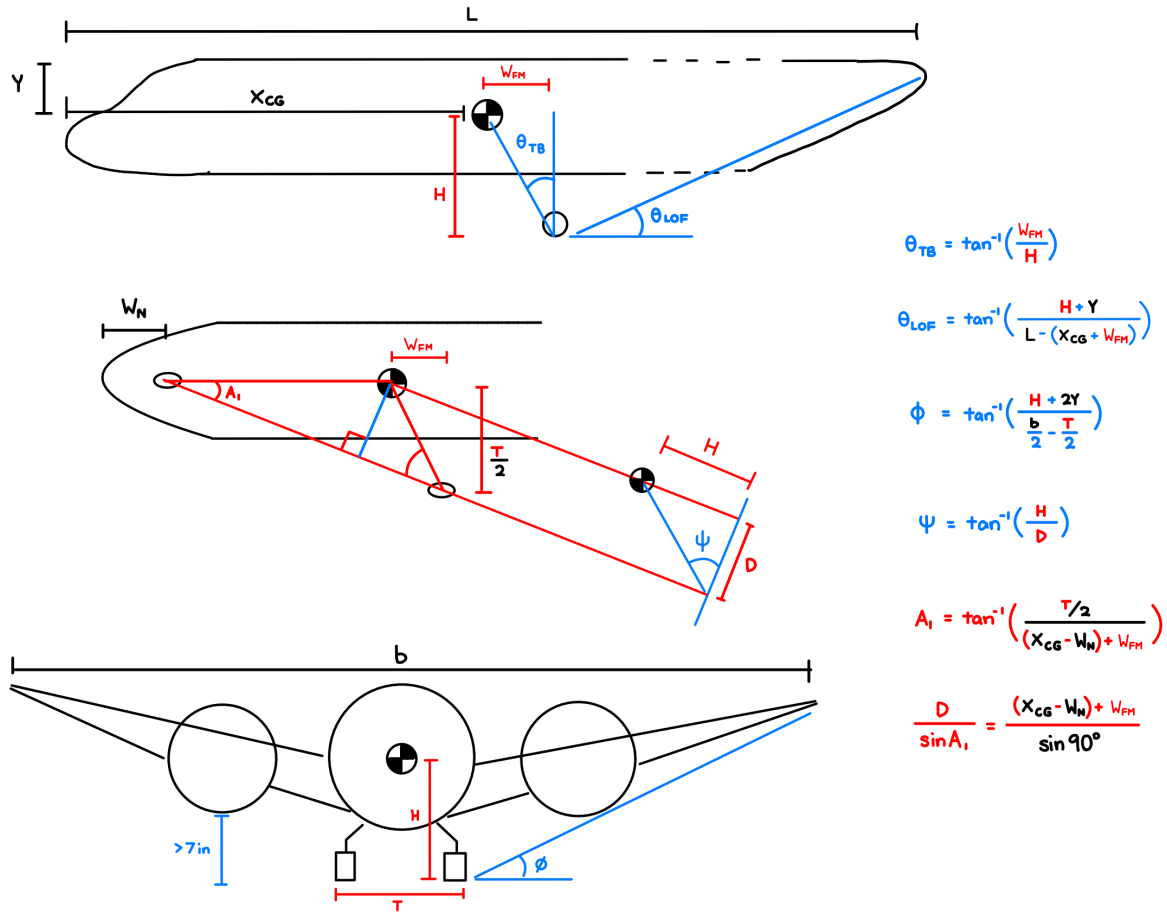
Fig. 39   Sketch of Landing Gear Criteria Angles

B. Tire Size, Braking Energy, and Kinetic Loads

When calculating the the tire loads, the FAR 25 requires that a 7% [3] increase is added to all loads on the tires, however, we chose to add the recommended 25% [3] to the loads instead to allow for growth on our aircraft design. The landing gear is designed with 2 wheels for the nose gear and 4 wheels for the main gear in the tricycle configuration. The distances N_a, M_a, M_f, and B from Figure 40 are calculated from the known values of H, FWD_{cg}, AFT_{cg}, the location of nose gear, and the location of main gear. Those values are used in Eqn 117 and to satisfy the requirements in Eqn 118 that ensure the nose gear carries the right amount of the load. The nose landing gear should only carry 10% of the total static load [3]. Eqn 119 with A = 1.63 and B = 0.315 for the diameter and A = 0.1043 and B = 0.480 for the width are used to calculate the main wheel dimensions. Then, 80% of those values are used as an estimate for the nose wheel dimensions. However, sometimes the braking requirements will be the defining parameter when deciding the wheel sizes. The kinetic energy the brakes will have to absorb is calculated with equation 120 and uses Figure 41 to determine the wheel rim diameter, which is half of the total wheel diameter, and we assumed that our aircraft is comparable to a large transport. Larger wheels are needed so that the braking system is large enough to absorb all the kinetic energy.

The resulting wheel sizing is in Table 35.

$$(\text{Max Static Load})_{\text{main gear}} = W_0 \frac{N_a}{B} \tag{117}$$

$$\frac{M_a}{B} > 0.05, \qquad \frac{M_f}{B} < 0.20 \tag{118}$$

$$\text{Main Wheel Diameter or Width} = AW_0^B \tag{119}$$

$$KE_{\text{braking}} = \frac{1}{2} \frac{W_L}{g} V_{\text{Stall}}^2 \tag{120}$$
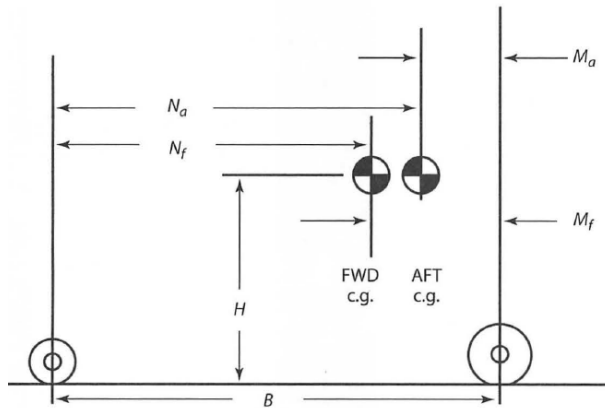
Fig. 40　Wheel Geometry [3]
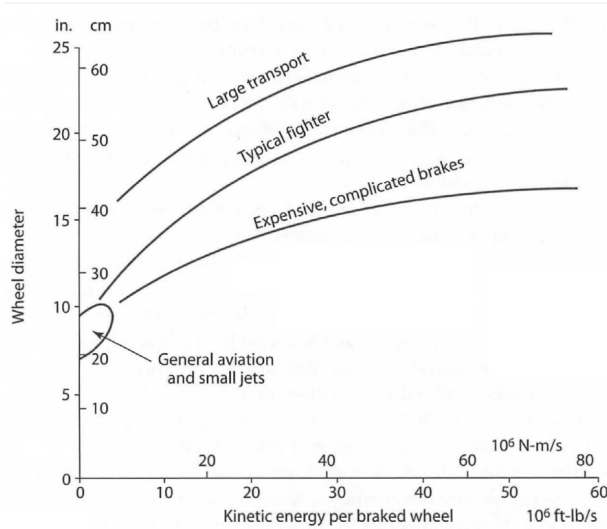
Fig. 41　Wheel Rim Diameter for Braking [3]

Table 35　Tire Sizing

Parameter	Value

Main Landing Gear Diameter	41.07 [in]
Main Landing Gear Width	11.80 [in]
Nose Landing Gear Diameter	32.85 [in]
Nose Landing Gear Width	9.45 [in]
Braking Kinetic Energy	$15.96x10^6$ [ft-lbf]

In Figures 42 and 43, the landing gears in wire form (colored blue) demonstrates how the landing gears are stored within the fuselage while the shaded landing gears represent the position they will adopt when deployed.
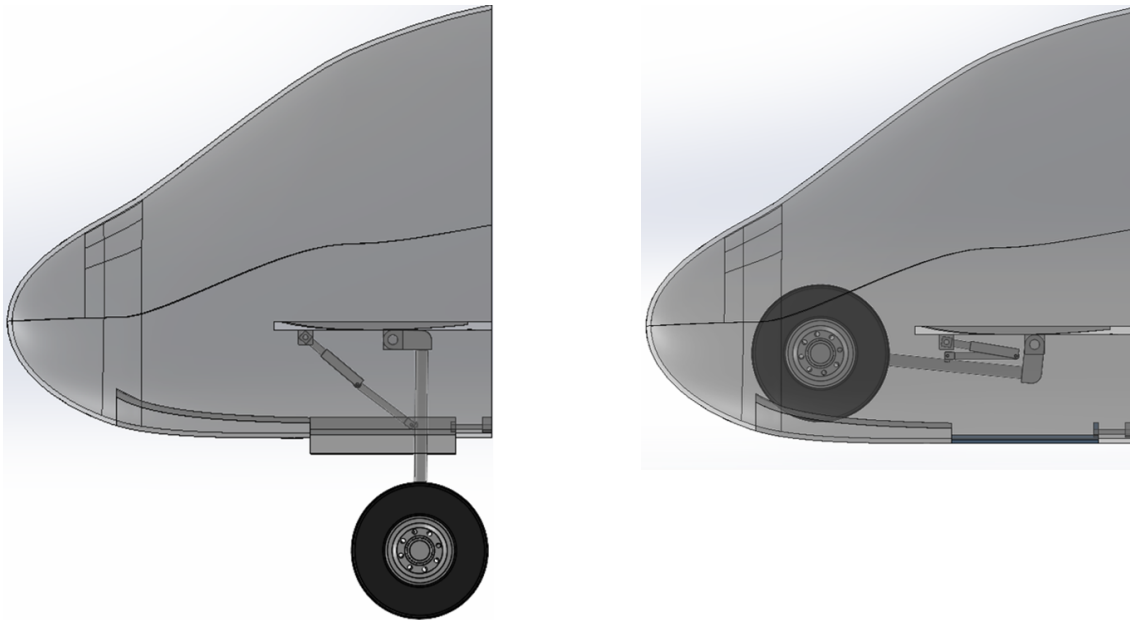
Fig. 42   Nose Landing Gear Extended (Left) and Retracted (Right)
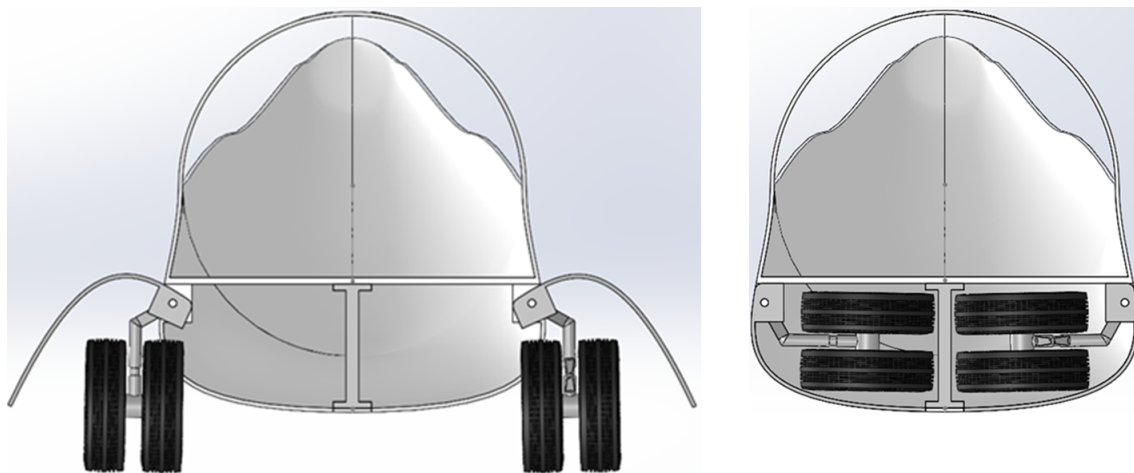
Fig. 43   Main Landing Gear Extended (Left) and Retracted (Right)

XII. Other Certifications and Considerations

A. Flight in Icing Conditions

For flight in known icing conditions, we recommend the use of heated propellers to prevent icing. De-icing boots on the vertical and horizontal tail can remove ice from those critical components. Potentially, de-icing boots can also be used for the leading edge, although the use of bleed air from the engines can be used to heat that area alternatively. The use use of electro-impulse de-icing systems was considered but decided against due to power and volume concerns.

B. VFR and IFR with Autopilot

For VFR flight we adhere to previously established pilot visibility regulations. For IFR flight, we accommodate equipment allowing for equipment defined in 14 CFR 91.205, such as two-way radios and other communication and control by ATC, adjustable altimeters, and gyroscopic indicators.

C. Autonomous Capability

We have currently not decided to implement autonomous functions for our aircraft. First, we would need to include a variety of additional sensors, such as a wide array of cameras or fully autonomous computer system, and this would add to the cost and complexity of the aircraft. Additionally, we have concerns about the feasibility of autonomous intelligence by the certification date of 2035. Autonomous capabilities are only now in preliminary testing for ground vehicles and some small drone aircraft. For our aircraft size, autonomous flight has not been certified or significantly tested for the amount of passengers and accompanying financial risk and potential loss of life. At this point in time, the technology does not seem ready for regional commercial airliners yet, and the market does not appear to have pushed for aircraft of these size to have full autonomy yet.

XIII. Cost

A. Design Trade-Study

To optimize the aircraft for our mission and performance requirements, we must conduct a trade study to consider the effects of different design parameters. For the design trade study, we will vary the battery specific energy, battery percentage, cruise speed, and the aspect ratio to optimize the block fuel burn for a 500 nmi trip.

For the first trade study, we varied the battery specific energy and the battery percentage. We created a contour plot to visualize how changing the variables affect the fuel weight and the overall takeoff weight. The results of the weights are shown in the figure below.
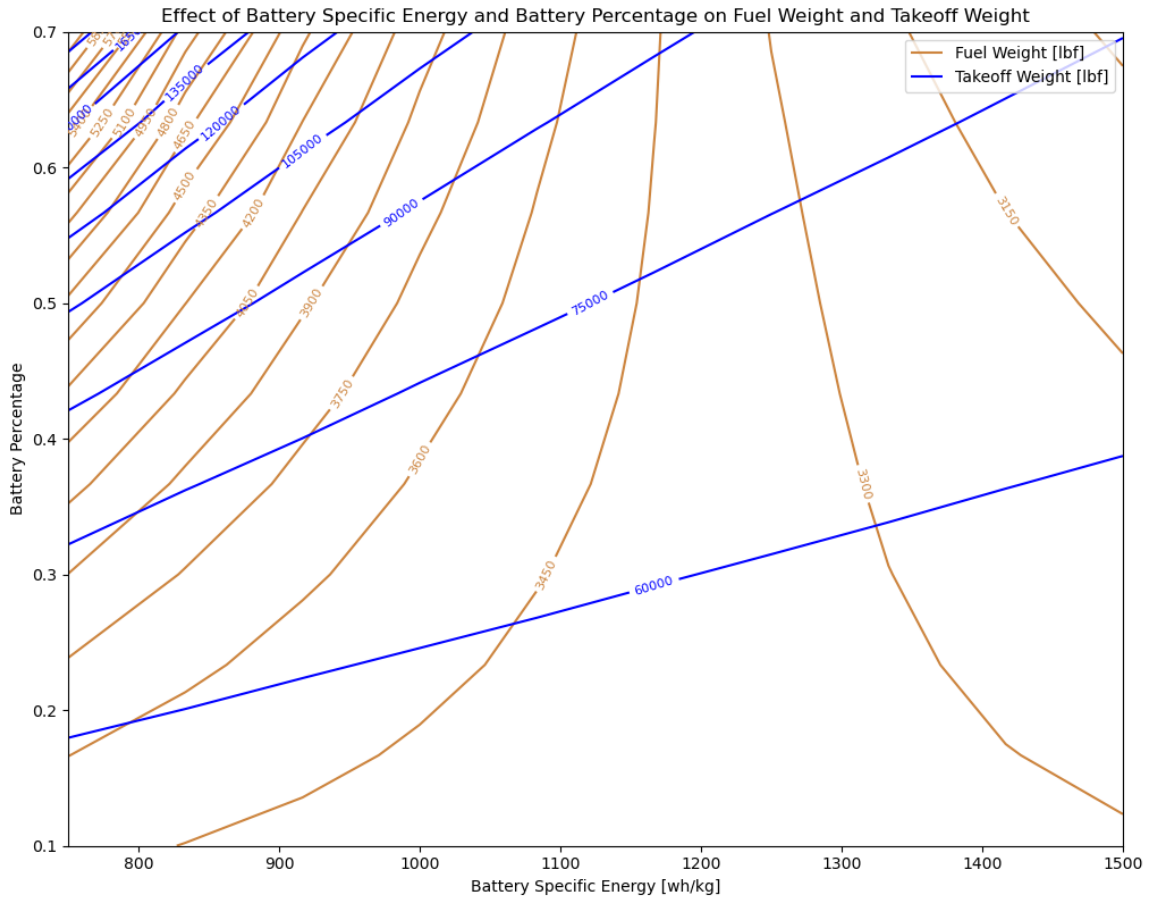
Fig. 44   Battery Specific Energy and Battery Percentage

As can be seen in the Figure 44, the fuel weight decreases as the battery specific energy is increased. The fuel weight is decreased by decreasing the battery percentage. Ideally, our goal is to increase the battery percentage to reduce fuel burn, however, increasing the battery percentage adds a lot of weight from the battery. This becomes counterintuitive as we now need to increase the fuel weight in order to meet the performance requirements. In order to optimize the block fuel burn, we need to increase the specific energy of the battery and decrease the battery percentage ratio.

For the second trade study, we varied the cruise speed to see how it affects the fuel weight. The results of the fuel, battery, and overall weights are shown below.
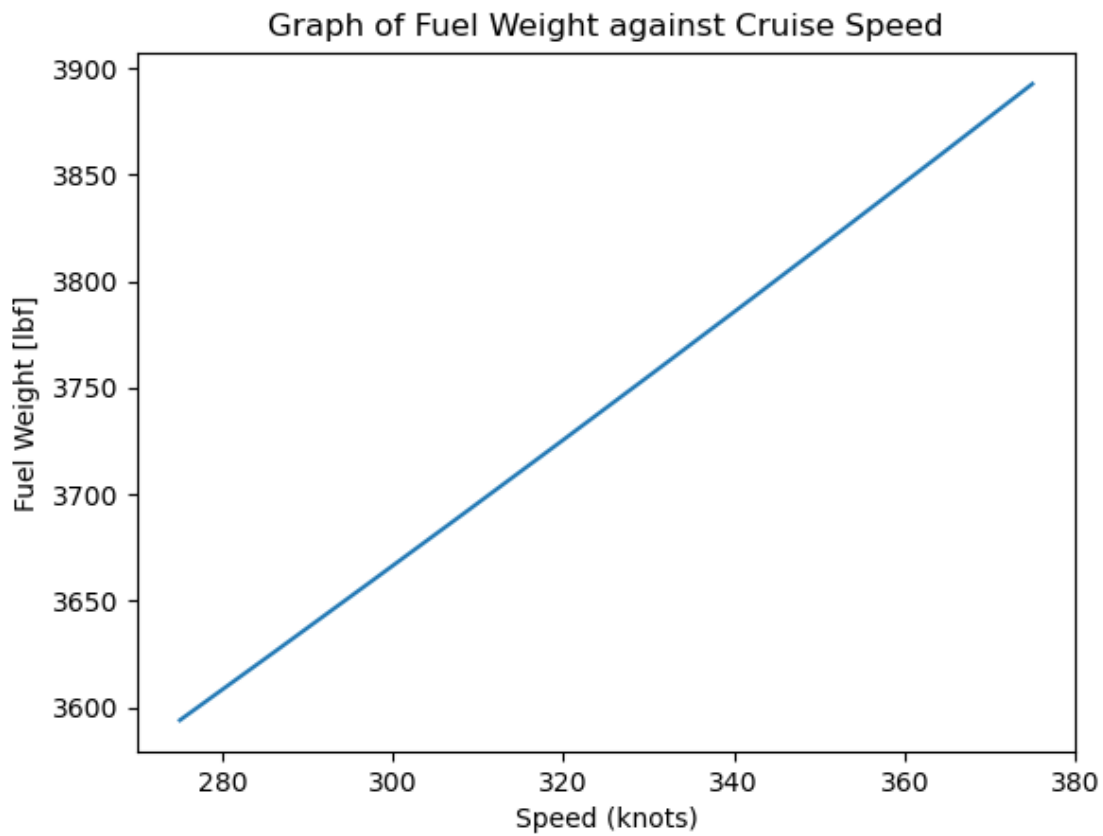
Fig. 45   Cruise Speed and Fuel Weight

From Figure45, it can be seen that the fuel weight increases as the cruise speed is increased. To optimize the block fuel burn, we chose to go with the slowest cruise speed as required by the RFP.

For the third trade study, we varied the aspect ratio to see how it affects fuel wight.
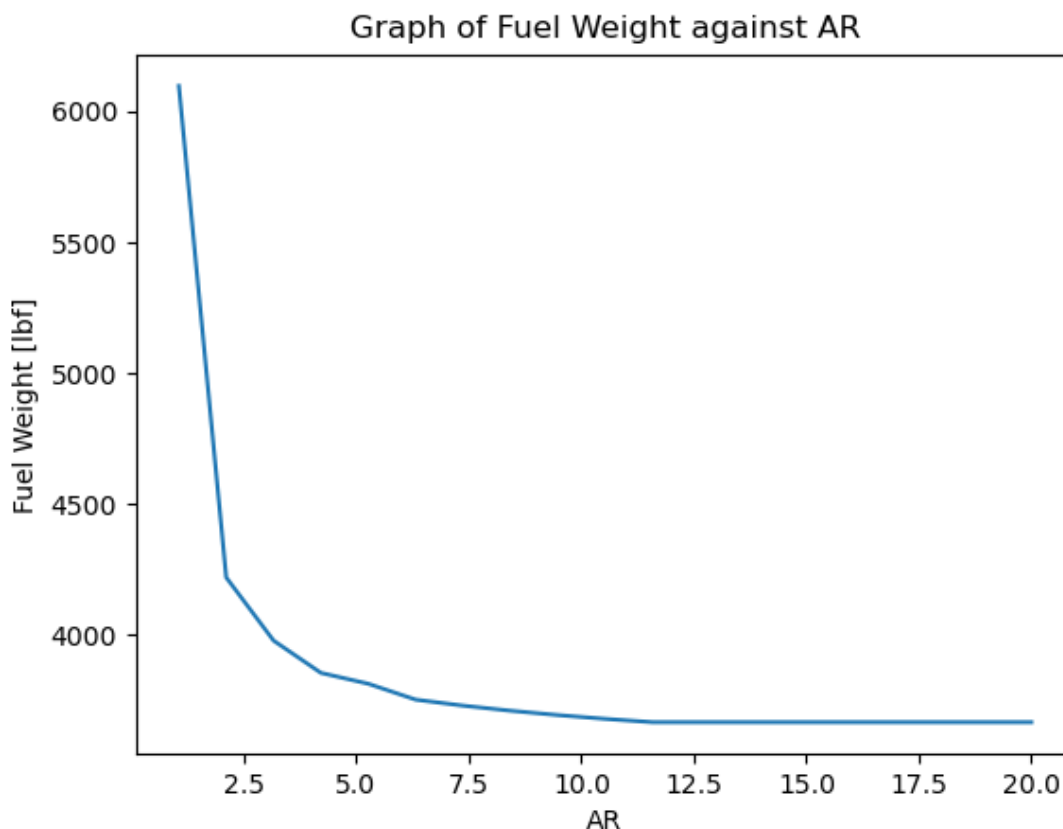
Fig. 46   Aspect Ratio and Fuel Weight

From Figure46, it can be seen that the fuel weight decreases as the aspect ratio is increased. The fuel weight plateaus once past the AR of 12. Our Aspect ratio is 13, which is within the optimum range for tthe fuel weight.

We have considered changing the geometry of our aircraft such as the airfoils, thickness to chord ratio, wing taper ratio, or wing sweep angle. However, doing so requires reworking the openVSP model and analysis done in AVL and MSES which is too complicated for the current design trade study. Instead, we will leave that to the individual project for wing design.

B. Per Unit Costs

In this section, we discuss the method used to estimate the per unit cost of our concept aircraft. The correction factors shown in Table 36 will be used in the equations shown later on.

The cost of engineering, C_{Eng}, is expressed as [8]:

$$C_{\text{Eng}} = 0.0873 \cdot W_{\text{Airframe}}^{0.791} \cdot V_{\text{H}}^{1.521} \cdot Q^{0.183} \cdot F_{\text{Cert}} \cdot F_{\text{Comp}} \cdot F_{\text{CF}} \cdot F_{\text{Press}} \cdot F_{\text{HYE}} \cdot R_{\text{Eng}} \cdot CPI \qquad (121)$$

where Q is the number of aircraft produced in 5 years, V_{H} if the maximum level airspeed in ktas, R_{Eng} is the engineering

Table 36   Correction Factors for Design Choices [8]

CER Category	F_{Cert} Factor for LSA certification	F_{Comp} Factor for 100% composites	F_{Taper} Factor for untapered wings	F_{CF} Factor for complex flap system	F_{Press} Factor for pressurized cabin	F_{HYE} Factor for hybrid-electric propulsion
Engineering Cost	0.67	2.00	-	1.03	1.03	1.33-1.66
Tooling Cost	-	2.00	0.95	1.02	1.01	1.10
Manufacturing Cost	0.75	1.25	-	1.01	-	1.10
Development Support Cost	0.50	1.50	-	1.01	1.03	1.05
Flight Test Operations Cost	0.50	-	-	-	-	1.50
Quality Control Cost	0.50	1.50	-	-	-	1.50
Materials Cost	0.75	-	-	1.02	1.01	1.05

labor rate in US$ per hour. A value of 92 was used for R_{Eng} [8]. CPI here refers to the consumer price index and the value of it used considers inflation since 2012.

The cost of tooling, C_{Tool}, is expressed as [8]:

$$C_{Tool} = 2.1036 \cdot W_{Airframe}^{0.764} \cdot V_H^{0.899} \cdot Q^{0.178} \cdot Q_M^{0.066} \cdot F_{Comp} \cdot F_{Taper} \cdot F_{CF} \cdot F_{Press} \cdot F_{HYE} \cdot R_{Tool} \cdot CPI \qquad (122)$$

where Q_M is the number of aircraft produced in 1 month. R_{Tool} is the tooling labor rate in US$/hour. A value of 61 was used for R_{Tool} [8].

The cost of manufacturing, C_{Mfg}, is expressed as [8]:

$$C_{Mfg} = 20.2588 \cdot W_{Airframe}^{0.74} \cdot V_H^{0.543} \cdot Q^{0.524} \cdot F_{Cert} \cdot F_{Comp} \cdot F_{CF} \cdot F_{HYE} \cdot R_{Mfg} \cdot CPI \qquad (123)$$

where R_{Mfg} is the manufacturing labor rate in US$ per hour. A value of 53 was used for R_{Mfg}[8].

The cost of development support, C_{Dev}, is expressed as [8]:

$$C_{Dev} = 0.06458 \cdot W_{Airframe}^{0.873} \cdot V_H^{1.89} \cdot Q_{Proto}^{0.346} \cdot F_{Cert} \cdot F_{Comp} \cdot F_{CF} \cdot F_{Press} \cdot F_{HYE} \cdot CPI \qquad (124)$$

where Q_{Proto} is the number of prototypes produced.

The cost of flight test operations, C_{Ft}, is expressed as [8]:

$$C_{Ft} = 0.009646 \cdot W_{Airframe}^{1.16} \cdot V_H^{1.3718} \cdot Q_{Proto}^{1.281} \cdot F_{Cert} \cdot F_{HYE} \cdot CPI \qquad (125)$$

The cost of quality control, C_{Qc}, is expressed as [8]:

$$C_{Qc} = 0.13 \cdot C_{Mfg}^{1.16} \cdot F_{Cert} \cdot F_{Comp} \cdot F_{HYE} \qquad (126)$$

The cost of materials, C_{Mat}, is expressed as [8]:

$$C_{Mat} = 24.896 \cdot W_{Airframe}^{0.689} \cdot V_H^{0.792} \cdot F_{Cert} \cdot F_{CF} \cdot F_{Press} \cdot F_{HYE} \cdot CPI \tag{127}$$

The equation for the cost of an electric motor, C_{Em} is [8]:

$$C_{Em} = 174 \cdot N_{Em} \cdot P_{Em} \cdot CPI \tag{128}$$

where N_{Em} is the number of electric motors and P_{Em} is the rated horsepower of the electric motor. For our purposes, we assume that P_{Em} is 2500 hp which is roughly the average value for an aircraft in this class.

The cost of the power management system, C_{Pms} is given with the equation [8]:

$$C_{Pms} = 150 \cdot P_{EmTotal} \cdot CPI \tag{129}$$

where $P_{EmTotal}$ is the total power of all electric motors.

The cost of the batteries, C_{Bat} is given with the equation [8]:

$$C_{Bat} = 200 \cdot E_{0,bat} \cdot CPI \tag{130}$$

The cost of the propellers, C_{Prop} is given with the equation [8]:

$$C_{Prop} = 210 \cdot N_P \cdot CPI \cdot D_P^2 \cdot \left(\frac{P_{SHP}}{D_P}\right)^{0.12} \tag{131}$$

where N_P is the number of propellers and D_P is the diameter of the propeller in feet.

The total estimated cost of a single plane is then:

$$C_{Total} = \left(\frac{(C_{Eng} + C_{Tool} + C_{Mfg} + C_{Dev} + C_{Ft} + C_{Mat} + C_{Em} + C_{Pms} + C_{Prop})}{Q} + C_{Bat}\right) \cdot 1.15 \tag{132}$$

We multiply by 1.15 to account for our 15% profit margin. Summing all the previous costs gives us the total cost of the entire program. Therefore, we need to divide by Q to get the cost of a single plane. Table 37 is the breakdown of all the costs associated with each design concept.

Table 37   Per Unit Costs for EcoProp [USD]

Item/Process	Amount [$]
Engineering	13,000,000
Tooling	4,700,000
Manufacturing	6,900,000
Development Support	430,000
Flight Test Operations	96,000
Quality Control	1,000,000
Materials	620,000
Electric Motor	32,000
Power Management System	30,000
Battery	600,000
Propeller	4,000
Cost to Produce	31,000,000

From the cost to produce from Table 37, we found the cost per passenger-nmi to be 620 $/passenger-nmi. Note that the costs shown in Table 37 for the electric motor and battery seem to be too low, therefore in the future these cost values will have to be verified.

C. Direct Operating Costs

In this section, we discuss the methods used for calculating the direct operating costs.

The cost of the crew, C_{Crew}, is expressed as [8]:

$$C_{\text{Crew}} = R_{\text{Crew}} \cdot N_{\text{Crew}} \cdot 1.5 \cdot t_{\text{flight}} \tag{133}$$

where R_{Crew} is the rate per hour for the flight crew, which is assumed to be $60 [8], and t_{flight} is the time of flight in hours which we calculated to be 2.25 hours for a 500 nmi flight.

The cost of the attendants, C_{Attd}, is expressed as [4]:

$$C_{\text{Attd}} = 60 N_{\text{attd}} (\text{CEF}) \left(t_{\text{flight}} \right) \tag{134}$$

where CEF is the cost escalation factor.

The cost of the fuel, C_{Fuel}, is expressed as [4]:

$$C_{\text{Fuel}} = 1.02 W_f \frac{P_f}{\rho_f} \tag{135}$$

where W_f is the weight of the fuel in lb, P_f is the price of fuel per gallon, and ρ_f is the density of fuel in lb per gallon.

The cost of the electricity, C_E, is expressed as [8]:

$$C_E = \frac{\tau_E \cdot E_{\text{flight}}}{\eta_{\text{charge}}} \tag{136}$$

where τ_E is the electricity price per kWh, and E_{flight} is the battery energy consumed during flight in kWh, and η_{charge} is the charging efficiency, 0.9 [8].

The cost of the oil, C_{Oil}, is expressed as [4]:

$$C_{\text{oil}} = 1.02 W_{\text{oil}} \frac{P_{\text{oil}}}{\rho_{\text{oil}}} \tag{137}$$

where P_{oil} is the price per gallon of oil, ρ_{oil} is the density of oil in lb per gallon, and the weight of the oil W_{oil} is given by [4]:

$$W_{\text{oil}} = 0.0125 W_f \frac{t_{\text{flight}}}{100} \tag{138}$$

The cost of the landing fees, C_{Airport}, is expressed as [4]:

$$C_{\text{Airport}} = 1.5 \left(\frac{\text{MTOW}}{1000} \right) (\text{CEF}) \tag{139}$$

The cost of the navigation fees, C_{Nav}, is expressed as [4]:

$$C_{\text{Nav}} = 0.5 (\text{CEF}) \left(\frac{1.852 R}{t_{flight}} \right) \sqrt{\frac{0.00045359237 \, \text{MTOW}}{50}} \tag{140}$$

where R is the flight range in nmi.

The cost of the maintenance, C_{Maint}, is expressed as [8]:

$$C_{\text{Maint}} = R_{\text{A\&P}} \cdot F_{MF} \cdot t_{\text{flight}} \tag{141}$$

where $R_{\text{A\&P}}$ is the mechanic rate at \$60 per hour [8], and F_{MF} is the ratio between flight hours to maintenance hours which is typically 0.20.

The cost of the aircraft insurance, C_{Ins}, is expressed as [8]:

$$C_{\text{Ins}} = 500 + 0.015\tau_{\text{AC}} \tag{142}$$

where τ_{AC} is the purchasing price of the aircraft which we assume to be the Cost to Produce in Table 37.

The cost of the aircraft depreciation, C_{ACD}, is expressed as [8]:

$$C_{\text{ACD}} = \frac{\tau_{AC}}{N_{\text{flights}}} \tag{143}$$

where N_{flights} is the number of flights over the depreciation period.

The cost of the battery depreciation, C_{BatD}, is expressed as [8]:

$$C_{\text{BatD}} = C_{\text{Bat}} \cdot \frac{E_{\text{flight}}}{n_{\text{cycles}} \cdot E_{\text{BAT}} \cdot \left(1 - \left(\frac{1 - \frac{E_{BAT,\text{ end-of-life}}}{E_{BAT,\text{ nominal}}}}{2}\right)\right)} \tag{144}$$

where n_{cycles} is the assumed life cycle of 1000 [8] and the ratio of the battery energy at the end of life to the nominal, $\frac{E_{\text{BAT, end-of-life}}}{E_{\text{BAT, nominal}}}$ is assumed to be 0.2 [8].

Table 38   Direct Operating Costs for EcoProp [USD]

Item/Process	Amount [\$/hr]
Crew	180
Attendants	60
Fuel	1,700
Electricity	450
Oil	0.31
Landing Fees	41
Navigation fees	140
Maintenance	12
Insurance	1,300
Aircraft depreciation	4.6
Battery depreciation	2,100
Total	5984.91

Table 38 is a breakdown of the cost per airplane flight hour for the direct operating costs.

XIV. Method Validation

In order to validate our code, we will use the specifications of the ATR-72 provided in Table 2 in our code. If our methodology is accurate, the takeoff weight returned by our code should give us a somewhat similar value to the actual

takeoff weight of the ATR-72.

From this analysis, the code returns a max takeoff weight of 56,000 lb for the ATR-72. This value is more than the actual takeoff weight shown in Table 2. Such a discrepancy is to be expected as accurate data for the lift coefficients and L/D of the ATR-72 could not be found and estimates had to be used. Furthermore, a component of the code estimates the 'everything else' weight, W_e, from historical data. This portion of the code is subject to much error since the coefficients used will vary greatly depending on the aircraft chosen.

XV. Computation Procedure and Software Design

We designed the code to be easily modifiable because the design process would require constant adjustment. We decided early on that creating an excel sheet to input our aircraft parameters would accelerate our design process since we needed a quick way to check the performance of different aircraft configurations. This excel sheet contains the variables that will affect the aircraft weight calculations. The python code we created then extract the variables from that excel sheet to carry out the calculations.

The code then uses the variables to carry out the calculations shown in the previous sections and outputs the drag polars and power loading against wing loading graphs as png files. The results of the calculations and the graphs are also written into a pdf file which includes the calculated parameters of our aircraft.

The empennage sizing code is then used to size our vertical and horizontal tail. The data from the excel sheet, combined code, and empennage sizing code are then used in the component weight code to calculate our component weights.

Lastly, the CG, neutral point and static margin of the aircraft is calculated by the NP_CG_SM code which uses outputs from the component weight code and empennage code. A block diagram of the code can be seen in Figure 47. The code can be found at https://github.com/BombBagel/2023_UC_DAVIS_AIAA_DESIGN_COMPETITION_GROUP8.git.

Fig. 47   Code block diagram
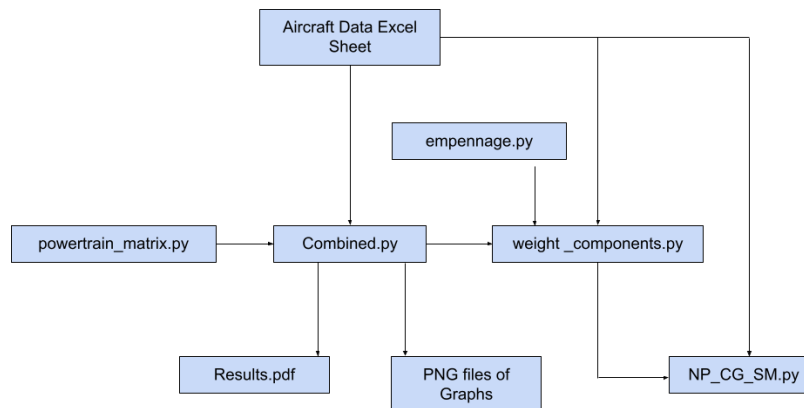
XVI. Conclusions

As our current design is still in the preliminary stage, there is room for further refinement. Most of the values obtained were based on estimates and historical approaches, and as a result, the values may not truly reflect the performance parameters of our aircraft. For instance, the estimated weight of our aircraft is significantly heavier compared to similar aircraft. Due to the weight of our aircraft, a large aspect ratio is needed. Hence, we may consider other designs such as a truss braced folding wing or a box wing in the future. These designs will allow us to increase the AR of our aircraft while remaining below the RFP wingspan limit.

Moving forward, we will need to conduct further analyses to obtain more accurate design parameters. The aerodynamic performance of our wing and empennage can be further analyzed through XFOIL. In addition, the aerodynamic performance of the whole aircraft can be analyzed with computational fluid dynamics to determine the true neutral point. Also, the accuracy of the weight, CG, and the static margin can be improved as the design progresses. Furthermore, the structure of the fuselage and wings will need careful design and optimization in order to minimize the weight of our aircraft. With that said, we have shown that our current design meets most of the requirements stated in the RFP. Our aircraft achieves 35% block fuel reduction for a 500 nmi mission, and with a hybrid propulsion system, we have reduced carbon and NOX emissions.

XVII. References

[1] Jux, B., Foitzik, S., and Doppelbauer, M., "A Standard Mission Profile for Hybrid-Electric Regional Aircraft based on Web Flight Data," *2018 IEEE International Conference on Power Electronics, Drives and Energy Systems (PEDES)*. URL `https://ieeexplore.ieee.org/document/8707564?figureId=fig2#fig2`.

[2] "Battery Cell-to-Pack Scaling Trends for Electric Aircraft," , . URL `https://ntrs.nasa.gov/api/citations/20210017488/downloads/Battery_Cell_to_Pack_Scaling_Trends_for_Electric_Aircraft_6_14.pdf`.

[3] Raymer, D. P., *Aircraft design: A conceptual approach*, 6th ed., AIAA education series, American Institute of Aeronautics and Astronautics, Reston, Va., 2018.

[4] Martins, J. R. R. A., *The Metabook of Aircraft Design*, 2016.

[5] "Astro Instruments," URL `https://astroinstruments.com/`.

[6] Roskam, J., *Airplane Design: Layout Design of Cockpit, Fuselage, Wing, and Empennage: Cutaways and Inboard Profiles*, Airplane Design, DARcorporation, 1985.

[7] Roskam, J., *Airplane Design: Preliminary sizing of airplanes*, Airplane Design, DARcorporation, 1985.

[8] Finger, D., Götten, F., Braun, C., and Bil, C., "Cost Estimation Methods for Hybrid-Electric General Aviation Aircraft," 2019.

[9] "Q400 Specifications." , . URL `https://web.archive.org/web/20161006005926/http://www2.bombardier.com/q400/en/specifications.jsp`.

[10] "ATR aircraft | home," . URL `https://www.atr-aircraft.com/wp-content/uploads/2022/06/ATR_Fiche72-600-3.pdf`.

[11] "SAAB 2000," *Jetstream Aviation Capitol*, . URL `https://www.jetstreamavcap.com/wp-content/uploads/2022/01/JAC-SAAB-2000-Cargo-Data-Sheet-2022-01-27-A.pdf`.

[12] "ATR: The N°1 choice in the Regional Market Advanced Technology - SKYbrary," . URL `https://skybrary.aero/sites/default/files/bookshelf/3696.pdf`.

[13] "Saab 2000," *Airliners*, . URL `https://www.airliners.net/aircraft-data/saab-2000/348#:~:text=Wing%20span%2024.76m%20(81ft,m2%20(600.0sq%20ft)`.

[14] "Saab 2000 - price, Specs, photo gallery, history," *Aero Corner*, . URL `https://aerocorner.com/aircraft/saab-2000/`.

[15] "ATR 72-600 - price, Specs, photo gallery, history," *Aero Corner*, . URL `https://aerocorner.com/aircraft/atr-72-600/#aircraft-specifications`.

[16] "Proposed Engine Modifications and Re-engining," 2007. URL `https://nap.nationalacademies.org/read/11837/chapter/5`.

[17] "BOMBARDIER Dash 8 Q400," . URL `https://www.skybrary.aero/aircraft/dh8d`.

[18] "ATR ATR-72-600," . URL `https://www.skybrary.aero/aircraft/at76`.

[19] "SAAB 2000," . URL `https://skybrary.aero/aircraft/sb20`.

[20] "Saab 2000 Private Jet Charter," *Paramount Business Jets*, . URL `https://www.paramountbusinessjets.com/private-jet-charter/aircraft/saab-2000`.

[21] "CemAir De Havilland-Dash 8 Q300," URL `https://www.flycemair.co.za/general_r/dehavilland_dash8-q300.php`.

[22] *ATR 72-600 The first choice for operators*, . URL `https://www.atr-aircraft.com/wp-content/uploads/2022/06/ATR_Fiche72-600-3.pdf`.

[23] "Bombardier Q Series," , . URL `https://web.archive.org/web/20180416074022/https://commercialaircraft.bombardier.com/content/dam/Websites/bombardiercom/supporting-documents/BA/Bombardier_Q/%20Series_Final.pdf`.

[24] "ATR 72-600 - amelia pro," . URL `https://pro.flyamelia.com/wp-content/uploads/2019/08/EN-Aircraft-specifications-ATR-72-600.pdf`.

[25] "Airliners.net," . URL https://www.airliners.net/aircraft-data/de-havilland-canada-dhc-8-400-dash-8/122.

[26] "Charter or Hire a De Havilland Dash 8 Q400." . URL https://www.paramountbusinessjets.com/private-jet-charter/aircraft/dash-8-q400.

[27] "Charter an ATR 72-600 turboprop airliner by Aérospatiale," *Paramount Business Jets*, . URL https://www.paramountbusinessjets.com/private-jet-charter/aircraft/atr-72-600.

[28] "Regional Jet Market Size, share & covid-19 impact, by platform (commercial aircraft and military aircraft), by engine type (turboprop and turbofan), by seating capacity (35 to 80 and 80 to 125), and by maximum takeoff weight (20,000 lbs to 80,000 lbs and 81,000 lbs to 1,60,000 lbs) and Regional Forecast, 2021-2028," *Regional Jet Market Share & Forecast | Industry Outlook [2028]*, . URL https://www.fortunebusinessinsights.com/regional-jet-market-106235.

[29] "Turboprop market forecast 2022-2041," *ATR Aircraft*, . URL https://www.atraircraft.com/wp-content/uploads/2022/07/ATR_MarketForecast_2022_Digital_HD.pdf.

[30] "Regional aircraft," *Clean Aviation*, . URL https://www.clean-aviation.eu/regional-aircraft.

[31] Richardson, M., "In great demand," *Aerospace Manufacturing*, 2022. URL https://www.aero-mag.com/in-great-demand.

[32] Hadhazy, A., "Fly the Electric Skies," *Aerospace America*. URL https://aerospaceamerica.aiaa.org/features/fly-the-electric-skies/.

[33] Lees, E., and Watson, C., "The rebirth of short-haul aviation," *ICF*, 2021. URL https://www.icf.com/insights/transportation/short-haul-electric-aviation.

[34] Menon, O., "The Economics Of Short & Long-Haul Flights," *Simple Flying*, 2022. URL https://simpleflying.com/short-long-haul-flights-economics-guide/.

[35] Cummins, N., and Pande, P., "How Much Does It Cost To Fuel A Commercial Airliner?" *Simple Flying*, 2022. URL https://simpleflying.com/commercial-airliner-fuel-cost/.

[36] "4 ways airlines are planning to become carbon neutral," *World Economic Forum*. URL https://www.weforum.org/agenda/2021/11/airlines-industry-climate-neutral-travel/.

[37] *Challenges Associated to High Power Hybrid Electric Propulsion in Aerospace*, 2019. https://doi.org/10.14339/STO-MP-AVT-323-04-PDF, URL https://www.sto.nato.int/publications/STO%20Meeting%20Proceedings/STO-MP-AVT-323/MP-AVT-323-04.pdf.

[38] Fletcher, S., Flynn, M.-C., Jones, C. E., and Norman, P. J., "Hybrid Electric Aircraft: State of the Art and Key Electrical System Challenges," *IEEE Transportation Electrification Community Newsletter*, 2016. URL https://tec.ieee.org/newsletter/september-2016/hybrid-electric-aircraft-state-of-the-art-and-key-electrical-system-challenges.

[39] Wheeler, P., Sirimanna, T. S., Bozhko, S., and Haran, K. S., "Electric/Hybrid-Electric Aircraft Propulsion Systems," *Proceedings of the IEEE*, Vol. 109, No. 6, 2021, pp. 1115 – 1127. https://doi.org/10.1109/JPROC.2021.3073291, URL https://ieeexplore.ieee.org/abstract/document/9419369.

[40] "Lightweight, Durable, and Multifunctional Electrical Insulation Material Systems for High Voltage Applications," , . URL https://ntrs.nasa.gov/api/citations/20180005559/downloads/20180005559.pdf.

[41] Mark Voskuijl, A. G. R., Joris van Bogaert, "Analysis and design of hybrid electric regional turboprop aircraft," 2017. URL https://link.springer.com/article/10.1007/s13272-017-0272-1.

[42] Bright Appiah Adu-Gyamfi, C. G., "Electric aviation: A review of concepts and enabling technologies," *Transportation Engineering*, Vol. 9, 2022. URL https://www.sciencedirect.com/science/article/pii/S2666691X2200032X.

[43] "The Future of Mobility eFanX," URL https://www.siemens.com/innovation/en/home/pictures-of-the-future/mobility-and-motors/the-future-of-mobility-e-fan-x.html.

[44] de Vries, R., "Hybrid-Electric Aircraft with Over-the-Wing Distributed Propulsion: Aerodynamic Performance and Conceptual Design," Ph.D. thesis, Delft University of Technology, 2022. https://doi.org/10.4233/uuid:ef87dc11-e7b2-4726-a41f-28588d64c58d.

[45] "ULD Container Types," URL https://www.searates.com/reference/uld/.

[46] "14 CFR Part 25 Subpart D: Emergency Provisions," URL https://www.ecfr.gov/current/title-14/chapter-I/subchapter-C/part-25/subpart-D/subject-group-ECFR88992669bab3b52/section-25.807.

[47] "Influence of Fuselage Bulkhead Stiffness on Composite Wing Weight of a Civil Aircraft," URL https://nal-ir.nal.res.in/12125/1/cp159.pdf.

[48] Löbberding, H., Wessel, S., Offermanns, C., Kehrer, M., Rother, J., Heimes, H., and Kampker, A., "From Cell to Battery System in BEVs: Analysis of System Packing Efficiency and Cell Types," *World Electric Vehicle Journal*, Vol. 11, No. 4, 2020. https://doi.org/10.3390/wevj11040077, URL https://www.mdpi.com/2032-6653/11/4/77.

[49] Roskam, J., *Airplane Design*, No. pt. 5 in Airplane Design, DARcorporation, 1985. URL https://books.google.com/books?id=mMU47Ld7yQkC.

[50] Roskam, J., and of Kansas, U., *Airplane Design: Part 2 - preliminary configuration design and integration of the propulsion system*, DARcorporation, 1985. URL https://books.google.com/books?id=lIa-tAEACAAJ.

[51] Torenbeek, E., *Synthesis of Subsonic Airplane Design*, Delft University Press, Delft, 1982.

[52] Reynard de Vries, a. R. V., Maurice F. M. Hoogreef, "Preliminary Sizing of a Hybrid-Electric Passenger Aircraft Featuring Over-the-Wing Distributed-Propulsion," 2019. https://doi.org/0.2514/6.2019-1811.

[53] Reynard de Vries, R. V., Malcom T. Brown, "Preliminary Sizing Method For Hybrid Electric Aircraft Including Aero-Propulsive Interaction Effects," 2018. URL https://doi.org/10.2514/6.2018-4228.

[54] Roskam, D. J., *Layout Design of Landing Gear and Systems*, DAR Corporation, 2018.

XVIII. Appendix

A. Cited Figures and Tables

Figures and Tables from Raymer [3]
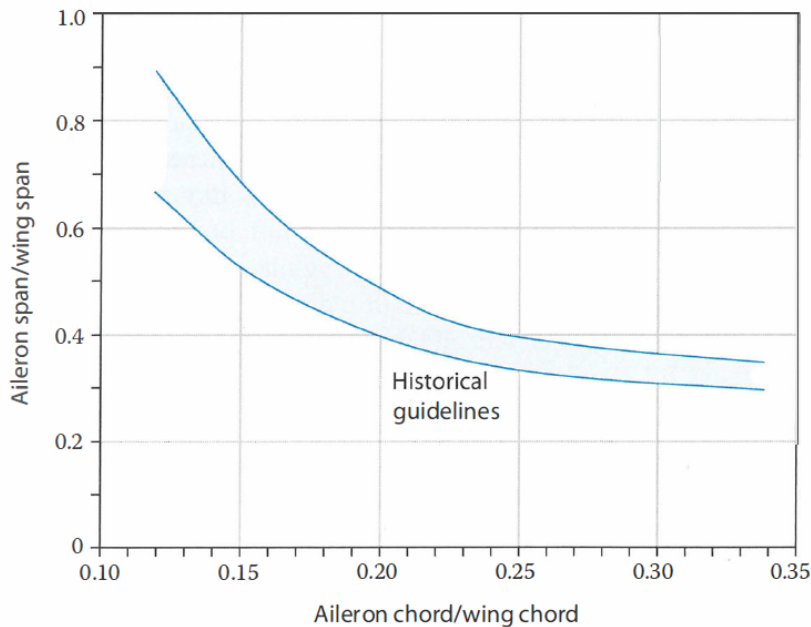
Fig. 6.3 Aileron guidelines.
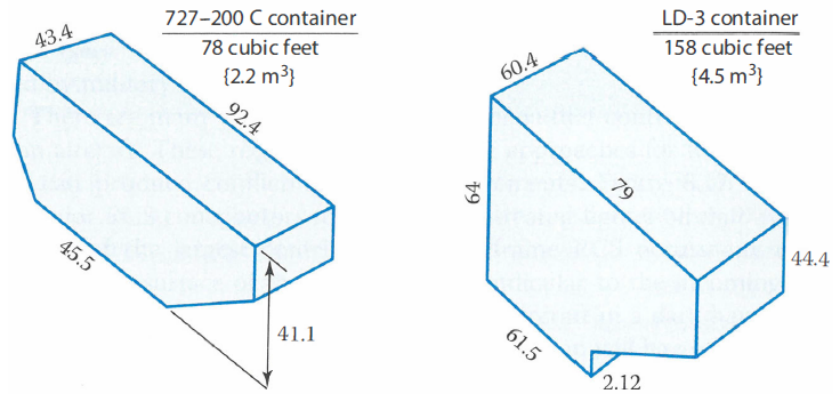
Fig. 9.4   Cargo containers.

Table 3.1   Empty Weight Fraction vs W_0

$W_e/W_0 = A W_0^C K_{vs}$	A	{A-metric}	C
Sailplane—unpowered	0.86	{0.83}	−0.05
Sailplane—powered	0.91	{0.88}	−0.05
Homebuilt—metal/wood	1.19	{1.11}	−0.09
Homebuilt—composite	1.15	{1.07}	−0.09
General aviation—single engine	2.36	{2.05}	−0.18
General aviation—twin engine	1.51	{1.4}	−0.10
Agricultural aircraft	0.74	{0.72}	−0.03
Twin turboprop	0.96	{0.92}	−0.05
Flying boat	1.09	{1.05}	−0.05
Jet trainer	1.59	{1.47}	−0.10
Jet fighter	2.34	{2.11}	−0.13
Military cargo/bomber	0.93	{0.88}	−0.07
Jet transport	1.02	{0.97}	−0.06
UAV—Tac Recce & UCAV	1.67	{1.47}	−0.16
UAV—high altitude	2.75	{2.39}	−0.18
UAV—small	0.97	{0.93}	−0.06

Table 3.2   Historical Mission-Segment Weight Fractions

Mission Segment	(W_i/W_{i-1})
Warmup and takeoff	0.970
Climb	0.985
Landing	0.995

Table 3.4   Propeller-Specific Fuel Consumption, C_{bhp}

Propeller: $C = C_{power} V/\eta_p = C_{bhp} V/(550\eta_p)$ Typical C_{bhp}: lb/hr/bhp {mg/W-s}	Cruise	Loiter
Piston-prop (fixed pitch)	0.4 {0.068}	0.5 {0.085}
Piston-prop (variable pitch)	0.4 {0.068}	0.5 {0.085}
Turboprop	0.5 {0.085}	0.6 {0.101}

Table 6.4 Tail Volume Coefficient

	Typical Values	
	Horizontal c_{HT}	Vertical c_{VT}
Sailplane	0.50	0.02
Homebuilt	0.50	0.04
General aviation—single engine	0.70	0.04
General aviation—twin engine	0.80	0.07
Agricultural	0.50	0.04
Twin turboprop	0.90	0.08
Flying boat	0.70	0.06
Jet trainer	0.70	0.06
Jet fighter	0.40	0.07–0.12*
Military cargo/bomber	1.00	0.08
Jet transport	1.00	0.09

*Long fuselage with high wing loading needs larger value.

Table 6.5 Control Surface Sizing Guidelines

Aircraft	Elevator C_e/C	Rudder C_r/C
Fighter/attack	0.30*	0.30
Jet transport	0.25†	0.32
Jet trainer	0.35	0.35
Biz jet	0.32†	0.30
GA single	0.45	0.40
GA twin	0.36	0.46
Sailplane	0.43	0.40

*Supersonic usually all-moving tail without separate elevator.
†Often all-moving plus elevator.

Table 9.1 Typical Passenger Compartment Data

	First Class	Economy	High-Density/Small Aircraft
Seat pitch, in. {cm}	38–40 {97–102}	34–36 {86–91}	30–32 {76–81}
Seat width, in. {cm}	20–28 {51–71}	17–22 {43–56}	16–18 {41–46}
Head room, in. {cm}	>65 {165}	>65 {165}	—
Aisle width, in. {cm}	20–28 {51–71}	18–20 {46–51}	≥12 {30}
Aisle height, in. {cm}	>76 {193}	>76 {193}	>60 {152}
Passengers per cabin staff (international-domestic)	16–20	31–36	≤50
Passengers per lavatory (40 × 40 in.) {1 × 1 m}	10–20	40–60	40–60
Galley volume per passenger, ft³ {m³}	5–8 {0.14–0.23}	1–2 {0.03–0.06}	0–1 {0–0.03}

Table 12.3 Equivalent Skin-Friction Coefficients

$C_{D0} = C_{fe}(S_{wet}/S_{ref})$	C_{fe}
Bomber	0.0030
Civil transport	0.0026
Military cargo (high upsweep fuselage)	0.0035
Air Force fighter	0.0035
Navy fighter	0.0040
Clean supersonic cruise aircraft	0.0025
Light aircraft—single engine	0.0055
Light aircraft—twin engine	0.0045
Prop seaplane	0.0065
Jet seaplane	0.0040

Table 15.2 Approximate Empty Weight Buildup

	Fighters		Transport & Bomber		General Aviation		Multiplier	Approximate Location
	lb/ft²	kg/m²	lb/ft²	kg/m²	lb/ft²	kg/m²		
Wing	9	44	10	49	2.5	12	$S_{exposed\ planform}$	40% MAC
Horizontal tail	4	20	5.5	27	2	10	$S_{exposed\ planform}$	40% MAC
Vertical tail	5.3	26	5.5	27	2	10	$S_{exposed\ planform}$	40% MAC
Fuselage	4.8	23	5	24	1.4	7	$S_{wetted\ area}$	40–50% length
	Weight Ratio		Weight Ratio		Weight Ratio			
Landing gear*	0.033		0.043		0.057		TOGW	centroid
Landing gear—Navy	0.045		—		—		TOGW	centroid
Installed engine	1.3		1.3		1.4		Engine weight	centroid
"All-else empty"	0.17		0.17		0.1		TOGW	40–50% length

*15% to nose gear, 85% to main gear; reduce gear weight by 0.014 W_0 if fixed gear.

Tables from Roskam Part 1 [7]

```
Table 3.1 Typical Values For Maximum Lift Coefficient
========================================================
```

Airplane Type	$C_{L_{max}}$	$C_{L_{max_{TO}}}$	$C_{L_{max_L}}$
1. Homebuilts	1.2 - 1.8	1.2 - 1.8	1.2 - 2.0*
2. Single Engine Propeller Driven	1.3 - 1.9	1.3 - 1.9	1.6 - 2.3
3. Twin Engine Propeller Driven	1.2 - 1.8	1.4 - 2.0	1.6 - 2.5
4. Agricultural	1.3 - 1.9	1.3 - 1.9	1.3 - 1.9
5. Business Jets	1.4 - 1.8	1.6 - 2.2	1.6 - 2.6
6. Regional TBP	1.5 - 1.9	1.7 - 2.1	1.9 - 3.3
7. Transport Jets	1.2 - 1.8	1.6 - 2.2	1.8 - 2.8
8. Military Trainers	1.2 - 1.8	1.4 - 2.0	1.6 - 2.2
9. Fighters	1.2 - 1.8	1.4 - 2.0	1.6 - 2.6
10. Mil. Patrol, Bomb and Transports	1.2 - 1.8	1.6 - 2.2	1.8 - 3.0
11. Flying Boats, Amphibious and Float Airplanes	1.2 - 1.8	1.6 - 2.2	1.8 - 3.4
12. Supersonic Cruise Airplanes	1.2 - 1.8	1.6 - 2.0	1.8 - 2.2

* The Rutan Varieze reaches 2.5, based on stall speed data from Ref.9.

Notes: 1. The data in this table reflect existing (1984) flap design practice.
2. Considerably higher values for maximum lift coefficient are possible with more sophisticated flap designs and/or with some form of circulation control.
3. Methods for computing $C_{L_{max}}$ values are contained in Ref.6.

```
Table 3.2 Ground Friction Coefficient, μ_G
==========================================
```

Surface Type	μ_G
Concrete	0.02 - 0.03 (0.025 per Ref.15)
Asphalt	0.02 - 0.03
Hard Turf	0.05
Short Grass	0.05
Long Grass	0.10
Soft Ground	0.10 - 0.30

```
Table 3.5 Regression Line Coefficients for Take-off
===================================================
          Weight Versus Wetted Area (Eqn.(3.22))
          =====================================
```

Airplane Type	c	d
1. Homebuilts	1.2362	0.4319
2. Single Engine Propeller Driven	1.0892	0.5147
3. Twin Engine Propeller Driven	0.8635	0.5632
4. Agricultural	1.0447	0.5326
5. Business Jets	0.2263	0.6977
6. Regional Turboprops	-0.0866	0.8099
7. Transport Jets	0.0199	0.7531
8. Military Trainers*	0.8565	0.5423
9. Fighters*	-0.1289	0.7506
10. Mil. Patrol, Bomb and Transport	0.1628	0.7316
11. Flying Boats, Amph. and Float	0.6295	0.6708
12. Supersonic Cruise Airplanes	-1.1868	0.9609

* For these airplanes, wetted areas were correlated with 'clean', maximum take-off weights. No stores were accounted for.

```
Table 3.6 First Estimates for ΔC_D_o and 'e'
============================================
          With Flaps and Gear Down
          =========================
```

Configuration	ΔC_{D_o}	e
Clean	0	0.80 - 0.85
Take-off flaps	0.010 - 0.020	0.75 - 0.80
Landing Flaps	0.055 - 0.075	0.70 - 0.75
Landing Gear	0.015 - 0.025	no effect

Figures and Tables from Roskam Part 2 [50]

Table 8.13 Planform Design Parameters for Horizontal Tails

Type	Dihedral Angle, Γ_h deg.	Incidence Angle, i_h deg.	Aspect Ratio, A_h	Sweep Angle, $\Lambda_{c/4_h}$ deg.	Taper Ratio, λ_h
Homebuilts	+5 – –10	0 fixed to variable	1.8 – 4.5	0 – 20	0.29 – 1.0
Single Engine Prop. Driven	0	–5 – 0 or variable	4.0 – 6.3	0 – 10	0.45 – 1.0
Twin Engine Prop Driven	0 – +12	0 fixed to variable	3.7 – 7.7	0 – 17	0.48 – 1.0
Agricultural	0 – +3	0	2.7 – 5.4	0 – 10	0.59 – 1.0
Business Jets	–4 – +9	–3.5 fixed	3.2 – 6.3	0 – 35	0.32 – 0.57
Regional Turbo-Props.	0 – +12	0 – 3 fixed to variable	3.4 – 7.7	0 – 35	0.39 – 1.0
Jet Transports	0 – +11	variable	3.4 – 6.1	18 – 37	0.27 – 0.62
Military Trainers	–11 – +6	0 fixed to	3.0 – 5.1	0 – 30	0.36 – 1.0
Fighters	–23 – +5	0 fixed to variable	2.3 – 5.8	0 – 55	0.16 – 1.0
Mil. Patrol, Bomb and Transports	–5 – +11	0 fixed to variable	1.3 – 6.9	5 – 35	0.31 – 0.8
Flying Boats, Amph. and Float Airplanes	0 – +25	0 fixed	2.2 – 5.1	0 – 17	0.33 – 1.0
Supersonic Cruise Airplanes	–15 – 0	0 fixed to variable	1.8 – 2.6	32 – 60	0.14 – 0.39

Table 8.14 Planform Design Parameters for Vertical Tails

Type	Dihedral Angle, Γ_v deg.	Incidence Angle, i_v deg.	Aspect Ratio, A_v	Sweep Angle, $\Lambda_{c/4_v}$ deg.	Taper Ratio, λ_v
Homebuilts	90	0	0.4 – 1.4	0 – 47	0.26 – 0.71
Single Engine Prop. Driven	90	0	0.9 – 2.2	12 – 42	0.32 – 0.58
Twin Engine Prop Driven	90	0	0.7 – 1.8	18 – 45	0.33 – 0.74
Agricultural	90	0	0.6 – 1.4	0 – 32	0.43 – 0.74
Business Jets	90	0	0.8 – 1.6	28 – 55	0.30 – 0.74
Regional Turbo-Props.	90	0	0.8 – 1.7	0 – 45	0.32 – 1.0
Jet Transports	90	0	0.7 – 2.0	33 – 53	0.26 – 0.73
Military Trainers	90	0	1.0 – 2.9	0 – 45	0.32 – 0.74
Fighters	75 – 90	0	0.4 – 2.0	9 – 60	0.19 – 0.57
Mil. Patrol, Bomb and Transports	90	0	0.9 – 1.9	0 – 37	0.28 – 1.0
Flying Boats, Amph. and Float Airplanes	90	0	1.2 – 2.4	0 – 32	0.37 – 1.0
Supersonic Cruise Airplanes	75 – 90	0	0.5 – 1.8	37 – 65	0.20 – 0.43

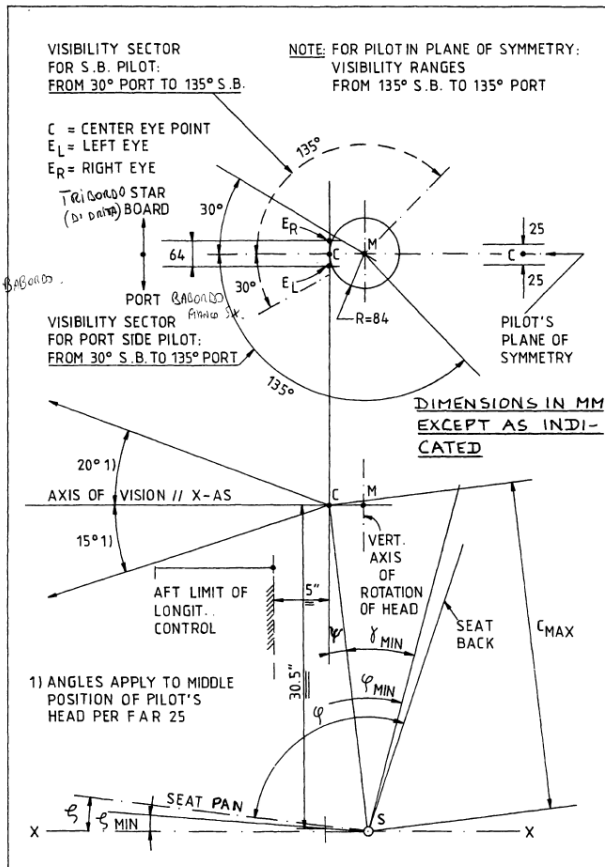Figures and Tables from Roskam Part 3 [6]

Figure 2.16 Visibility Requirements for the Port and for the Starboard Side and the Connection with Acceptable Seat Arrangements
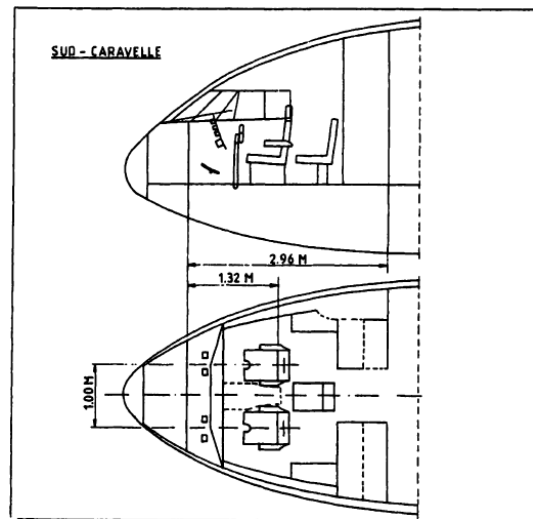

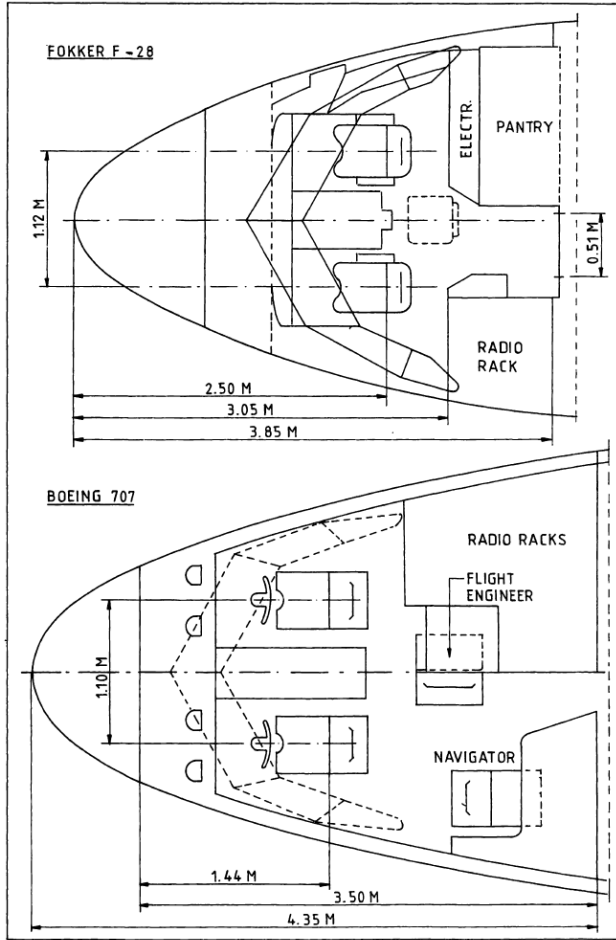Figure 2.22 Cockpit Layout: Sud Caravelle

93

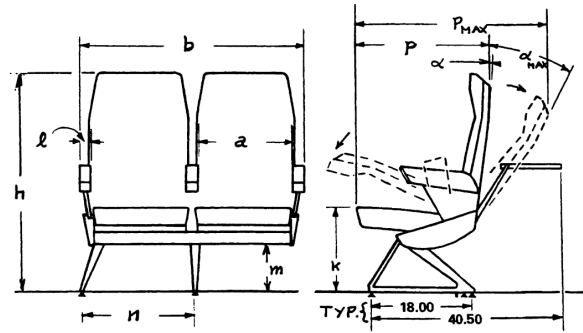Figure 2.24 Cockpit Layout: Fokker F28 and Boeing 707

Figure 3.28 Definition of Seat Dimensions in Table 3.1

Table 3.1 Seat Classification and Seat Dimensions
==

Note: see Figure 3.28 for definition of seat dimensions.

		Seat Classification		
Symbol	Unit	De Luxe	Normal	Economy
a	in.	20(18.5-21)	17(16.5-17.5)	16.5(16-17)
b	in.	47(46-48.5)	40(39-41)	39(38-40)
		for two seats per block		
b	in.	---	60(59-63)	57
		for three seats per block		
l	in.	2.75	2.25	2.0
h	in.	42(41-44)	42(41-44)	39(36-41)
k	in.	17	17.75	17.75
m	in.	7.75	8.5	8.5
n	in.	32(24-34)	32(24-34)	32(24-34)
p/p_{max}	in./in.	28/40	27/37.5	26/35.5
α/α_{max}	deg/deg	15/45	15/38	15/38

The data in brackets indicate the range of numbers found.

Table 3.6 Typical Dimensions of Galleys, Lavatories and
==
Wardrobes Used in Several Airplanes
===================================

Airplane Type	N_{pax}	Range	Galleys No. Dim.		Lavatories No. Dim.		Wardrobes No. Dim.	
Business Jets								
HFB 320	7	1,000	1	24x24	1	30x26	1	24x15
Falcon 20F	10	1,500	1	27x18	1	44x30	1	51x25
BAe HS 125	8	1,450	none		1	35x28	1	24x12
Regional Turboprops								
Nord 262	29	400	1	23x20	1	41x28	1	40x24
Gulfstr. I	19	2,100	1	34x25	1	67x37	1	36x32
Bae HS 748	44	1,000	1	37x14	1	53x35	none	
Fokker F27	48	1,100	1	43x35	1	47x46	1	31x16
DHC-7	44	800	1	26x24	1	46x30	1	26x24
Electra	95	2,300	2	46x26	4	46x41	2	46x34
Jet Transports								
VFW 614	40	700	1	35x28	1	55x32	1	65x40
Fokker F28	60	1,025	1	44x25	1	58x25	1	25x21
BAC 111	74	900	2	49x22	2	65x35	1	49x22
McDD DC9-10	80	1,100	1	48x33	2	48x48	2	48x21
B 737-200	115	1,800	1	55x43	2	43x34	1	55x43
Caravelle	118	1,000	1	51x43	2	55x43	2	24x17
D Mercure	140	800	none		2	47x34	2	49x16
B 727-200	163	1,150	2	51x32	3	43x39	Overhead	
A 300 B4	295	1,600	3	?	5	59x35	Overhead	
L 1011	330	2,700	1	240x162*	7	45x36	Overhead	
McDD DC10	380	3,000	1	240x162*	9	40x40	2	76x22
B 747	490	5,000	4	79x25	12	40x40	2	71x28

*under floor galley

All dimensions in inches. Data based on Ref.12, page 80.
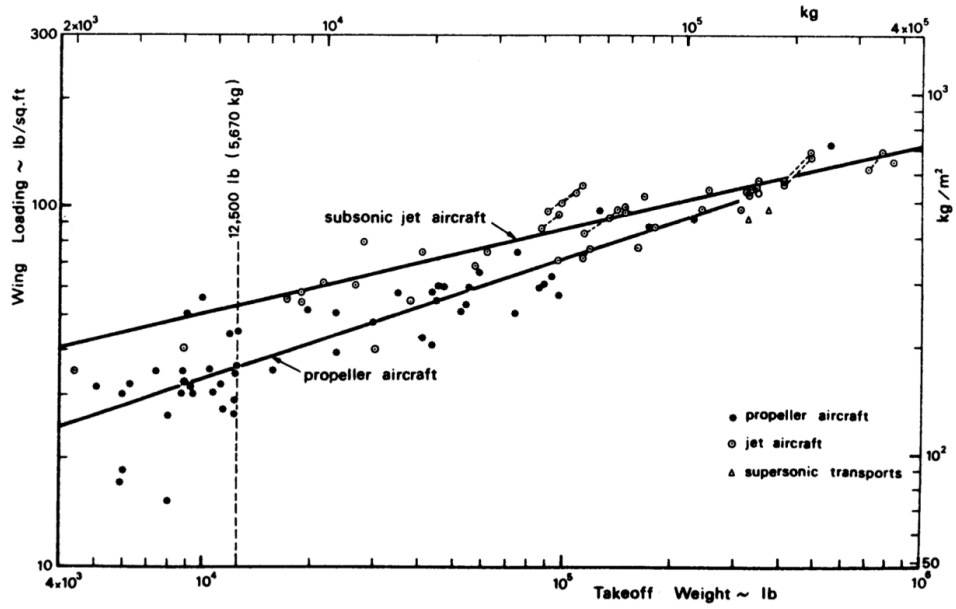
Figures from Torenbeek [51]

Fig. 7-4. Wing loading trends.

Nomenclature

$\bar{c}$ Mean aerodynamic chord

$\bar{c}_{\text{w}}$ Wing mean aerodynamic chord

η_{CTL} Efficiency of controller/converter

η_{EM} Efficiency of electric motor

η_{GB} Efficiency of gearbox

η_{GT} Efficiency of gas turbine

η_{PM} Efficiency of power management system

η_{p} Propulsive efficiency

$\frac{L}{D}$ Lift-to-drag ratio

$\frac{W_0}{P_0}$ Sea level density

$\frac{W_0}{S_{\text{w}}}$ Wing loading [lbf/ft^2]

Λ Wing sweep angle

λ Wing taper ratio

Λ_{ht} Horizontal tail sweep angle

Λ_{vt} Vertical tail sweep angle

Φ Supplied power ratio

ψ Shaft power ratio

ρ_{SL} Sea level density

AEO All engines operative

$AIAA$ American Institute of Aeronautics and Astronautics

APU Auxiliary power unit

AR Wing aspect ratio

AR_{h} Horizontal tail aspect ratio

AR_{v} Vertical tail aspect ratio

B_{h} Horizontal tail span

B_{w} Wing span

C Specific fuel consumption[lb/(lbf hr)]

$C_{\text{D}_{\text{o}}}$ Zero lift drag coefficient

C_{D} Coefficient of drag

$C_{\text{f}_{\text{c}}}$ Skin friction drag coefficient

$C_{\text{L}_{\text{max,Cr}}}$ Max cruise lift coefficient

$C_{\text{L}_{\text{max,L}}}$ Max landing lift coefficient

$C_{\text{L}_{\text{max,TO}}}$ Max takeoff lift coefficient

C_{L} Coefficient of lift

C_{l} Airfoil sectional coefficient of lift

c_{root} Chord length at root

c_{tip} Chord length at tip

C_{bat} Cost of batteries

C_{bhp} Amount of fuel needed to produce one horsepower at the propeller shaft [lb/hr/hp]

C_{Dev} Cost of development support

C_{Eng} Cost of engineering

C_{Ft} Cost of flight test operations

C_{mat} Cost of materials

C_{Mfg} Cost of manufacturing

C_{pms} Cost of power management system

C_{prop} Cost of propeller

C_{Qc} Cost of quality control

C_{Tool} Cost of tooling

CG Center of gravity

CPI Consumer price index

d_{f} Fuselage diameter

D_{P} Propeller diameter

E Endurance

e Oswald's efficiency factor

$E_{0,\text{bat}}$ Energy supplied by battery

$E_{0,\text{f}}$ Energy supplied by fuel

FAR Federal aviation regulations

$ICAO$ International Civil Aviation Organization

L Lift

l_{f} Fuselage length

M Mach Number

MAC Mean aerodynamic chord

N Number of engines

N_{bl} Number of propeller blades

N_{c} Number of crew

N_{lt} Nacelle length

N_{pers} Number of crew and passengers

N_{t} Number of fuel tanks

N_{w} Nacelle width

N_{z} Ultimate load factor

$N_{\text{Attendants}}$ Number of attendants

$N_{\text{Passengers}}$ Number of passengers

N_{Pilots} Number of pilots

N_p	Number of propellers	W_Airframe	Structural Weight
OEI	One engine inoperative	W_APUin	Installed APU weight
$P_\mathrm{0,prop}$	Required takeoff power per propeller [hp]	W_avio	Avionics weight
P_bat	Power from battery	W_dIce	Anti-icing weight
P_elec	Electric shaft power	$W_\mathrm{e'}$	'Everything else' Weight
P_f	Power from fuel	W_eCon	Engine control weight
P_other	Non-electric shaft power	W_ele	Electrical weight
P_0	Takeoff power [hp]	W_em	Weight of electric motor
Q	Number of aircraft produced in 5 years	W_eng	Engine Weight
Q_M	Number of aircraft produced in 1 month	W_fc	Flight controls weight
Q_Proto	Number of prototypes produced	W_fs	Fuel system weight
R	Range	W_fur	Furnishing weight
RFP	Request for proposal	W_fus	Fuselage weight
S_a	Obstacle clearance distance	W_f	Fuel weight
S_csw	Wing control surface area	W_ht	Horizontal tail weight
S_cs	Control surface area	W_hyd	Hydraulics weight
S_FL	Takeoff field length	W_inst	Instrument weight
S_f	Fuselage wetted area	W_L	Landing weight
S_ht	Horizontal tail area	W_mlg	Main landing gear weight
S_n	Nacelle wetted area	W_ng	Nacelle group weight
S_TOG	Takeoff groundrun	W_nlg	Nose landing gear weight
S_vt	Vertical tail area	W_pms	Weight of power management system
S_wet	Wetted area	W_prop	Propeller Weight
S_w	Wing reference area	W_seat	Seat weight
t	Structural depth	W_start	Pneumatic starter weight
T_0	Takeoff thrust	W_vt	Vertical tail weight
V_H	maximum level airspeed [ktas]	W_w	Wing weight
V_Cruise	Cruise speed	W_0	Takeoff weight
V_H	Maximum level airspeed [ktas]	W_bat	Battery weight
V_i	Integral tanks volume [gal]	W_Crew	Weight of crew and crew baggage
V_pr	Volume of pressurized section	W_e	Empty weight
V_p	Self sealing tanks volume [gal]	$W_\mathrm{Passengers}$	Weight of passengers and passenger baggage
V_Stall	Stall speed	x_cg	Center of gravity location
V_t	Total fuel volume [gal]	x_np	Neutral point location
W_ac	Air conditioning weight		